New Insights into the Biochemistry and Cell Biology of RNA Recapping

Dissertation

Presented in Partial Fulfillment of the Requirements for the Degree Doctor of Philosophy in the Graduate School of The Ohio State University

By

Jackson B. Trotman, B.S.

Graduate Program in Ohio State University Biochemistry Program

The Ohio State University

2018

Dissertation Committee

Daniel R. Schoenberg, Advisor

Dawn S. Chandler

Venkat Gopalan

Michael Ibba

Abstract

Eukaryotic gene expression depends on the 5′ cap structure added to all mRNAs. The biology of RNA capping is more dynamic than originally thought, with cytoplasmic recapping enabling spatial and temporal control of translation and other aspects of the RNA life cycle. Despite progress over the past decade, critical gaps remain in our understanding of the biochemistry of RNA recapping and its context within the cell, which are addressed in this dissertation.

Recapping an uncapped RNA in the cytoplasm begins with the combined activities of a 5′ monophosphate RNA kinase and capping enzyme (CE). Recapped RNAs are also methylated at the N7 position of the cap guanine, enabling recognition by cap-binding proteins such as the translation initiation factor eIF4E. However, it was unknown how caps synthesized in the cytoplasm acquire this critical methyl group. Here I describe the identification of the enzyme that completes the synthesis of mature caps in the cytoplasm. This enzyme, RNA guanine-7 methyltransferase (RNMT), was originally thought to be restricted to the nucleus, but I show that it also functions in the cytoplasm. Cytoplasmic RNMT activity is unexpectedly robust compared to that of nuclear RNMT, and RNMT knockdown points to RNMT being the predominant, if not only cap guanine-N7 methyltransferase in the cytoplasm. These results were obtained using an adapted cap methyltransferase activity assay, the details of which are provided. RNMT directly

interacts with CE through its C-terminal catalytic domain, allowing it to associate with the multifunctional cytoplasmic capping complex. Cytoplasmic RNMT activity is additionally stimulated by dimerization with the small protein cofactor RAM. Inhibiting cytoplasmic cap methylation with a dominant-negative form of RNMT caused recapping target RNAs to destabilize, suggesting surveillance by decapping enzymes specific for unmethylated caps.

The full complement of proteins required for cytoplasmic recapping is also unknown. Toward this end, I used in vivo crosslinking and bottom-up proteomics to identify novel proteins that interact with the cytoplasmic population of capping enzyme. The identified proteins perform diverse functional roles and include metabolic enzymes, nucleocytoplasmic transporters, and cytoskeletal proteins. Many of these proteins are known to bind mRNA and may underlie the observed specificity of recapping target RNAs. Western blotting confirmed the association of cytoplasmic CE with the candidate interactors FASN, XPO2, HSP90, EEF2, RUVBL1, and RUVBL2. Further investigation of HSP90 revealed that its interaction with CE causes stabilization of the levels of both nuclear and cytoplasmic CE. HSP90 stabilization may provide a link between cytoplasmic recapping and the cellular stress response, which is discussed.

Dedication

Dedicated to Melissa, for her love and support.

Acknowledgments

I first would like to give thanks to my collaborators for their contributions to this work. Thanks to Chandrama for her initial work on RNMT and stress granules, but most importantly for her effort and patience as my mentor when I first joined the lab. Thanks to Andrew for all his hard work getting our BioID experiments up and running and for his attention to detail in generating some beautiful figures. Lastly, thanks to Bernice and Vicki for providing us with the springboard for our proteomics project that has revealed some interesting avenues for future research.

Thank you to the Center for RNA Biology, the Department of Biological Chemistry and Pharmacology, and the OSU Graduate School for supporting my work with funding and awards and for providing excellent facilities to research and to meet new scientists. Thanks to the NIH as well for funding my work.

I would also like to acknowledge my committee members, Venkat, Mike, and Dawn, for always giving helpful comments, for providing different perspectives on my work, and for working with me on sometimes tight deadlines. Thanks to Jane Jackman and Juan Alfonzo for additional discussions and advice.

Thanks to all the other past and present Schoenberg lab members who have taught me so much about biology and have been wonderful colleagues and friends, including Julie, Sean, Shan-Qing, Danny, Mikaela, Danny, and Alex. I would like to especially

thank Dan Kiss for our frequent discussions about recapping and life in general. I wish him the best of luck in his new lab.

And an enormous thank-you to Dan Schoenberg for giving me the environment to develop independence and for his guidance in making me a better scientist. The past four and a half years of work have been a blast, and I am so grateful that I have had the opportunity to work together.

Lastly, endless thanks to Melissa for being my sounding board when experiments fail and for always wanting to celebrate when things do work. I thank her for her endless patience when I work late and on weekends, and most importantly for the fun we have had working toward our PhDs together.

Vita

2009 ..... Emsley A. Laney High School, Wilmington, North Carolina

2013 ..... B.S. Chemistry and Biology, University of North Carolina at Chapel Hill

2013 to present ..... Graduate Research Fellow and Graduate Research Associate, The Ohio State University

Publications

Trotman, J.B., Giltmier, A.J., Mukherjee, C., and Schoenberg, D.R. (2017). RNA guanine-7 methyltransferase catalyzes the methylation of cytoplasmically recapped RNAs. *Nucleic Acids Res.* 45, 10726–10739.

Trotman J.B. and Schoenberg D.R. (2018). RNA cap methyltransferase activity assay. *Bio Protoc.* 8, e2767.

Fields of Study

Major Field: Ohio State University Biochemistry Program

Table of Contents

List of Tables

List of Figures

Chapter 1. Introduction: A Recap of RNA Recapping

Abstract

The N7-methylguanosine cap is a hallmark feature at the 5′ end of eukaryotic messenger RNAs and is required for gene expression. Nearly a decade ago, it was discovered that mammalian cells contain enzymes capable of restoring caps onto uncapped RNAs in the cytoplasm. In this review, I summarize recent advances in our understanding of cytoplasmic RNA recapping, with regard to both its biochemistry and its impact on the transcriptome. Most studies have focused on the mammalian recapping system, but I also highlight new observations that recapping is observed in disparate eukaryotic organisms, with the trypanosome recapping system appearing to be a fascinating example of convergent evolution. I conclude with emerging insights into the biological significance of cytoplasmic RNA recapping and prospects for the future of this evolving area of study.

Introduction

Messenger RNA, or mRNA, is the critical molecule that directs the production of proteins according to the genetic blueprint of DNA. The flow of genetic information through mRNA is highly complex in eukaryotes, with regulated processes acutely controlling where, when, and how much of each individual protein is produced in

different cell types according to cellular and environmental conditions. A mature eukaryotic mRNA contains at its core a protein-coding sequence (CDS) that is flanked on its 5′ and 3′ ends by untranslated regions (UTRs). The 5′ terminus is characterized by an N7-methylguanosine (m^7G) residue joined through a 5′-5′ triphosphate bridge to the first transcribed nucleotide, a structure referred to as a cap. The m^7GpppN cap structure (where N is the first transcribed nucleotide) was first elucidated in the 1970s through studies of viral and HeLa cell mRNA (Furuichi, 2015; Furuichi et al., 1975a, 1975b; Moss, 2017; Wei and Moss, 1975). Thirty years later, the genes encoding mammalian cap synthesis enzymes had been identified, and the molecular biology of capping had been established: the cap is added co-transcriptionally to the 5′ end of an mRNA in the nucleus, protects the mRNA from degradation by exoribonucleases, and is required for almost every aspect of the mRNA life cycle. This picture has since become more complex with the identification of a cytoplasmic complex of enzymes that can restore a cap onto uncapped RNA. In the last decade, much has been learned through characterizing the recapped transcriptome and studying the enzymes and cofactors responsible for cytoplasmic recapping. It has also been learned that recapping is not unique to mammals but also functions in *Drosophila* and *Trypanosoma*.

Because other reviews published in recent years comprehensively cover the synthesis and biological roles of the cap (Cowling, 2010a; Ghosh and Lima, 2010; Ramanathan et al., 2016), the purpose of this review is to focus on cytoplasmic recapping. This review serves as an update to a previous survey (Schoenberg and Maquat, 2009) that was written at the onset of the investigation into cytoplasmic capping.

Many of the questions raised previously have been answered and will be discussed at length in this review. However, several outstanding questions still remain that I also highlight in an effort to guide future studies of RNA recapping.

The Cap: Canonical Nuclear Synthesis and Functions in mRNA Metabolism

The canonical nuclear cap synthesis pathway modifies the 5′ end of every RNA polymerase II (Pol II) transcript with a cap during the early stages of transcription and is generally conserved among eukaryotes. Pol II transcripts include precursors of all mRNAs but also include microRNA (miRNA) precursors, long non-coding RNAs (lncRNAs), small nucleolar RNAs (snoRNAs), and small nuclear RNAs (snRNAs). As a nascent RNA transcript emerges from Pol II in mammalian cells, its 5′ triphosphate end is rapidly acted upon by capping enzyme (CE, or alternatively, RNGTT), which is anchored to the phosphorylated C-terminal repeat domain of Pol II (Ho et al., 1998a; Yue et al., 1997). First, the CE triphosphatase domain removes the γ-phosphate of the 5′ triphosphate to yield a diphosphate. Next, the guanylyltransferase domain of CE transfers a GMP moiety (covalently bound to lysine 294) to the diphosphate to create the 5′-5′ triphosphate-linked guanosine cap. The cap guanosine is then methylated at the N7 position by the S-adenosylmethionine (SAM)-dependent cap methyltransferase RNMT, which functions as a heterodimer with the small RNMT-activating miniprotein (RAM) (Gonatopoulos-Pournatzis et al., 2011; Pillutla et al., 1998). This generates a mature N7-methylated cap (termed cap 0) that is sufficient for recognition by cap-binding effector proteins (Calero et al., 2002; Marcotrigiano et al., 1997; Niedzwiecka et al., 2002).

Further 2′-O-ribose methylations of the first and second transcribed nucleotides (forming cap 1 and cap 2, respectively) can occur via the respective activities of the methyltransferases CMTR1 and CMTR2 (Bélanger et al., 2010; Werner et al., 2011). These additional methylations function to enhance translation (Kuge et al., 1998) and to mark an RNA as "self" to evade innate immunity responses against viral RNAs (Hyde and Diamond, 2015; Schuberth-Wagner et al., 2015).

Following its synthesis, the cap is bound by the nuclear cap-binding complex (CBC) of CBP20 and CBP80 (Gonatopoulos-Pournatzis and Cowling, 2014). Binding of the CBC to the cap serves as an RNA quality control step to ensure that only capped RNAs are spliced (Izaurralde et al., 1994; Schwer and Shuman, 1996), cleaved and polyadenylated at the 3′ end (Flaherty et al., 1997; Gilmartin et al., 1988), and exported to the cytoplasm (Jarmolowski et al., 1994; Visa et al., 1996). Following nuclear export, the CBC is replaced by another cap-binding protein, the translation initiation factor eIF4E, which directs the majority of translation (von der Haar et al., 2004). Additional cap binding proteins have been identified in recent years, including the alternative CBP80-interacting protein NCBP3 (Gebhardt et al., 2015), the SMN complex member gemin5 (Bradrick and Gromeier, 2009), and the translation initiation factor eIF3d, which can support cap-dependent translation in an eIF4E-independent manner (Lee et al., 2016). Such diversity of cap-binding proteins illustrates the importance of the cap in mRNA metabolism.

As part of mRNA decay, the cap can be removed by several decapping enzymes with distinct and overlapping functions (Arribas-Layton et al., 2013; Song et al., 2010,

2013). Removal of N7-methylated caps has generally been thought to produce m^7GDP and 5′ monophosphate RNA, which is degraded by cytoplasmic XRN1 or nuclear XRN2. Additionally, the recently characterized decapping enzyme DXO (Chang et al., 2012; Jiao et al., 2013) and several Nudix family decapping enzymes (Song et al., 2013) function in cap quality control with activities that can act on 5′ triphosphate ends and/or unmethylated caps.

Early Evidence of Cytoplasmic Recapping

The view that uncapped 5′ ends are irreversibly destined for exonucleolyic decay was challenged by early studies of nonsense-mediated decay (NMD) and its role in the genetic blood disorder β-thalassemia. In erythroid cells of a β-thalassemic mouse model, decay intermediates from nonsense codon-containing β-globin mRNA were found that lacked portions of their 5′ ends but were surprisingly stable (Lim et al., 1989). These decay intermediates were polyadenylated like their parent mRNAs and were only detected in the cytoplasm (Lim et al., 1989; Stevens et al., 2002). Loss of parent mRNA levels upon transcription inhibition was coincident with the accumulation of the decay intermediates, further pointing to their generation being a cytoplasmic process independent of transcription (Lim et al., 1992). Further analysis of these decay intermediates revealed an unexpected explanation for their unusual stability: that their 5′ ends had been modified by a cap or cap-like structure (Lim and Maquat, 1992). Supporting this conclusion, the decay intermediates bound to anti-cap antibody like their parent mRNAs and were competitively eluted with m^7G, a result that was blocked by pre-

treatment with tobacco acid pyrophosphatase. These results were confirmed by the Schoenberg laboratory, with additional evidence that the decay intermediates bind to recombinant eIF4E, are resistant to 5′ exonuclease treatment, and can be decapped by the well-characterized decapping enzyme DCP2 (Otsuka et al., 2009). It was later found that the NMD-associated endonuclease SMG6 is responsible for generating these decay intermediates (Mascarenhas et al., 2013). NMD is a cytoplasmic process, and because capping was thought to be restricted to the nucleus, no mechanism was known at the time that could restore cap structures on uncapped, cytoplasmic RNA.

Recapping Enzymes and Cofactors

The first mechanistic insight into how a cap could be synthesized on a 5′-end-processed, cytoplasmic RNA came with the observation that CE is not restricted to the nucleus as originally thought (Otsuka et al., 2009; Wen et al., 1998). While a predominantly nuclear enzyme, CE also localizes to the cytoplasm in multiple mammalian cell types, including U2OS, Huh7, MEL, Cos-1 (Otsuka et al., 2009), HEK293 (Mukherjee et al., 2014), RH-30 (Thul et al., 2017), and primary astrocytes and cardiomyocytes (C. Mukherjee, unpublished observations). Immunofluorescence of mammalian CE shows evenly distributed, punctate staining throughout the cytoplasm (Otsuka et al., 2009). Furthermore, *Drosophila* CE (RNA-cap) also has a population that localizes to the cytoplasm (Chen et al., 2017).

A common characteristic among diverse eukaryotic cap synthesis machineries is that multiple enzymatic activities are frequently brought together within the same

polypeptide or through protein-protein interactions, facilitating efficient substrate channeling according to the concept of a metabolon (Srere, 1985). Examples include the bifunctional triphosphatase-guanylyltransferase activites of mammalian CE; in *S. cerevisiae*, these activities belong to the separate proteins Cet1 and Ceg1 that nonetheless interact with one another (Ho et al., 1998b). The trypanosome nuclear capping enzyme TbCgm1 is a bifunctional guanylyltransferase-methyltransferase (Takagi et al., 2007), while the trifunctional capping enzymes of poxviruses, African swine fever virus, and mimivirus contain triphosphatase, guanylyltransferase, and methyltransferase activities (Benarroch et al., 2008; Kyrieleis et al., 2014). Consistent with this theme, mammalian CE forms a cytoplasmic capping complex also containing a 5′ monophosphate kinase that generates a diphosphate substrate for CE guanylyltransfersase activity (Otsuka et al., 2009). The cytoplasmic capping complex assembles on the cytoplasmic adaptor protein Nck1, which consists of three SH3 domains and a C-terminal SH2 domain. Mutational analyses revealed that CE binds to the second SH3 domain of Nck1 through its proline-rich C-terminus, while the as-of-yet unidentified monophosphate kinase binds to the second SH3 domain, presumably through a proline-rich peptide sequence of its own (Mukherjee et al., 2014).

In addition to the nuclear guanylyltransferase-methyltransferase TbCgm1, trypanosomes possess a second guanylyltransferase, TbCe1. Investigation of TbCe1 revealed that it localizes predominantly to the cytoplasm and that it strikingly contains a novel 5′ monophosphate RNA kinase domain at its N-terminus, making TbCe1 the only enzyme with such activity identified to date (Ignatochkina et al., 2015). TbCe1 kinase

activity is magnesium-dependent and can use ATP or dATP as a phosphate donor. Of the 5′ monophosphate RNA substrates tested, recapping with TbCe1 was most efficient on those containing spliced leader (SL) sequence, but it is unclear whether recapping activity was stimulated by SL sequence or is instead simply more efficient on substrate RNAs with a 5′ terminal G or A. As a bifunctional kinase-guanylyltransferase, TbCe1 is the first dedicated cytoplasmic recapping enzyme to be described. The authors also speculate that an additional standalone guanine-N7 methyltransferase, TbCmt1, functions to methylate recapped RNAs in trypanosomes (Hall and Ho, 2006; Ignatochkina et al., 2015). The isolation of TbCe1 homology to the kinetoplastid clade (NCBI BLAST analysis) suggests a different evolutionary origin of recapping compared to organisms that have purposed the same enzymes (e.g., CE) for both nuclear and cytoplasmic cap synthesis.

Other enzymes reported in the literature may play roles in recapping or in generating substrates for recapping. A 5′ monophosphate RNA kinase that can yield di- or triphosphate ends was purified from vaccinia viral cores by following its enzymatic activity (Spencer et al., 1978), but the identity of this enzyme remains unknown, despite the limited number (~200) of protein-coding genes that have been annotated in vaccinia (Moss, 2017). Cytoplasmic recapping has not been reported in yeast, but the yeast L-A virus has been found to synthesize RNA transcripts with a 5′ diphosphate, and the ATP-dependent generation of 5′ diphosphate ends from GMP-primed transcripts points to the possibility of 5′ monophosphate RNA kinase activity (Fujimura and Esteban, 2010). Perhaps most relevant to cytoplasmic recapping is the discovery that mammals possess multiple decapping enzymes capable of generating 5′ diphosphate ends in addition to 5′

monophosphate ends (Song et al., 2013). Such 5′ diphosphate ends are resistant to XRN1 activity (Fujimura and Esteban, 2010) and may be readily recapped by the cytoplasmic capping complex in a kinase-independent manner (Figure 1). Likewise, the trypanosome decapping enzyme TbALPH1 was also recently shown to produce 5′ diphosphate (or potentially triphosphate) termini (Kramer, 2017).

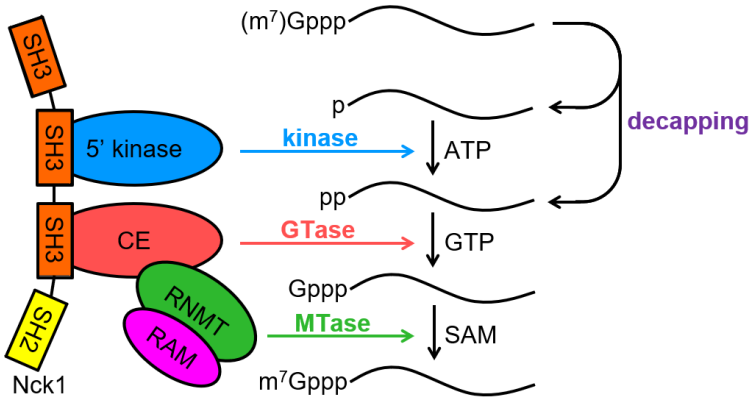

Figure 1. Model of the mammalian cytoplasmic capping complex and the biochemistry of recapping.

The identification of the cytoplasmic cap methyltransferase (green) is a subject of investigation in Chapter 2.

Recapping Target RNAs and Functional Consequences of Recapping

To determine the RNA targets and functional consequences of mammalian cytoplasmic recapping without disrupting nuclear capping, the Schoenberg laboratory

developed an inducible stable cell line expressing a cytoplasmically restricted, catalytically inactive form of CE (termed K294A, referring to its active-site mutation; Otsuka et al., 2009). Overexpression of K294A inhibits endogenous cytoplasmic CE in a dominant-negative manner, likely through disruption of functional cytoplasmic capping complexes. Recapping target mRNAs were identified globally using in vitro XRN1 sensitivity as an indicator of capped/uncapped status of cytoplasmic RNAs harvested from K294A-expressing and uninduced control cells (Mukherjee et al., 2012). This analysis suggested that only a subpopulation of the transcriptome is subject to recapping, as the vast majority of transcripts (51,486) had their cap status unaffected by inhibiting cytoplasmic recapping with K294A expression. However, 675 transcripts were found to be uncapped exclusively in K294A-expressing cells and thus represent a "capping-inhibited" class of mRNAs that are likely to be rapidly recapped whenever an uncapped form appears in the cytoplasm. Another 2666 transcripts were found to be uncapped exclusively in uninduced cells and thus exist in a "natively uncapped" form that may or may not be subject to recapping. Finally, 835 "common" transcripts were found to be uncapped in both K294A-expressing and uninduced cells; these mRNAs are natively uncapped to some degree but have an increased proportion that appears uncapped upon inhibiting cytoplasmic recapping.

Cyclic decapping and recapping, or "cap homeostasis", serves to regulate the stability and/or translatability of recapping target mRNAs (Mukherjee et al., 2012). Notably, recapping targets were found to accumulate as non-translating mRNPs in a stably uncapped state when cytoplasmic capping was inhibited. Despite regulation of

poly(A) tail length as a translational control strategy (Weill et al., 2012) and the general view that deadenylation precedes decapping in mRNA decay (Muhlrad et al., 1994), cap homeostasis does not involve changes in poly(A) tail length (Kiss et al., 2016). Both uncapped and capped forms of the recapping target ZNF207 were found to have similar poly(A) tail length distributions capable of supporting translation. Poly(A) tail length distributions of recapping targets were unchanged by K294A expression and were also essentially the same whether analyzed from non-translating mRNP or translating polysome fractions. These observations support a model where long poly(A) tails are retained on stably uncapped target mRNAs, enabling these transcripts to be stored in a translationally silenced form that is primed for rapid reentry into the translating pool upon recapping. Recent advances in live-cell imaging of translation events have revealed sporadic on-off "bursting" kinetics (Wu et al., 2016; Yan et al., 2016) that could be explained by cycles of decapping and recapping regulating translation in a temporal manner.

Due to the inability to distinguish between caps added in the nucleus from those added in the cytoplasm, it is not yet clear whether cytoplasmic recapping occurs more frequently at the canonical 5′ end following decapping or at downstream sites generated by endonucleolytic cleavage (Mercer et al., 2010; Schmidt et al., 2015) or partial exonucleolytic decay (Moon et al., 2015). Nonetheless, growing evidence suggests a role for cytoplasmic recapping in generating novel capped ends at downstream sites. A number of methods have been developed for the transcriptome-wide identification of capped sites (Afik et al., 2017; Batut et al., 2012; Cartolano et al., 2016; Gu et al., 2012;

Machida and Lin, 2014), with cap analysis of gene expression (CAGE; Shiraki et al., 2003) being the most commonly used. CAGE was originally developed for the annotation of transcription start sites (TSSs); however, analysis as part of the ENCODE Project uncovered the prevalence of human CAGE tags downstream of annotated TSSs mapping across exon-exon junctions (Fejes-Toth et al., 2009). Such downstream CAGE tags represent the recapping of post-transcriptionally processed mRNAs, as the tags are considered too short to be generated by the splicing of mRNAs produced from alternative TSSs (Fejes-Toth et al., 2009; Le Hir et al., 2000, 2001) and do not coincide with the active chromatin marks or Pol II occupancy that would be expected of alternative transcription initiation (Mercer et al., 2010, 2011). Further analysis by the ENCODE Project concluded that only ~72% of human CAGE tags map to actual TSSs, leaving the remaining 30% as possible recapping sites (Djebali et al., 2012). A targeted ligation-based approach identified locations of uncapped 5′ ends in recapping targets (Mukherjee et al., 2012) that mapped exactly to or in the vicinity of downstream CAGE tags (Kiss et al., 2015a), supporting a role for the cytoplasmic recapping machinery in generating novel capped ends.

Downstream capped ends are also frequent in *Drosophila*. These are similarly unlikely to be generated by alternative TSSs on the basis of promoter motifs and chromatin immunoprecipitation sequencing data for the transcription factors TBP TRF2 (Hoskins et al., 2011; Ni et al., 2010). Targeted validation by two independent methods,

cap-trapping and oligo-capping, confirmed that 10 out of 12 candidate downstream sites indeed represented capped RNAs (Ni et al., 2010).

These studies are in agreement that post-transcriptional processing and recapping is responsible for a large portion of capped sites mapping to exonic sequences of the genome. However, even recent studies of noncanonical capped sites (Afik et al., 2017; Reyes and Huber, 2018; Tamarkin-Ben-Harush et al., 2017) have not considered this possibility. With a diversity of techniques now available to profile capped sites, future studies should continue to focus attention to delineating whether downstream capped ends arise due to alternative TSSs or recapping of processed mRNAs. Inhibiting cytoplasmic recapping via K294A or a similar method may be an effective tool for enabling this distinction. Such studies will be crucial for unraveling the mechanisms that underlie the generation of capped transcripts with shortened 5′ UTRs, shortened ORFs encoding N-terminally truncated proteins, or even new classes of non-coding RNAs consisting of primarily 3′ UTR sequences (Mayr, 2017; Mercer et al., 2011).

Biological Significance of Recapping

Temporal regulation of translation and RNA stability through cap homeostasis may serve important roles in the cell cycle and in the cellular response to stress. Gene ontology (GO) analysis of recapping targets in Mukherjee et al. (2012) revealed that the "capping-inhibited" class of transcripts was enriched for proteins involved in mitotic cell cycle control, consistent with more recent reports suggesting some level of coordination between cap synthesis and the cell cycle (Aregger and Cowling, 2017; Aregger et al.,

2016). Cellular stresses, such as oxidative stress and heat shock, are known to generally repress cap-dependent translation through the sequestration of translationally repressed mRNPs in stress granules (SGs; Sheinberger and Shav-Tal, 2017). The cap status of mRNAs in SGs is unknown, but recent observations suggest that cytoplasmic recapping may serve to translationally reactivate uncapped mRNAs as SGs dissociate during recovery from stress. When cytoplasmic recapping is inhibited, cells are impaired in their ability to recover from oxidative stress (Otsuka et al., 2009). This study did not find co-localization of an epitope-tagged form of CE with SGs, but direct immunofluorescence of endogenous CE has since shown a strong association of CE with SGs (C. Mukherjee, unpublished observations), suggesting that the epitope tag may have interfered with the recruitment of CE to SGs. Taken together, cytoplasmic recapping may function to promote the post-stress resumption of cap-dependent translation.

New findings have also indicated a role for RNA recapping in animal development via the hedgehog signaling pathway (Chen et al., 2017). An siRNA screen of ~7000 genes conserved between *Drosophila* and mammals revealed that CE is required for *Drosophila* wing development. Unexpectedly, CE-knockdown-induced wing defects could be rescued by expression of a cytoplasmically restricted form of CE (cCE) but not by the corresponding active-site mutant (K294A), establishing cytoplasmic recapping as necessary for wing development. As hedgehog signaling is a key regulator of development, it was also found that in mouse 3T3 cells, hedgehog signaling is upregulated upon cCE overexpression but downregulated upon K294A expression. The dependence of this phenomenon on cytoplasmic CE catalytic activity suggests that

cytoplasmic recapping enables changes in the translation and/or stability of transcripts involved in the hedgehog signaling pathway. Hedgehog signaling is dysregulated in a wide range of human diseases, including cancer and neurodevelopmental disorders (Fattahi et al., 2018), so further studies into the involvement of cytoplasmic recapping may lead to novel therapeutic strategies.

Problems to Be Addressed

The aims of to be addressed in this dissertation are two-fold. First is the identification and characterization of the enzyme responsible for N7-methylation of caps added in the cytoplasm. Multiple lines of evidence point to the N7-methylation of cytoplasmically synthesized caps. Decay intermediates of nonsense codon-containing β-globin mRNA bind to recombinant eIF4E and anti-cap antibody and are competitively eluted by m^7GDP but not GDP. Additionally, inhibiting cytoplasmic recapping affects the translation of recapping target mRNAs, and cap-dependent translation requires N7-methylation of the cap.

The second aim is to identify novel proteins involved in cytoplasmic recapping through the proteomic analysis of proteins that interact with the cytoplasmic population of CE. Very little is known how the recapping machinery selects target mRNAs for recapping or how the process might be regulated or linked to other cellular processes.

Chapter 2. RNA Guanine-7 Methyltransferase Catalyzes the Methylation of Cytoplasmically Recapped RNAs[1] [2]

Abstract

Cap homeostasis is a cyclical process of decapping and recapping that impacts a portion of the mRNA transcriptome. The metastable uncapped forms of recapping targets redistribute from polysomes to non-translating mRNPs, and recapping is all that is needed for their return to the translating pool. Previous work identified a cytoplasmic capping metabolon consisting of capping enzyme (CE) and a 5′-monophosphate kinase bound to adjacent domains of Nck1. The current study identifies the canonical cap methyltransferase (RNMT) as the enzyme responsible for guanine-N7 methylation of recapped mRNAs. RNMT binds directly to CE, and its presence in the cytoplasmic capping complex was demonstrated by pulldown assays, gel filtration, and proximity-dependent biotinylation. The latter also identified the RNMT cofactor RAM, whose presence is required for cytoplasmic cap methyltransferase activity. These findings

[1] This chapter has benefited from the writing and editing contributions of all four authors: Jackson B. Trotman[a,b,c], Andrew J. Giltmier[a,c], Chandrama Mukherjee[a,c] and Daniel R. Schoenberg[a,c] ([a]Center for RNA Biology, [b]Ohio State Biochemistry Program, [c]Department of Biological Chemistry and Pharmacology, The Ohio State University, Columbus, Ohio).

[2] This chapter is modified from an article originally published in *Nucleic Acids Research* (Trotman et al., 2017; Oxford University Press) and is used here in accordance with a Creative Commons license agreement.

guided development of an inhibitor of cytoplasmic cap methylation whose action resulted in a selective decrease in levels of recapped mRNAs.

Introduction

The 5′ end of every mRNA is modified by addition of an N7-methylguanosine (m^7G) cap that is required for proper mRNA processing and function (Ramanathan et al., 2016). Until recently, the prevailing view was that mRNA capping is confined to the nucleus, that loss of the cap in the cytoplasm is irreversible, and that uncapped 5′ ends are rapidly degraded by Xrn1. The first evidence to the contrary came with the identification of stable decay intermediates of nonsense-containing β-globin mRNA in the cytoplasm of erythroid cells from transgenic mice. These 5′-truncated RNAs are polyadenylated (Stevens et al., 2002), and recent work showed they are generated by SMG6 cleavage of the nonsense-containing mRNA (Mascarenhas et al., 2013). Unexpectedly, the shortened transcripts were also modified on their 5′ ends by a cap or cap-like structure (Lim and Maquat, 1992). The mechanism responsible for this modification was unknown at the time; however, in confirming the m^7G cap status of these RNAs, my group identified a cytoplasmic pool of capping enzyme (CE; alternatively, RNGTT) that co-purifies with a 5′ monophosphate RNA kinase (5′ kinase) activity that generates diphosphate ends necessary for guanylate transfer by CE (Otsuka et al., 2009). The existence of cytoplasmic machinery capable of recapping 5′ monophosphate ends suggested that decapping (and/or endonucleolytic cleavage) does not invariably lead to complete degradation and can instead generate substrates for subsequent recapping. My group

identified a number of recapping targets by their accumulation with uncapped 5′ ends when cytoplasmic capping was inhibited by overexpression of a catalytically inactive, cytoplasmically restricted form of CE (Mukherjee et al., 2012). Capped Analysis of Gene Expression (CAGE) performed as part of ENCODE provided additional evidence for cytoplasmic capping by identifying capped ends that do not map to transcription start sites but instead map to sites within spliced exons (Fejes-Toth et al., 2009). It is estimated that these downstream cap sites account for 25% of capped ends (Djebali et al., 2012), and a number of these capped ends were recently shown to map to the 5′ ends of recapped transcripts (Kiss et al., 2015b). Cytoplasmic capping targets undergo a cyclical process of decapping and recapping, termed cap homeostasis, that impacts the translation of a subset of the mRNA transcriptome (Mukherjee et al., 2012). When cytoplasmic capping is blocked, these transcripts move from polysomes to non-translating mRNPs, where they accumulate in a stable yet uncapped form. Importantly, these non-translating transcripts are polyadenylated, and the length of their poly(A) tails is sufficient to facilitate translation initiation after recapping (Kiss et al., 2016).

Nuclear capping involves three successive reactions that are catalyzed by two enzymes, CE and RNA guanine-7 methyltransferase (RNMT). CE converts the 5′-triphosphate end of the nascent transcript to a 5′-diphosphate and then transfers GMP bound covalently at lysine 294 onto this. Synthesis of the basic cap structure (cap 0) is completed by methylation at N7 of the transferred guanosine by RNMT, and both CE and RNMT are juxtaposed to the nascent 5′ end by binding to the C-terminal domain of RNA polymerase II. Cytoplasmic capping also involves three successive reactions but differs

from nuclear capping by the process that generates the 5′-diphosphate intermediate. In cytoplasmic capping, the recapping substrate is generated by transfer of the γ-phosphate of ATP onto a 5′-monophosphate end by a polynucleotide 5′-monophosphate kinase. Mutual binding to the cytoplasmic adapter protein Nck1 brings the 5′ kinase and CE together in a single complex (Mukherjee et al., 2014). Nck1 consists of three SH3 domains and a C-terminal SH2 domain. The 5′ kinase binds to the second SH3 domain, and CE binds to the third SH3 domain through its proline-rich C-terminus. This organization of sequential enzymes in a metabolic pathway into a supramolecular complex, or metabolon, allows effective transport of substrates from one active site to the next and enhances the rate of catalysis by increasing the local concentration of substrates for downstream enzymes (Srere, 1987; Wu and Minteer, 2015). Overexpression of forms of Nck1 that are unable to bind CE or the 5′ kinase caused uncapped forms of recapping targets to accumulate (Mukherjee et al., 2014), thus establishing the cytoplasmic capping complex as a metabolon that recaps 5′ monophosphate ends. Echoing the multifunctionality of the cytoplasmic capping complex, trypanosomes have a cytoplasmic, bifunctional enzyme with 5′ monophosphate kinase and guanylyltransferase activities that may likewise facilitate translational control through recapping (Ignatochkina et al., 2015).

The majority of translation is directed by the cap-binding translation initiation factor eIF4E, which, through the eIF4F complex, ultimately recruits the small ribosomal subunit to the mRNA 5′ end (Kumar et al., 2016). In order for recapped mRNAs to recapitulate the behavior of nuclear capped transcripts, the added cap guanosine must

undergo N7 methylation. In the crystal structure of eIF4E, the cap guanine base is recognized by sandwich-stacking between two tryptophan side chains. Binding is strengthened by cation-π interactions with the N7-methylguanine (Marcotrigiano et al., 1997; Niedzwiecka et al., 2002), such that the affinity of eIF4E for the m^7G cap is three to four orders of magnitude stronger than that for the unmethylated equivalent. Guanine-N7 methylation is also needed to maintain mRNA stability in the presence of surveillance mechanisms that degrade mRNAs with improperly methylated caps (Grudzien-Nogalska and Kiledjian, 2017; Jiao et al., 2013).

The current study sought to identify the source of cytoplasmic cap methylation. Nuclear cap methylation is a regulated process (Aregger and Cowling, 2017) in which RNMT activity is stimulated by the binding of RNMT-activating miniprotein (RAM) to its C-terminal catalytic domain (Gonatopoulos-Pournatzis et al., 2011) and inhibited by loss of RAM (Grasso et al., 2016). Regulation of RNMT and RAM by site-specific phosphorylation points to cap methylation as an evolving nexus of post-transcriptional control. Results presented here identify a cytoplasmic pool of RNMT, show this is a component of the cytoplasmic capping complex, and demonstrate its function as the methyltransferase that catalyzes the final maturation step in cap homeostasis.

Materials and Methods

Cell Lines and Cell Culture. Human osteosarcoma (U2OS) cells obtained from ATCC (HTB-96) were cultured in McCoy's 5A medium (Thermo Fisher 116600-108) supplemented with fetal bovine serum (FBS) to 10% (v/v). Human embryonic kidney

(HEK293) cells were cultured in Dulbecco's Modified Eagle Medium (Thermo Fisher 11995-073) supplemented with FBS to 10% (v/v). Cells were maintained at 37 °C under 5% CO_2 and were discarded after no more than 20 passages.

Transfection and Subcellular Fractionation

Prior to transfection, cells were given fresh, pre-warmed medium. HEK293 cells were 60-70% confluent at time of transfection with 10 μg plasmid DNA per 10-cm dish using jetPRIME transfection reagent (Polyplus 114-15) according to manufacturer's protocol. Cells were cultured 24 or 48 h before being harvested. U2OS cells were 70-75% confluent at time of transfection with 6 μg plasmid DNA per 10-cm dish using FuGENE 6 transfection reagent (Promega E2691) according to manufacturer's protocol. These cells were then cultured 24 h before being harvested. One 10-cm dish of U2OS cells was used per siRNA treatment. At the time of the first siRNA transfection, cells were 50% confluent. siRNA transfection mixtures were prepared with jetPRIME transfection reagent (Polyplus) and added to culture medium to bring siRNA to a concentration of 10 nM. After 24 h, the culture medium was removed, and the same procedure was repeated for a second transfection. After another 24 h, the cells were harvested. Trilencer-27 siRNAs (OriGene) used in this study are as follows: universal scrambled control siRNA (SR30004), RNMT siRNA (SR305750B), RAM siRNA (SR313193A). To harvest, cells were washed with PBS and then scraped into 1 mL PBS. After centrifugation at 70 x g for 10 min at 4 °C, pellets were resuspended in 5 to 10 volumes of ice-cold YO Lysis Buffer (10 mM HEPES pH 7.3, 10 mM KCl, 10 mM $MgCl_2$, 0.2% (v/v) IGEPAL CA-

630, 2 mM DTT, 0.5 mM PMSF, 7.5 µL/mL protease inhibitor cocktail (Sigma P8340), 7.5 µL/mL phosphatase inhibitor cocktail 2 (Sigma P5726), 7.5 µL/mL phosphatase inhibitor cocktail 3 (Sigma P0044)) by pipetting 10 times. Resuspended cells were incubated on ice for 10 min, pipetted 5 times, and centrifuged at 16,100 x g for 10 min at 4 °C. The supernatants (cytoplasmic extracts) were removed and kept on ice. Residual supernatants were completely removed from the nuclear pellets before resuspending in 4 to 10 cell-pellet volumes of ice-cold YO Buffer A (10 mM HEPES pH 7.3, 25% (v/v) glycerol, 420 mM NaCl, 1.5 mM $MgCl_2$, 0.2 mM EDTA, 1 mM DTT, 0.5 mM PMSF, 7.5 µL/mL protease inhibitor cocktail (Sigma), 7.5 µL/mL phosphatase inhibitor cocktail 2 (Sigma), 7.5 µL/mL phosphatase inhibitor cocktail 3 (Sigma)) by pipetting 15 times. This was incubated end-over-end for 20 min at 4 °C and then centrifuged (16,100 x g for 5 min at 4 °C) to pellet nuclear debris. Supernatants (nuclear extracts) were removed and kept on ice. Total protein concentration in each extract was determined by Bradford assay using Bio-Rad Protein Assay Dye Reagent (Bio-Rad 5000006) normalized against a standard curve of BSA (Fisher Scientific BP1600-100). For cap methyltransferase activity assays, nuclear and cytoplasmic extracts were brought to the same protein concentration and buffer composition (Combo Buffer) by diluting to 50% with YO Lysis Buffer or YO Buffer A, respectively, and stored in small aliquots at -80 °C. For SDS-PAGE analysis, extracts were diluted to 75% with 4X Laemmli Sample Buffer.

Immunoprecipitation

Nuclear and cytoplasmic extracts corresponding to the same mass of protein (1000 μg for Fig. 1B, 125 μg for Fig. 4C) were brought to 500 μL under the same buffer composition (Combo Buffer) and pre-cleared with 15 μL slurry-equivalent of Dynabeads Protein G (Thermo Fisher 10003D) at 4 °C for 45 min with end-over-end rotation. At the same time, 15 μL slurry-equivalent Dynabeads Protein G was incubated with 2 μg antibody in 500 μL Combo Buffer (for each immunoprecipitation) at 25 °C for 45 min. Pre-cleared extract samples were then incubated with bead-bound antibodies end-over-end at 4 °C overnight. Beads were washed three times with 500 μL Combo Buffer, 10 min end-over-end at 4 °C per wash. Beads were resuspended in 20 μL Combo Buffer; a portion of this mixture was brought to 1X Laemmli Sample Buffer for SDS-PAGE, and the remaining mixture was stored in small aliquots at -80 °C for cap methyltransferase activity assays.

Generation of GpppRNA Substrate for Cap Methyltransferase Activity Assay

In vitro transcription with the MEGAscript T3 Transcription Kit (Ambion 1138) was used to produce a 32-nt 5′-triphosphate RNA (pppRNA) with the same sequence as that used in Yue et al., 1997. pppRNA was purified using a NucAway Spin Column (Thermo Fisher AM10070) and stored at -20 °C. To generate radiolabeled GpppRNA, a 40-μL in-vitro capping reaction was prepared, containing 10 mM Tris-HCl pH 7.5, 3 mM $MgCl_2$, 1 mM dithiothreitol, 0.1 mM EDTA, 20% (v/v) glycerol, 24 pmol pppRNA, 24 pmol [α-32P]GTP (3000 Ci/mmol, PerkinElmer BLU006H250UC), and 2 pmol

recombinant His-CE. This reaction was incubated for 3 h at 30 °C and then heat-inactivated for 10 min at 65 °C. RNA was purified using the RNA Clean & Concentrator-5 kit (Zymo Research R1016), eluting with 30 µL RNase-free water. Yield of purified radiolabeled GpppRNA was measured by scintillation counting relative to input.

Cap Methyltransferase Activity Assay

Reactions were prepared, each containing 5 fmol radiolabeled GpppRNA, 50 mM Tris pH 8.0, 6 mM KCl, 1.25 mM $MgCl_2$, 100 nM S-adenosylmethionine, 2 mM DTT, and 20 U SUPERase-In (Thermo Fisher AM2696). Each reaction volume was 10 µL and contained either 4 µg (Fig. 1B) or 1 µg (Fig. 1D, 4E, and 5C) nuclear or cytoplasmic extract, 1 µL immunoprecipitated (5% of total) bead slurry (Fig. 1B), or 4 µL gel filtration fraction (Fig. 2B). Reactions were incubated for 30 min at 37 °C, and RNA was then immediately purified using the RNA Clean & Concentrator-5 kit (Zymo Research), eluting with 7 µL RNase-free water. Purified RNA was digested in a 7-µL reaction containing 5 µL purified RNA, 50 mM sodium acetate pH 5.2, and 0.44 U nuclease P1 (US Biological N7000). After incubating for 30 min at 37 °C, 2 µL of each reaction was spotted on the origin of a pre-run PEI cellulose thin-layer chromatography plate (Macherey-Nagel 801053), which was then developed in 0.4 M ammonium sulfate. After overnight exposure to a storage phosphor screen, images were obtained with a Typhoon 9200 (Amersham).

Streptavidin Pulldown

HEK293 cells were transiently transfected with pQCXIP-MS2-bio or pcDNA3-bio-myc-NES-mCE ΔNLS (Fig. 2C) or a 1:1 (w/w) ratio of pcDNA3-bio-myc-mCE with pcDNA4/TO-myc-GFP-FLAG, pcDNA3-FLAG-RNMT, pcDNA3-FLAG-RNMT 1-120, or pcDNA3-FLAG-RNMT 121-476 (Fig. 2F). Prior to harvesting, cells for Fig. 2F were incubated for 10 min at room temperature in PBS containing 0.15% formaldehyde before adding glycine (in PBS) to 115 mM, mixing well, and allowing incubation for 5 min at room temperature to quench free formaldehyde. Cytoplasmic extracts were prepared, and protein concentrations were measured. Equivalent protein amounts of each cytoplasmic extract were brought to 500 µL with YO Lysis Buffer, and concentrated NaCl solution was added to a final concentration of 150 mM. To each sample, 50 µL pre-equilibrated slurry-equivalent MyOne Streptavidin T1 Dynabeads (Thermo Fisher 65601) was added. Samples were incubated end-over-end at 4 °C for 2 h before washing the protein-bound beads four times with 500 µL PD Buffer (YO Lysis Buffer containing 150 mM NaCl) at 4 °C for 10 min. Beads were resuspended in 30 µL 2X Laemmli Sample Buffer for analysis by SDS-PAGE and Western blot.

GST Pulldown

To 5 µg bead-bound GST or GST-RNMT, 30 µL glutathione Sepharose 4B beads (GE Healthcare) was added to better visualize the bead pellets. The bead mixtures were equilibrated in PD Buffer and then resuspended in 500 µL PD Buffer containing 1 µg His-CE. The mixtures were incubated end-over-end at 4 °C for 2 h and then washed four

times with 500 µL PD Buffer at 4 °C for 10 min each. Beads were resuspended in 15 µL 2X Laemmli Sample Buffer and analyzed alongside an input sample by SDS-PAGE and Western blot.

Proximity-Dependent Biotinylation

Triplicate cultures of HEK293 cells were transiently transfected with a 1:3 (w/w) ratio of pcDNA3-FLAG-RNMT and either pcDNA3.1-myc-BirA* or pcDNA3.1-myc-BirA*-cCE. After 6 h, a stock solution of 10 mM biotin (Sigma-Aldrich B4639-1G) in DMSO was prepared and added directly to medium to final concentrations of 0, 5, and 25 µM biotin. Additional DMSO was added where necessary to normalize the volume of mix added to each dish. Cells were incubated 14 h before harvesting and preparing cytoplasmic extracts as described above. Streptavidin pulldown was performed as described above, using 300 µg total cytoplasmic protein. Beads were resuspended in Laemmli Sample Buffer and analyzed by SDS-PAGE and Western blot. Using the same cytoplasmic extracts, anti-FLAG immunoprecipitation was performed as described above for Fig. 3B, except that the binding and washing steps used PD Buffer instead of Combo Buffer.

Preparation of Cytoplasmic RNA

Triplicate cultures of U2OS cells were transiently transfected with a 1:9 ratio (w/w) of pECE-EGFP-bio and either empty pcDNA3 or pcDNA3-FLAG-NES-RNMT 121-476 D203A. After 24 h, cells were harvested, and nuclear and cytoplasmic extracts

were prepared, with the YO Lysis Buffer being supplemented with RNaseOUT (Thermo Fisher 10777019) to 0.4 U/μL. Total cytoplasmic RNA was prepared from cytoplasmic extracts using the Direct-zol RNA MiniPrep Kit (Zymo Research R2053) according to manufacturer's protocol, including on-column DNase I digestion. Purity and concentration of the prepared RNA were measured with a NanoDrop ND-1000 spectrophotometer.

Recovery of Capped RNA with GST-eIF4E

For each pulldown, 8 μL slurry-equivalent Glutathione MagBeads (GenScript L00327) was equilibrated in Cap PD Buffer (150 mM NaCl, 0.1% (v/v) IGEPAL CA-630, 10 mM Tris pH 7.5, 1 mM DTT) before resuspending beads in 200 μL Cap PD Buffer with 4 μg GST-eIF4E K119A. Mixtures were incubated end-over-end at 4 °C for 70 min, and then beads were washed five times with 200 μL Cap PD Buffer. RNA mixtures of 400 μL were prepared for each pulldown, each containing 1 μg cytoplasmic RNA, 0.04 ng G-capped luciferase RNA, and 80 U RNaseOUT (Thermo Fisher) in Cap PD Buffer. Washed protein-bound beads were resuspended in 200 μL RNA mixtures, and the remaining 200 μL RNA mixtures were kept on ice for analysis as input samples. Bead-RNA mixtures were incubated end-over-end at 4 °C for 2 h, and the beads were then washed thrice with 200 μL Cap PD Buffer at 4 °C for 10 min. Washed beads were resuspended in 200 μL Cap PD Buffer. RNA from each 200 μL input and eIF4E-bound sample was purified using the Direct-zol RNA MiniPrep Kit (Zymo Research), eluting with 25 μL RNase-free water.

Quantitative Reverse Transcription PCR

To 0.5 µg cytoplasmic RNA spiked with 0.02 ng luciferase RNA (Fig. 5E) or 10 µL purified input or eIF4E-bound RNA (Fig. 5F), 100 ng random hexamers and 10 nmol each dNTP was added to a total volume of 13 µL. Mixtures were incubated at 65 °C for 5 min and immediately placed on ice. Mixtures were brought to 20-µL reverse transcription reactions containing 1X First Strand Buffer, 5 mM DTT, 40 U RNaseOUT (Thermo Fisher), and 200 U SuperScript III reverse transcriptase (Thermo Fisher 18080044). Reactions were placed on a thermocycler with the following program: 25 °C for 5 min, 50 °C for 60 min, 70 °C for 15 min. The resulting cDNAs were analyzed by quantitative reverse transcription PCR in triplicate 10-µL reactions containing 0.5 µM forward and reverse gene-specific primer (see Table 3) and 1X SensiFAST SYBR No-ROX mix (Bioline BIO-98020) with a Bio-Rad CFX Connect real-time PCR detection system. PCRs were performed with the program: 95 °C for 3 min, 40 cycles of (95 °C for 10 s, 55 °C for 30 s).

Quantification and Statistical Analysis

Cap methyltransferase activity data (Fig. 1B, 1D, 2D, 4E, and 5C) were quantified using ImageQuant TL software (GE Healthcare) to determine relative amounts of GpppG and m^7GpppG for each sample. GraphPad Prism 6 software was used to conduct ratio paired (Fig. 1D and 4E) and unpaired two-tailed (Fig. 5C) t-tests to analyze independent biological triplicate experiments. Results with $p<0.05$ were considered significant. RT-

qPCR data (Fig. 5E and 5F) were analyzed using Bio-Rad CFX Manager 3.1 software. Cq values were determined by regression mode. For Fig. 5E, the the ΔΔCq method was used to calculate relative mRNA quantities among the samples for each gene, normalized to the luciferase spike control and to the non-recapping-target internal control BOP1. Normalized quantities were arbitrarily set to 1 for the vector control treatment. For Fig. 5F, the ΔCq method was used to calculate relative mRNA quantities among the samples for each gene, and the technical mean quantity of each gene in the eIF4E-bound samples was normalized to the corresponding input quantity. The mean of independent biological replicates was presented ± SEM using GraphPad Prism 6 software, and unpaired two-tailed t-tests were performed for each gene to compare vector control and ΔN-RNMT samples. Results with $p<0.05$ were considered significant. Additional information can be found in Supplementary Materials and Methods in Appendix A.

Results

RNMT is Present in Both the Nucleus and the Cytoplasm

The core of the cytoplasmic capping complex consists of CE and a 5′-monophosphate kinase bound to adjacent SH3 domains of adapter protein Nck1 (Mukherjee et al., 2014). From results in Otsuka et al., 2009, I knew that recapped 5′ ends are methylated; however, the responsible methyltransferase remained to be identified. The most likely candidate was RNA guanine-7 methyltransferase (RNMT, or cap methyltransferase). RNMT is highly specific for unmethylated caps (Varshney et al.,

2016), and there was evidence in Otsuka et al., 2009 for a cytoplasmic pool of this enzyme.

Immunofluorescence showed the expected nuclear staining for RNMT but also revealed the presence of RNMT throughout the cytoplasm (Figure 2A). RNMT staining concentrated in the perinuclear region, and varying degrees of punctate cytoplasmic staining were seen in every cell I examined. Cytoplasmic RNMT staining has also been reported for U2OS, A431, and U251 cells in the Cell Atlas (Thul et al., 2017) and is independent of whether cells are fixed with methanol (Figure 2A) or with formaldehyde (Figure 3). A pattern of punctate cytoplasmic staining was also seen previously for CE (Otsuka et al., 2009). Western blotting of nuclear and cytoplasmic extracts and immunoprecipitation with anti-RNMT antibody provided further evidence for a cytoplasmic pool of RNMT (Figure 2B, upper panels). Phosphorylation of RNMT on threonine at position 77 interferes with RNMT binding to the KPNA2 subunit of importin-α (Aregger et al., 2016), and while it was conceivable this might be responsible for the observed cytoplasmic pool, I saw no evidence for this by Western blotting of immunoprecipitated RNMT with anti-phosphothreonine antibody (Figure 4).

The functionality of cytoplasmic RNMT was evaluated by the ability of protein present in crude extract and immunoprecipitated RNMT to methylate G-capped RNA. In Figure 2B, nuclear and cytoplasmic extracts (lanes 1 and 2) or immunoprecipitated nuclear and cytoplasmic RNMT (lanes 3 and 4) were incubated with [^{32}P]G-capped RNA and S-adenosylmethionine. The reaction products were digested with P1 nuclease, separated by PEI cellulose thin layer chromatography (TLC) and visualized by

phosphorimager. GpppG and m^7GpppG were identified by comparing their mobilities to known standards. Cytoplasmic extract contained unexpectedly robust RNMT activity, and the activity of immunoprecipitated protein confirmed both the functional nature of this protein and the broad subcellular distribution seen in Figure 2A.

RNA interference provided additional confirmation for the existence of a cytoplasmic pool of RNMT. In Figure 2C, U2OS cells were transfected with control or RNMT siRNAs. Western blotting confirmed parallel loss of RNMT from nuclear and cytoplasmic fractions, and this was matched by a parallel decrease in nuclear and cytoplasmic RNMT activity (Figure 2D). Together, the results in Figure 2 demonstrate that cells have a pool of cytoplasmic RNMT that is as functional as its nuclear counterpart in catalyzing cap methylation.

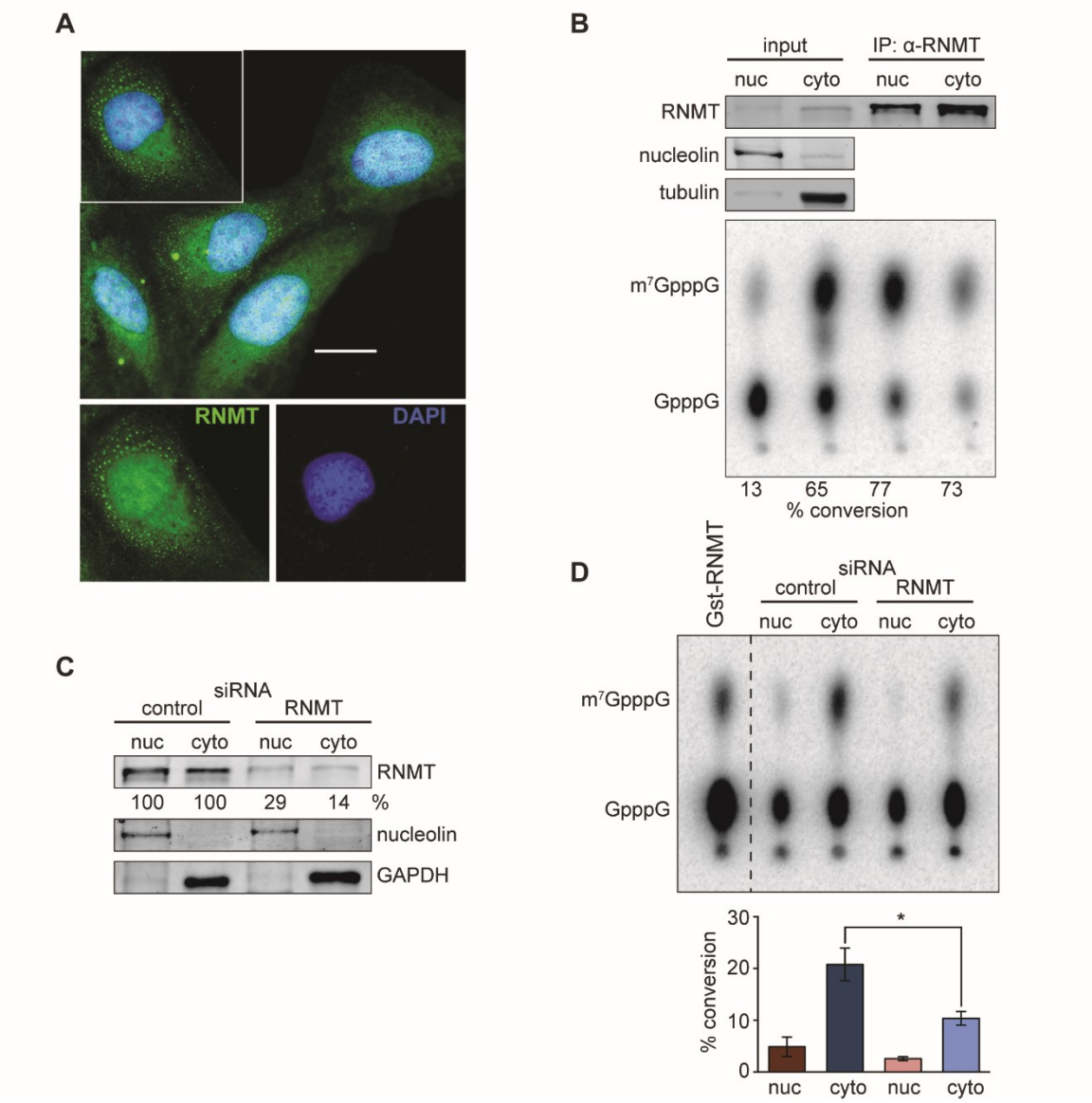

Figure 2. Identification of a cytoplasmic pool of RNMT.

A. U2OS cells were fixed with methanol, stained with rabbit anti-RNMT antibody and DAPI, co-stained with Alexa Fluor 488-labeled anti-rabbit antibody, and imaged with a fluorescence microscope. The scale bar indicates 15 μm. B. HEK293 cells were fractionated into nuclear and cytoplasmic extracts. These were analyzed directly by Western blotting (lanes 1 and 2) or recovered by immunoprecipitation with rabbit anti-

RNMT prior to Western blotting (lanes 3 and 4). The same extracts were analyzed by cap methyltransferase activity assay, in which equal mass amounts of extract were incubated with S-adenosylmethionine and a 32-nt long [^{32}P]cap-labeled RNA. The reaction products were digested with P1 nuclease prior to separation by PEI cellulose TLC and visualization by phosphorimager. The identity of each P1 digestion product was determined by comparison to known standards run on the same plate. C. U2OS cells were transfected with control or RNMT siRNA, and the extent of knockdown was determined by Western blotting and is shown quantitatively below the gel. D. Cap methyltransferase activity was determined for nuclear and cytoplasmic extracts from control and RNMT knockdown cells. A representative autoradiogram is shown in the upper panel, and the quantified results from 3 independent experiments (mean ± SEM) is shown in the lower panel. The asterisk (∗) indicates $p<0.05$ by ratio paired t-test.

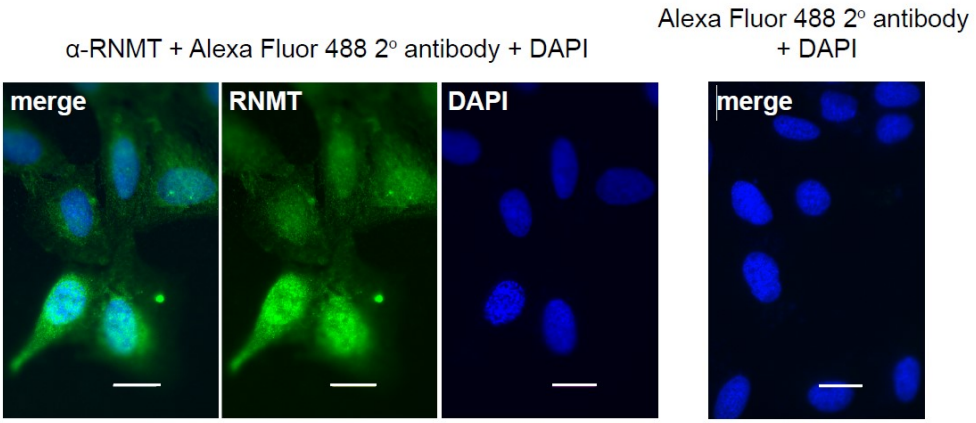

Figure 3. Identification of cytoplasmic RNMT in formaldehyde-fixed cells.

U2OS cells were fixed with formaldehyde and stained with (left panels) or without (right panel) rabbit anti-RNMT antibody, DAPI and Alexa Fluor 488-labeled anti-rabbit antibody. The scale bar indicates 15 μm.

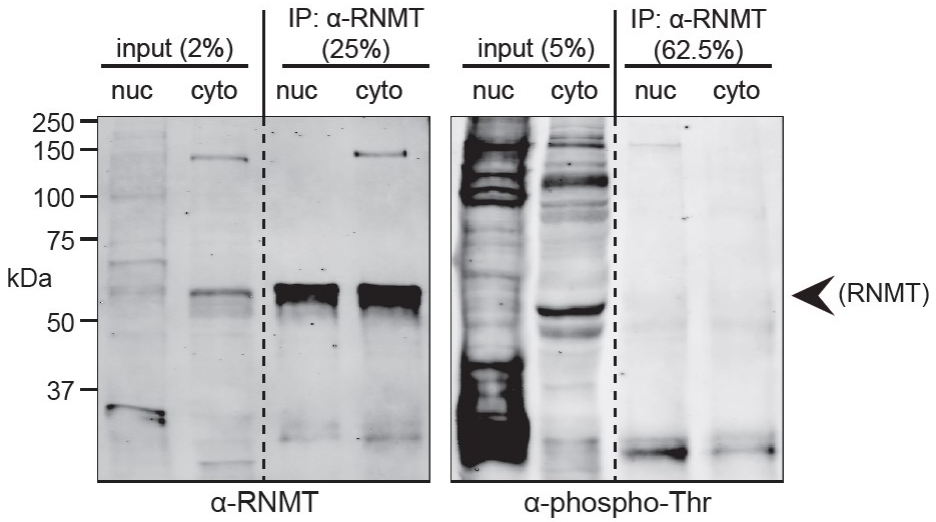

Figure 4. Analysis of RNMT threonine phosphorylation.

Nuclear and cytoplasmic extracts from HEK293 cells were immunoprecipitated with rabbit anti-RNMT antibody. In the left panel 2% of the input and 25% of immunoprecipitated protein was analyzed by Western blotting with anti-RNMT antibody. In the right panel these were analyzed by Western blotting with antiphosphothreonine antibody. The arrow on the right panel indicates the position of RNMT.

RNMT is a Component of the Cytoplasmic Capping Complex

In order to methylate recapped transcripts, RNMT must either be associated with the cytoplasmic capping complex or have some way of targeting these after guanylylation. As a first test, I examined the recovery of endogenous protein with the cytoplasmic capping complex. Gel filtration performed in Mukherjee et al., 2014 showed that the cytoplasmic capping complex eluted just past the void volume of a calibrated

Sephacryl S-200 column. The stored fractions were re-examined by Western blotting with antibodies to RNMT, CE, and Nck1 (Figure 5A). RNMT co-eluted with CE and Nck1, and like CE, was not detected in later fractions. This is consistent with the cytoplasmic pool of RNMT being restricted to the cytoplasmic capping complex. Cap methyltransferase activity tracked with the intensity of Western blot staining for all 3 proteins (Figure 5B), indicating that RNMT associated with the cytoplasmic capping complex is functional. Next, HEK293 cells were transfected with plasmids expressing cytoplasmically restricted CE or a control protein consisting of multiple MS2 stem-loop binding sites, each with a biotinylation tag (bio-cCE or MS2-bio, Mukherjee et al., 2014) (Figure 5C). The selective streptavidin-bead recovery of both Nck1 and RNMT with cCE provided additional evidence for RNMT as a component of the cytoplasmic capping complex.

It was conceivable that RNMT might join the cytoplasmic capping complex by binding to the first SH3 domain or the SH2 domain of Nck1. However, RNMT lacks a proline-rich sequence necessary for SH3 domain binding, and while it does have a potential tyrosine phosphorylation site at Y10 (Aregger and Cowling, 2017), the sequence surrounding this tyrosine residue is incompatible with binding to the SH2 domain of Nck1 (Frese et al., 2006). Additionally, I saw no evidence for tyrosine phosphorylation by Western blotting of immunoprecipitated cytoplasmic RNMT with anti-phosphotyrosine antibody. I therefore sought to determine if RNMT is recruited to the complex through a direct interaction with CE or by binding to some other protein on one of the available domains of Nck1. In nuclear capping, CE and RNMT are brought

together at the phosphorylated C-terminal domain of RNA polymerase II (Chiu et al., 2002). The identification of m^7G-capped tRNA precursors (Ohira and Suzuki, 2016) suggested that CE and RNMT may interact in a manner independent of RNA polymerase II. Direct binding would be the most straightforward explanation, but there are conflicting reports as to whether RNMT and CE interact with one another (Aregger and Cowling, 2013; Pillutla et al., 1998). To examine this, GST-RNMT and His-CE were expressed in *E. coli* (Figure 5D), and these proteins were incubated prior to recovery on glutathione agarose. The recovery of CE with GST-RNMT but not with a GST control (Figure 5E) indicates that RNMT can interact directly with CE.

I next sought to identify the portion of RNMT that mediates its in vivo interaction with the cytoplasmic capping complex using an approach similar to that in Gonatopoulos-Pournatzis et al., 2011 to characterize functional domains of RNMT. Plasmids were generated that express FLAG-tagged forms of the full-length protein, the N-terminal 120 amino acids, and the catalytic C-terminal domain spanning amino acids 121-476. The subcellular distribution of each of these proteins was determined prior to their use in mapping CE-interacting sites (Figure 6**Error! Reference source not found.**). Although RNMT(1-120) was reported to contain several nuclear localization sequences (Shafer et al., 2005), this protein was found predominantly in the cytoplasmic fraction. RNMT(121-476) was both nuclear and cytoplasmic. Each of these plasmids was transfected into HEK293 cells alongside a plasmid expressing bio-CE, and cytoplasmic extracts were recovered on streptavidin beads (Figure 5F). Full-length (FL) RNMT and the portion spanning residues 121-476 were recovered with bio-cCE, but the N-terminal portion

spanning residues 1-120 was not. Thus, residues within the C-terminal methyltransferase domain are responsible for recruitment of RNMT into the cytoplasmic capping complex. Taken together, the results in Figures 1 and 2 show that cells contain a functional cytoplasmic pool of RNMT, that the entirety of cytoplasmic RNMT is associated with the cytoplasmic capping complex, and that it is recruited to the complex by direct binding to CE.

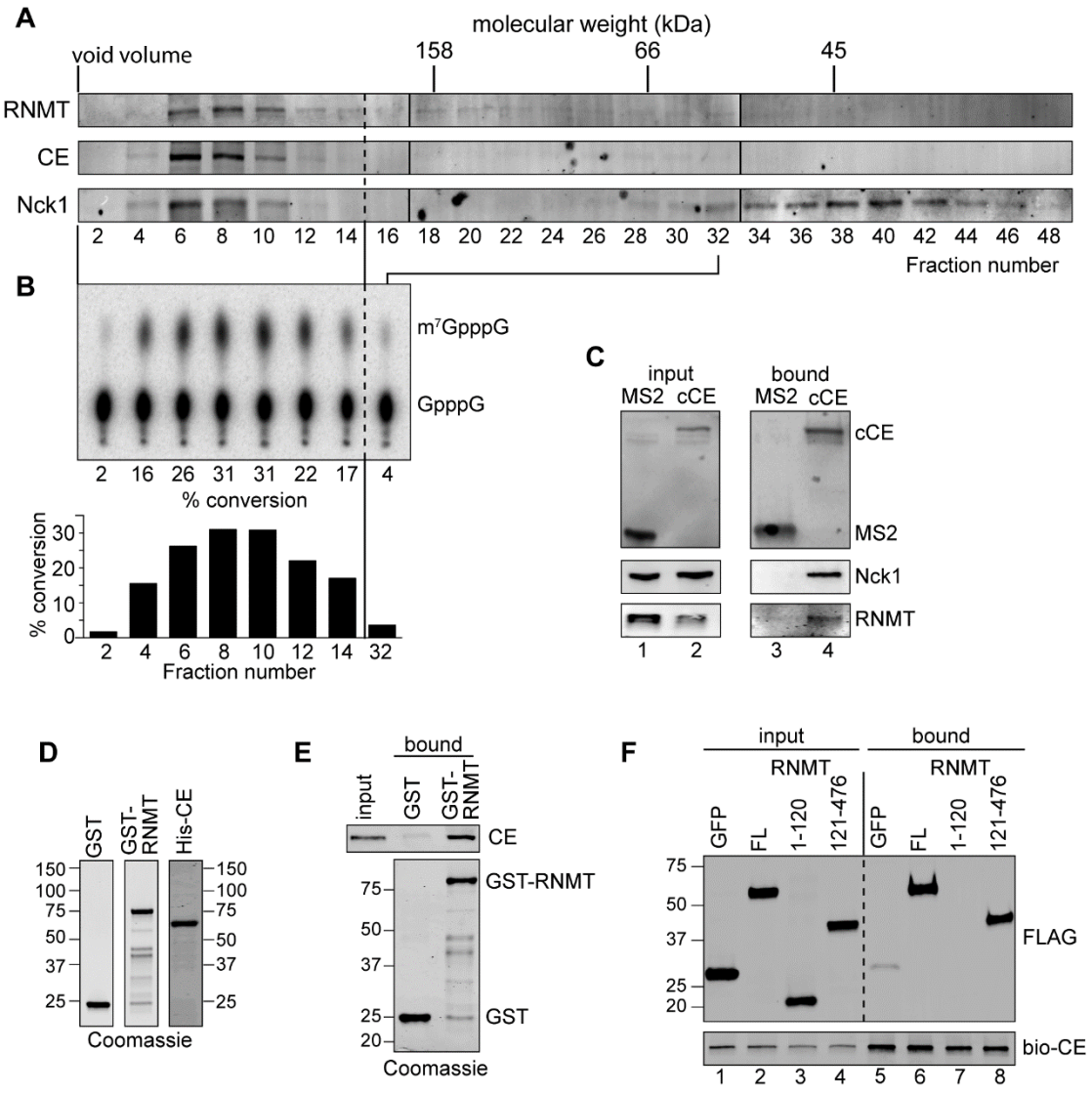

Figure 5. RNMT is a component of the cytoplasmic capping complex and binds to CE through its C-terminal catalytic domain.[3]

A. Stored Sephacryl S-200 column fractions from Mukherjee et al., 2014 were analyzed by Western blotting for RNMT, CE, and Nck1. B. Fractions 2-14 and fraction 34, which corresponds in size to monomeric RNMT, were analyzed for cap methyltransferase

[3] Figure 5C was generated by Chandrama Mukherjee in the lab of Daniel R. Schoenberg.

activity. The percent conversion of unmethylated to methylated caps is shown graphically beneath the autoradiogram C. HEK293 cells were transfected with plasmids expressing two MS2 binding domains or a cytoplasmically-restricted form of CE, each of which is coupled to a biotinylation tag (Mukherjee et al., 2014). Cytoplasmic extracts were recovered on streptavidin beads, and the input (lanes 1 and 2) and bound (lanes 3 and 4) samples were analyzed by Western blotting with streptavidin (upper panels) or antibodies to Nck1 and RNMT (lower panels). D. GST, GST-RNMT, and His-CE were expressed in *E. coli*, purified on glutathione-Sepharose or cobalt-agarose beads as appropriate, and analyzed by SDS-PAGE. Shown are Coomassie Blue stained gels of purified proteins. E. Mixtures containing 1 μg His-CE and 5 μg GST or GST-RNMT were prepared for subsequent GST pulldown assay. Because His-CE runs at the same size as GST-RNMT, its recovery was monitored by Western blotting with anti-CE antibody. This is shown in the upper panel, where 2% of input and 90% of bound protein was analyzed for CE recovery with GST-RNMT. The lower panel is a Coomassie-stained gel containing 10% of bead-bound protein. F. HEK293 cells were co-transfected with plasmids expressing CE with an N-terminal biotinylation tag (bio-CE) and FLAG-GFP (lanes 1 and 5) or FLAG-tagged forms of full-length RNMT (FL, lanes 2 and 6), the N-terminal portion of RNMT (1-120, lanes 3 and 7), or the C-terminal portion of RNMT (121-476, lanes 4 and 8). Cytoplasmic extracts recovered on streptavidin beads were analyzed by Western blotting with an anti-FLAG antibody and streptavidin.

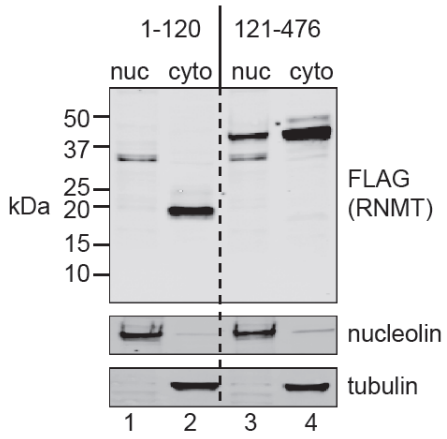

Figure 6. Subcellular distribution of RNMT(1-120) and RNMT(121-476). Nuclear and cytoplasmic extracts were prepared from HEK293 cells transfected with plasmids expressing FLAG-RNMT(1-120) or FLAG-RNMT(121-476). These were examined by Western blotting with anti-FLAG antibody to determine the subcellular distribution of each portion of RNMT. The same samples were examined by Western blotting for nucleolin and tubulin as controls for the effectiveness of subcellular fractionation.

Proximity-Dependent Biotinylation Identifies RNMT and RAM as Constituents of the Cytoplasmic Capping Complex

Proximity-dependent biotinylation (BioID) is a powerful tool for in vivo detection of proteins that are juxtaposed within a larger complex (Roux et al., 2012). Importantly, it reduces the possibility of scoring non-specific interactions that can occur during cell fractionation and allows for identification of transient in vivo interactions that may be lost during traditional pulldown methods. BirA* and Myc tags were added to the N-

terminus of a form of CE that is restricted to the cytoplasm due to loss of its NLS and addition of the HIV Rev NES (BirA*-cCE) (Otsuka et al., 2009). A parallel construct expressing Myc-tagged BirA* without CE was used as a control for nonspecific biotinylation. Plasmids expressing each of these proteins and FLAG-RNMT were transfected into HEK293 cells and cultured for 14 hr in medium containing 0, 5, or 25 μM biotin. Cytoplasmic extracts recovered on streptavidin beads were then analyzed by Western blotting.

Cytoplasmic BirA* and BirA*-cCE were expressed regardless of biotin supplementation (Figure 7A, upper left panel), and their recovery on streptavidin beads shows each of these was biotinylated only when the cells were supplemented with biotin (Figure 7A, upper right panel). The recovery of Nck1 from cells expressing BirA*-cCE but not BirA* (compare lanes 8 and 9 with lanes 11 and 12) confirmed the utility of BioID for identifying components of the cytoplasmic capping complex, and the selective recovery of RNMT confirmed its identification as a component of the cytoplasmic capping complex. In addition, the absence of GAPDH confirmed the specific biotin labeling of proteins in the cytoplasmic capping complex. RNMT functions as a heterodimer with a 118 amino acid protein termed RNMT-activating miniprotein (RAM) (Gonatopoulos-Pournatzis et al., 2011). RAM was present in the input cytoplasmic extract and, like Nck1 and RNMT, was selectively recovered with BirA*-cCE.

The preceding results do not indicate if RNMT and RAM were biotinylated by BirA*-cCE or if their recovery was secondary to their interaction with proteins of the cytoplasmic capping complex. To address this, RNMT was recovered from the same

extracts by anti-FLAG immunoprecipitation, and biotinylated proteins were visualized by streptavidin Western blot (Figure 7B). The recovery of RAM with RNMT confirmed that these proteins interact with each other in the cytoplasm. Streptavidin Western blotting showed RNMT was biotinylated by BirA*-cCE, but RAM was not. This could be do either to RAM being too far away from the BirA* moiety to be biotinylated or by its sequestration by RNMT. FLAG-RNMT also recovered a 30 kDa protein (solid dot) whose biotinylation by BirA*-cCE identified this as an unknown constituent of the cytoplasmic capping complex that may contribute to cap methylation.

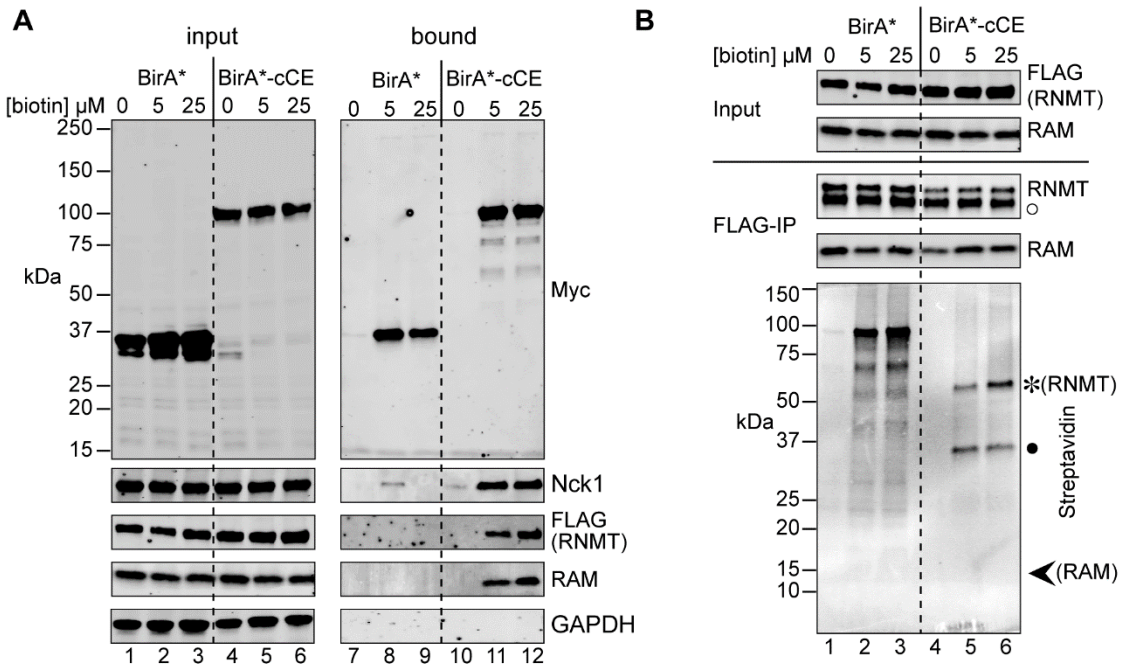

Figure 7. Proximity-dependent biotinylation identifies RNMT and RAM as components of the cytoplasmic capping complex.[4]

A. HEK293 cells were co-transfected with plasmids expressing Myc-tagged BirA* or BirA*-cCE together with FLAG-RNMT. Cells were cultured in medium containing 0, 5, or 25 µM biotin, and cytoplasmic extracts recovered on streptavidin beads were analyzed by Western blotting with antibodies to Myc (BirA* and BirA*-cCE), FLAG (RNMT), Nck1, RAM, and GAPDH. B. The cytoplasmic extracts from A were immunoprecipitated with anti-FLAG antibody. For comparison, the input samples from A are reproduced at the top of B. Western blotting with anti-RNMT and anti-RAM confirmed their recovery with anti-FLAG immunoprecipitation. The open circle (○) in the RNMT Western blot indicates IgG heavy chain. Biotinylated proteins recovered with anti-FLAG

[4]Figure 7 was generated by Andrew J. Giltmier in the lab of Daniel R. Schoenberg.

immunoprecipitation were identified by Western blotting with streptavidin. RNMT is indicated with an asterisk (∗), and an unknown 30-kDa protein is indicated with a filled circle (●).

Cytoplasmic RNMT is a Heterodimer with RAM

The identification of RAM in the cytoplasmic capping complex suggested this RNMT cofactor might also be required for optimal cytoplasmic cap methyltransferase activity. Immunofluorescence confirmed the nuclear localization of RAM but also showed that RAM is in the cytoplasm and has perinuclear staining similar to that of RNMT (Figure 8A). There was also evidence for punctate cytoplasmic staining in some cells, but this was less apparent than that for CE or RNMT. These results were complemented by Western blot analysis of nuclear and cytoplasmic extracts of U2OS and HEK293 cells (Figure 8B). To determine if cytoplasmic RNMT is a heterodimer with RAM, nuclear and cytoplasmic extracts were immunoprecipitated with anti-RNMT antibody and probed for RAM (Figure 8C). The indistinguishable recovery of RAM from both fractions is consistent with the existence of cytoplasmic RNMT as a heterodimer with RAM. In Gonatopoulos-Pournatzis et al., 2011, RAM knockdown suppressed cap methyltransferase activity present in whole-cell extracts. The experiment in Figure 8D and E compared cap methyltransferase activity in nuclear and cytoplasmic extracts of cells that were transfected with control or RAM siRNAs. RAM knockdown reduced the level of nuclear and cytoplasmic RAM to 18% and 30%, respectively (Figure 8D), and

the impact on nuclear and cytoplasmic cap methyltransferase activity (Figure 8E) was almost identical to that seen with RNMT knockdown in Figure 2D. In agreement with results in Gonatopoulos-Pournatzis et al., 2011, I also noted that RAM knockdown reduced the level of nuclear RNMT but had little impact on cytoplasmic RNMT. The reason for this difference is not known, but it may relate to differences in the complexes in which they reside.

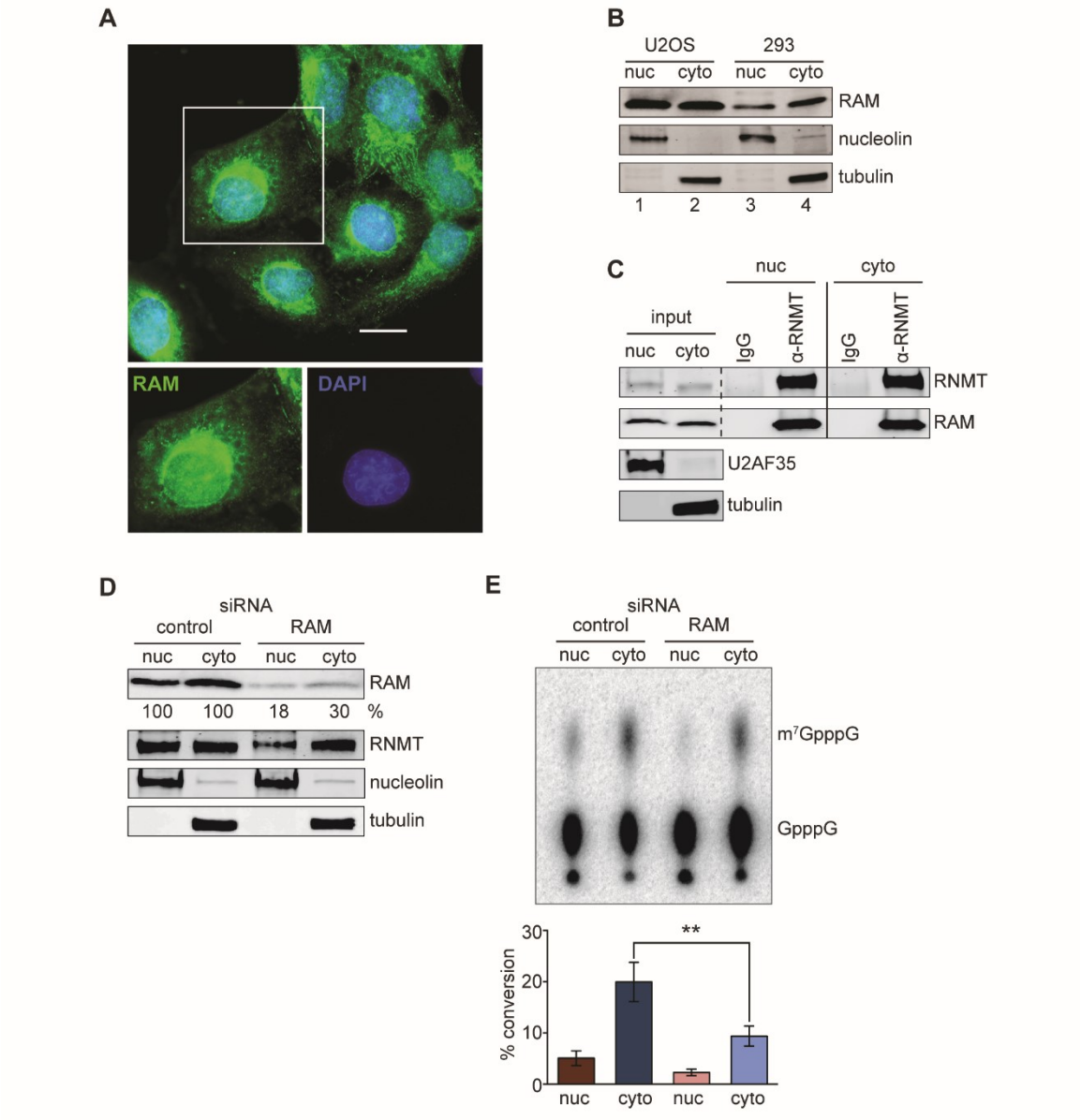

Figure 8. Identification of RAM as a cofactor that activates cytoplasmic RNMT.

A. U2OS cells were prepared and imaged as in Figure 2A, except that rabbit anti-RAM antibody was used for staining. The scale bar indicates 10 μm. B. Cytoplasmic and nuclear extracts from U2OS and HEK293 cells were examined for the presence of RAM by Western blotting with rabbit anti-RAM antibody. Nucleolin and tubulin were also

examined as controls for cross contamination between nuclear and cytoplasmic extracts. C. Nuclear and cytoplasmic extracts of U2OS cells were immunoprecipitated with control IgG or anti-RNMT antibody and analyzed by Western blotting for recovery of RAM and RNMT. The input samples were also probed for tubulin and U2AF35 as controls for cross contamination. D. U2OS cells were transfected with control or RAM siRNAs and separated into nuclear and cytoplasmic fractions. The effectiveness of knockdown was determined by Western blotting with anti-RAM antibody, and quantified results are shown beneath the upper panel. The same samples were also analyzed by Western blotting for RNMT, nucleolin, and tubulin. E. Cap methyltransferase activity of nuclear and cytoplasmic extracts from cells that were transfected with control or RAM-specific siRNAs was determined as in Figure 1D with the results from 3 independent experiments (mean ± SEM) shown beneath the autoradiogram. The double asterisk (∗∗) indicates $p<0.01$ by ratio paired t-test.

Methylation of Cytoplasmic Capping Targets

Cytoplasmic capping targets were originally identified by the appearance of uncapped transcripts in cells that overexpress a cytoplasmically restricted, inactive form of CE (Mukherjee et al., 2012). A conceptually similar approach was used to determine if the same mRNAs undergo cytoplasmic cap methylation. Interference with cap methylation should result in the appearance of transcripts with an unmethylated guanylate 5′ end whose presence would render these mRNAs susceptible to cap surveillance by one

or more decapping enzymes (Jiao et al., 2013; Song et al., 2010). The corollary to this is that the cytoplasmic capping targets that remain when cap methylation is inhibited should all have m^7G caps.

The development of a selective inhibitor of cytoplasmic cap methylation was based on results in Figure 5F showing that the C-terminal portion of RNMT mediates binding to CE. That portion of RNMT (spanning residues 121-476) also contains the active site and the RAM binding domain, but not the nuclear localization sequences. An inactive form of RNMT was created by changing the aspartic acid at position 203 in the SAM binding site to alanine (Saha et al., 1999). This particular site was chosen because it does not interfere with RAM binding (Figure 9**Error! Reference source not found.**). As in my group's previous work (Otsuka et al., 2009), the addition of the HIV Rev NES resulted in a protein, termed ΔN-RNMT (Figure 10A), that is almost entirely cytoplasmic (Figure 10D).

To be a functional inhibitor of cytoplasmic cap methylation, ΔN-RNMT should be incorporated into the cytoplasmic capping complex and bind to RAM such that the displaced endogenous RNMT is less active. The incorporation of ΔN-RNMT was examined by proximity-dependent biotinylation (Figure 10B) using cells transfected with plasmids expressing ΔN-RNMT and BirA* or BirA*-cCE. The selective biotinylation of ΔN-RNMT by BirA*-cCE but not BirA* alone confirmed the incorporation of this modified protein into the cytoplasmic capping complex. ΔN-RNMT also retains the ability to bind RAM (Figure 9), and I confirmed that ΔN-RNMT overexpression reduces the enzymatic activity of endogenous RNMT in cytoplasmic extracts (Figure 10C). It was

conceivable that ΔN-RNMT overexpression could interfere with nuclear cap methylation by changing the overall subcellular distribution of RAM. This proved not to be the case. In the experiment in Figure 10D, triplicate cultures of U2OS cells were transfected with empty vector or ΔN-RNMT plasmid, together with a plasmid expressing EGFP. ΔN-RNMT had no impact on the levels or nucleocytoplasmic distribution of RAM or of RNMT, thus confirming its impact should be limited to cytoplasmic cap methylation.

Cytoplasmic RNA from the same cells was analyzed by RT-qPCR (Figure 10E) for quantitative changes in 2 control mRNAs (RPLP0 and STRN4) and 6 recapping targets (POLR2B, ZNF207, VDAC3, EXOSC2, MAPK1, and STAT3), each of which accrues uncapped forms when cytoplasmic CE is inhibited. Because ΔN-RNMT does not affect levels of nuclear RNMT or RAM, it should not interfere with nuclear cap methylation of RPLP0 and STRN4, and this indeed was the case. In contrast, ΔN-RNMT expression resulted in a statistically significant decrease in the steady-state levels of POLR2B, ZNF207, and VDAC3 mRNA. The levels of the other target mRNAs also decreased but not to a degree that was statistically significant.

If mRNAs with unmethylated caps were degraded, the remainder should all have m^7G caps. This was examined by their recovery on immobilized eIF4E, which is highly selective for RNAs with properly methylated caps (Niedzwiecka et al., 2002). I reasoned that if the entire population of each remaining transcript has an m^7G cap, ΔN-RNMT expression should have no impact on the eIF4E-based recovery. However, if this population included G-capped transcripts, the amount of each mRNA recovered on eIF4E should be lower for cells expressing ΔN-RNMT compared to vector control. Prior to

binding to eIF4E, each preparation was spiked with G-capped luciferase RNA, and input and bound RNAs were quantified by RT-qPCR. As expected, there was minimal binding of G-capped luciferase RNA (Figure 10F), and eIF4E bound approximately 20% of m^7G-capped EGFP mRNA expressed from the co-transfection control plasmid. While the percent recovery on eIF4E differed for each of the control and target mRNAs, there was no difference in cap status between the two treatment groups, indicating that only mRNAs with m^7G caps remain when cytoplasmic cap methylation is inhibited.

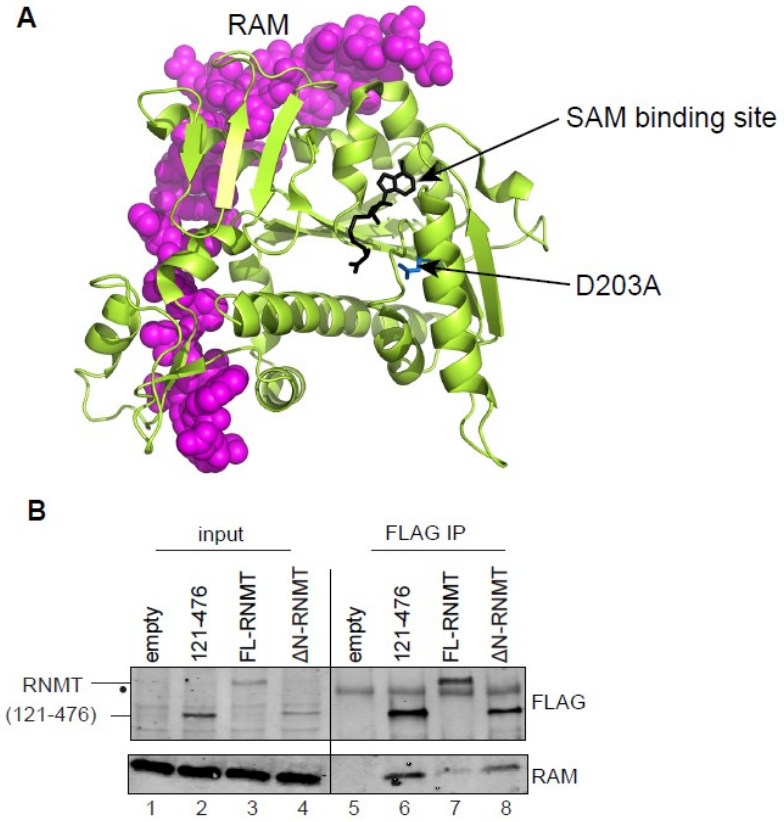

Figure 9. Development of an inhibitor of cytoplasmic cap methylation.

A. A portion of RNMT from Varshney et al., 2016 is shown in green, and RAM is shown in purple. The structure shown is part of the region of RNMT (residues 121-476) that also contains the active site residues and the CE-binding domain. Aspartic acid 203 is highlighted in blue. B. Plasmids were generated that express full-length RNMT (FL-RNMT), RNMT residues 121-476 (121-476) or the same region bearing a D203A mutation and the HIV Rev NES (ΔN-RNMT), each with an N-terminal FLAG tag. To confirm that ΔN-RNMT retains the ability to bind RAM cytoplasmic extracts of transfected cells were immunoprecipitated with anti-FLAG antibody and analyzed by Western blotting with antibodies to FLAG and RAM. The filled circle indicates the

position of IgG heavy chain in the immunoprecipitated material that was detected with the secondary antibody.

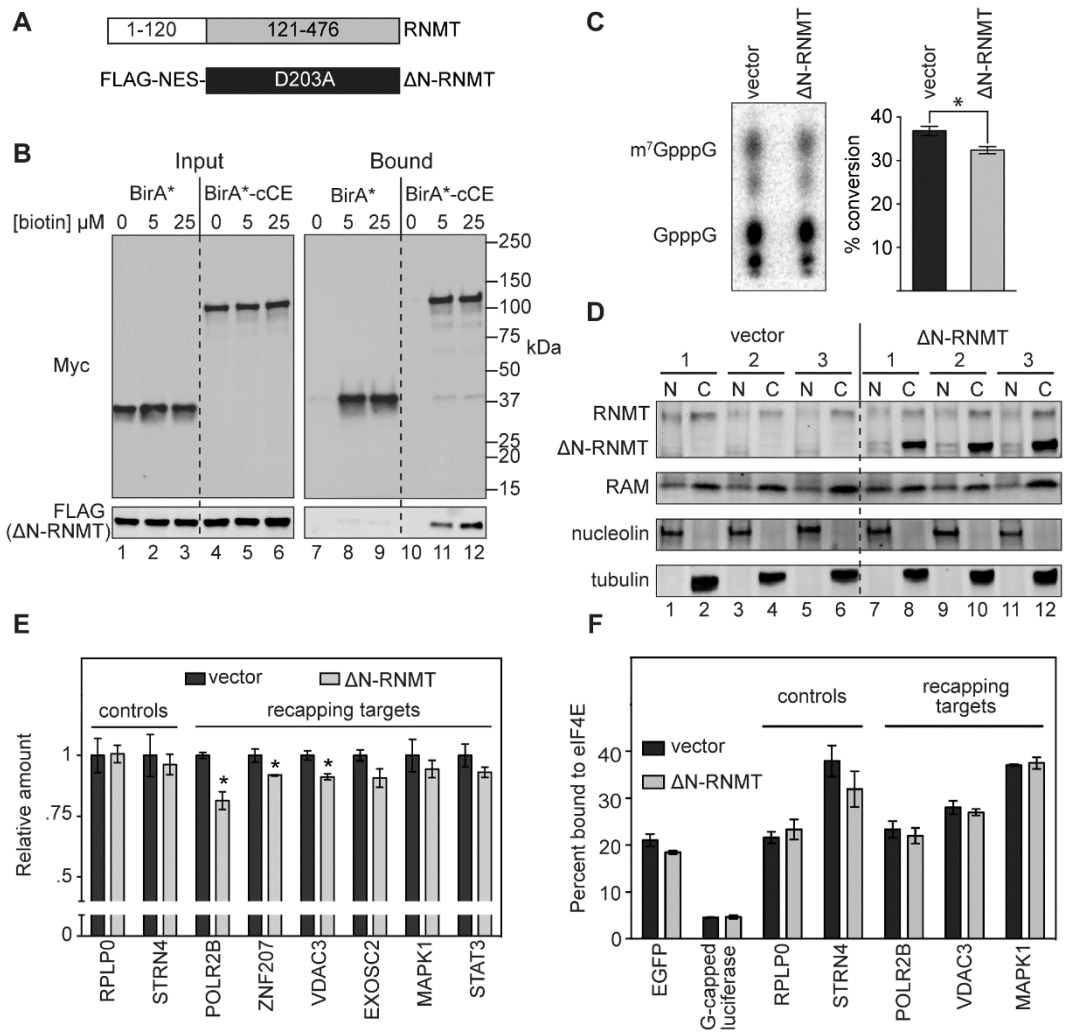

Figure 10. Levels of recapped mRNAs decline when cytoplasmic cap methylation is inhibited.[5]

A. Schematic showing the relationship of ΔN-RNMT to the native protein and the modifications that were made to create this inhibitor of cytoplasmic cap methylation. B. Cells were transfected as in Figure 3A with plasmids expressing FLAG-tagged ΔN-RNMT and Myc-tagged BirA* or BirA*-cCE and cultured with indicated biotin

[5] Figure 10B was generated by Andrew J. Giltmier in the lab of Daniel R. Schoenberg.

concentrations. Cytoplasmic protein recovered on streptavidin beads was analyzed by Western blotting with antibodies to the Myc and FLAG epitopes. C. Cap methyltransferase activity was determined for cytoplasmic extracts of HEK293 cells transfected with an empty vector or a plasmid expressing ΔN-RNMT. A representative autoradiogram is shown in the left panel, and the quantified results from 3 independent experiments (mean ± SEM) is shown in the right panel. The asterisk (*) indicates $p<0.05$ by unpaired two-tailed t-test. D. Triplicate cultures of U2OS cells were co-transfected with a plasmid expressing EGFP and either empty vector or plasmid expressing ΔN-RNMT. Nuclear and cytoplasmic extracts were analyzed by Western blotting with antibodies to RNMT, RAM, nucleolin, and tubulin. E. Cytoplasmic RNA recovered from each of the transfectants in D was analyzed by RT-qPCR for 2 control mRNAs (RPLP0 and STRN4) and 6 of the cytoplasmic capping targets identified in Mukherjee et al., 2012 (POLR2B, ZNF207, VDAC3, EXOSC2, MAPK1, STAT3). Relative abundances were normalized to spiked-in luciferase RNA and to the non-recapping control mRNA BOP1. Shown is the mean ± SEM (n=3). The asterisk (*) indicates $p<0.05$ by unpaired two-tailed t-test. F. The RNAs analyzed in E were spiked with G-capped luciferase RNA and incubated with GST-eIF4E bound magnetic beads. Input and bound RNAs were quantified by RT-qPCR, and the results were plotted as percent bound (normalized to input). Paired measurements were used for the vector control. For each mRNA there was no statistically significant difference in recovery between treatment groups.

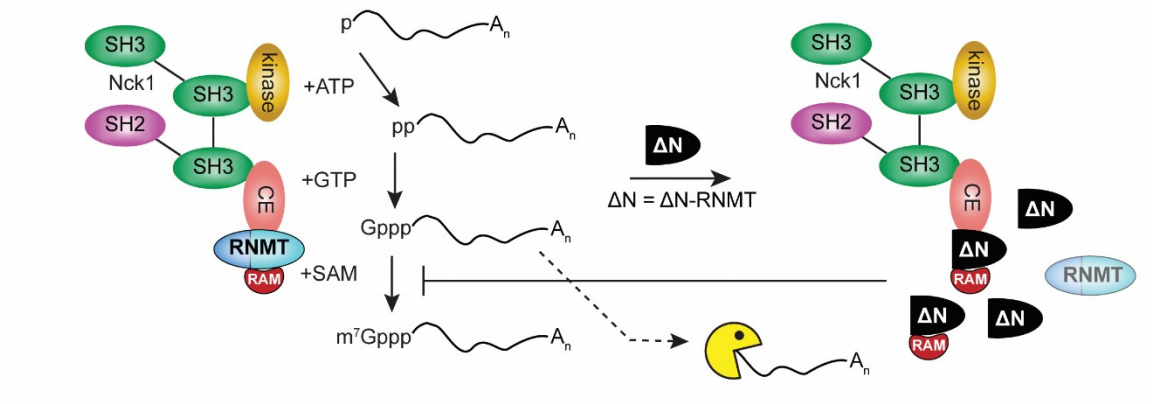

Figure 11. Model for the interaction of RNMT with the cytoplasmic capping complex. The left panel shows the organization of known components of the cytoplasmic capping complex. The 5′-kinase that generates a diphosphate capping substrate binds to the second SH3 domain of Nck1, and CE binds to the third SH3 domain. RNMT:RAM binds directly to CE, with binding mediated by sequences in the C-terminal portion spanning residues 121-476. In the right panel, cytoplasmic cap methylation is inhibited by overexpression of ΔN-RNMT. This displaces endogenous RNMT from the cytoplasmic capping complex and also sequesters cytoplasmic RAM without altering nuclear or cytoplasmic levels of RNMT or RAM.

Discussion

The discovery of cytoplasmic capping grew out of the observation that metastable β-globin decay intermediates have a cap structure that is indistinguishable from the m^7G caps on mRNAs that are capped in the nucleus (Lim and Maquat, 1992; Otsuka et al., 2009). Results in Mukherjee et al., 2012 showed that cytoplasmic capping targets cycle

between capped and uncapped states (cap homeostasis) and that recapping serves to maintain the stability of a portion of these targets and the translatability of another portion. Because cytoplasmic capping targets are polyadenylated (Kiss et al., 2016), recapping is all that is necessary to restore these uncapped transcripts from a non-translating state to a translating state. Three sequential reactions are needed for cytoplasmic capping: conversion of a 5′-monophosphate end of a decapped RNA to a 5′-diphosphate, addition of GMP, and methylation to generate the m^7G cap structure. The first two reactions are carried out by a 5′-monophosphate kinase and CE that are brought together in a single complex by binding to the second and third SH3 domains, respectively, of the cytoplasmic adapter protein Nck1 (Mukherjee et al., 2014). Here I identify RNMT as the third enzyme of the cytoplasmic capping metabolon.

RNMT heterodimerizes with RAM, and both were originally classified as nuclear proteins. Initial evidence for a cytoplasmic pool of RNMT was described in Otsuka et al., 2009, but because RNMT did not co-sediment with CE, it was not examined further. Structural studies in Varshney et al., 2016 showing that RNMT:RAM is specific for unmethylated caps led me to revisit cytoplasmic RNMT, and results in Figure 2 confirmed the existence of a cytoplasmic pool. Furthermore, the loss of nuclear and cytoplasmic cap methyltransferase activity following RNMT knockdown confirmed its identity as the major, if not only, cap methyltransferase in the cell. While it was conceivable that the cytoplasmic pool of RNMT (and RAM) results from loss of the nuclear envelope during mitosis, their cytoplasmic immunofluorescence staining in non-dividing cells and cytoplasmic abundance by subcellular fractionation suggest otherwise.

Evidence for RNMT as a component of the cytoplasmic capping complex was provided by co-precipitation experiments (Figure 5C and E) and by the gel filtration experiment in Figure 5A where RNMT, CE, and Nck1 eluted as a single entity. The fact that neither CE nor RNMT was present in later fractions suggests the entirety of their cytoplasmic populations is present in this complex. This was reinforced by the elution of cap methyltransferase activity in the same fractions as CE and Nck1 (Figure 5B) but not in a later fraction corresponding to the size of monomeric RNMT. Additional support for cytoplasmic cap methylation came from the identification of a cytoplasmic pool of RAM. RAM is a cofactor that dramatically stimulates cap methyltransferase activity (Gonatopoulos-Pournatzis et al., 2011). Initial evidence for the presence of RAM in the cytoplasmic capping complex came from proximity-dependent biotinylation with BirA*-tagged cCE (Figure 7). In this experiment, RNMT was biotinylated, but RAM was not, suggesting that RAM is either sequestered by RNMT or is sufficiently far from the BirA* moiety that it was not biotinylated. The existence of cytoplasmic RAM was confirmed by immunofluorescence (Figure 8A), biochemical fractionation (Figure 8B), and recovery with cytoplasmic RNMT (Figure 8C). Importantly, the impact of RAM knockdown was almost identical to that of RNMT knockdown (compare Figure 2D and Figure 8E), thus confirming both its presence in the cytoplasm and its obligate role in cytoplasmic cap methylation.

The left panel of Figure 11 shows a model of our current understanding of the organization of the cytoplasmic capping complex, with the 5′ kinase and CE bound to adjacent SH3 domains of Nck1. RNMT lacks a proline-rich sequence needed for binding

to Nck1, and my inability to visualize any interaction between these proteins ruled out the first SH3 domain as the RNMT binding site. Although PhosphoSite (Hornbeck et al., 2004) identified 3 tyrosine phosphorylation sites on RNMT, none of these matched the sequence needed for binding to the SH2 domain of Nck1 (Frese et al., 2006), and I saw no evidence for tyrosine phosphorylation of RNMT by Western blotting of immunoprecipitated protein with anti-phosphotyrosine antibodies. This suggested RNMT was recruited by direct interaction with CE or some other protein. An earlier report described evidence for a direct interaction between CE and RNMT (Pillutla et al., 1998), and this was confirmed with purified recombinant proteins (Figure 5E). RNMT has been operationally divided into two domains spanning amino acids 1-120 and 121-476 (Saha et al., 1999). RNMT(1-120) has several nuclear localization sequences and mediates the recruitment of RNMT to transcription initiation sites (Aregger and Cowling, 2013). RNMT(121-476) contains the active site and RAM-binding residues (Varshney et al., 2016). This latter domain mediates RNMT binding to CE (Figure 5F), and a direct association between these proteins is consistent with 5′ end capping of pre-tRNAs (Ohira and Suzuki, 2016).

Cells have surveillance mechanisms that degrade improperly capped transcripts (Grudzien-Nogalska and Kiledjian, 2017), and despite repeated attempts I was never able to detect unmethylated, G-capped forms of cytoplasmic capping targets. This contrasted with my ability to detect uncapped forms of the same mRNAs (Mukherjee et al., 2012). I used the loss of improperly capped target mRNAs as in vivo evidence for cytoplasmic cap methylation. As noted above, the portion of residues spanning 121-476 contains the

active site and RAM binding domain and mediates RNMT binding to CE. Mutating a single amino acid (D203A) in the SAM binding site and adding the HIV Rev NES generated an inactive protein (ΔN-RNMT) that is restricted to the cytoplasm but still able to bind RAM and be incorporated into the cytoplasmic capping complex. Overexpressed ΔN-RNMT competes with endogenous RNMT for binding to the cytoplasmic capping complex (Figure 10B, Figure 11, right panel) and to RAM (Figure 9B), reducing the overall cap methylation activity in the cytoplasm (Figure 10C). Importantly, ΔN-RNMT has no impact on nuclear RNMT or RAM (Figure 10D). Consistent with cellular surveillance for improperly capped transcripts, ΔN-RNMT reduced the steady-state level of each of 6 recapping targets but had no effect on 2 control mRNAs that are not subject to cytoplasmic recapping (Figure 10E). Although the degrees of loss were modest, they are consistent with results in Mukherjee et al., 2012 showing only a subfraction of any given recapping target is subject to cap homeostasis. The selective loss of improperly capped transcripts was confirmed by binding onto eIF4E, which is highly selective for methylated versus unmethylated caps (Niedzwiecka et al., 2002) (Figure 10F). This approach would have shown a difference in recovery between treatment groups if RNA from ΔN-RNMT-expressing cells contained transcripts with improperly methylated caps. The fact that no such difference was observed (Figure 10F) confirmed that the reduction in recapping targets was due to loss of unmethylated transcripts as a consequence of ΔN-RNMT inhibition of cytoplasmic cap methylation.

This observation has implications for regulation. Phosphorylation of RAM leads to its ubiquitination and degradation by the proteasome and an overall decrease in cellular

cap methyltransferase activity (Grasso et al., 2016). At this point in time it is unclear whether a similar process also applies to the cytoplasmic pool, but one can envision how loss of cytoplasmic RAM could result in downregulation of a portion of cytoplasmic capping targets. This also has implications for proteome complexity. Most of the cytoplasmic capping targets identified in Mukherjee et al., 2012 have downstream CAGE tags, and my lab showed in (Kiss et al., 2015b) that recapped ends map to the vicinity of these. These mRNAs also have a statistically higher representation of downstream in-frame start codons, and altering cytoplasmic cap methylation has the potential to affect production of N-terminally truncated proteins from recapped mRNAs.

Acknowledgments

I wish to thank Juan Alfonzo and members of the Schoenberg lab for their input and helpful comments.

Funding

This work was supported by the National Institutes of Health grant (GM084177 to D.R.S.). J.B.T. was supported by a training grant from the National Institutes of Health (GM08512) and a predoctoral fellowship from The Ohio State University Center for RNA Biology. C.M. was supported by an American Heart Association postdoctoral fellowship (13POST172700021). A.J.G. was supported by a Pelotonia undergraduate fellowship from the Ohio State University Comprehensive Cancer Center. The content is solely the responsibility of the authors and does not necessarily represent the official

views of Pelotonia, The Ohio State University, the American Heart Association, or the National Institutes of Health.

Chapter 3. RNA Cap Methyltransferase Activity Assay[6] [7]

Abstract

Methyltransferases that methylate the guanine-N7 position of the mRNA 5′ cap structure are ubiquitous among eukaryotes and commonly encoded by viruses. Here I provide a detailed protocol for the biochemical analysis of RNA cap methyltransferase activity of biological samples. This assay involves incubation of cap-methyltransferase-containing samples with a [^{32}P]G-capped RNA substrate and S-adenosylmethionine (SAM) to produce RNAs with N7-methylated caps. The extent of cap methylation is then determined by P1 nuclease digestion, thin-layer chromatography (TLC), and phosphorimaging. The protocol described here includes additional steps for generating the [^{32}P]G-capped RNA substrate and for preparing nuclear and cytoplasmic extracts from mammalian cells. This assay is also applicable to analyzing the cap methyltransferase activity of other biological samples, including recombinant protein preparations and fractions from analytical separations and immunoprecipitation/pulldown experiments.

[6] This chapter has benefitted from the writing and editing contributions of both authors: Jackson B. Trotman[a,b,c] and Daniel R. Schoenberg[a,c] ([a]Center for RNA Biology, [b]Ohio State Biochemistry Program, [c]Department of Biological Chemistry and Pharmacology, The Ohio State University, Columbus, Ohio).

[7] This chapter is modified from an original publication in *Bio-protocol* (Trotman and Schoenberg, 2018) and is used here in accordance with the journal's license-to-publish agreement.

Keywords: RNA, 5′ cap, Cap methyltransferase, RNMT, Enzyme activity assay, Subcellular fractionation, P1 nuclease, Thin-layer chromatography

Background

The N7-methylguanosine cap at the 5′ end of an mRNA is a modification essential for proper eukaryotic mRNA processing, localization, and translation. The N7 methyl group is particularly critical for the mRNA life cycle, as it drastically increases the binding affinity of cap-binding proteins (Niedzwiecka et al., 2002) and protects mRNAs from cap-quality control surveillance mechanisms (Jiao et al., 2013). I recently reported that the mammalian RNA guanine-7 methyltransferase (RNMT) functions beyond its canonical role in nuclear co-transcriptional cap synthesis to participate in cytoplasmic RNA recapping (Trotman et al., 2017). I used the protocol presented here to demonstrate that the cap methyltransferase activity of cytoplasmic RNMT is unexpectedly robust relative to nuclear RNMT. Additionally, siRNA-mediated knockdown of RNMT greatly reduced the cap methyltransferase activity of cytoplasmic extracts, suggesting that RNMT is the predominant, if not only cap methyltransferase in the cytoplasm of mammalian cells. Nuclear RNMT exists as a heterodimer with RNMT-activating miniprotein (RAM, Gonatopoulos-Pournatzis et al., 2011), and I demonstrated that cytoplasmic RNMT also binds to RAM. Reduced cytoplasmic cap methyltransferase activity upon RAM knockdown indicated that RAM is a required cofactor for cytoplasmic RNMT.

This protocol is adapted from two earlier publications characterizing human RNMT (Cowling, 2010b; Pillutla et al., 1998), with modifications that standardize generation of the substrate RNA, avoid cumbersome phenol-chloroform extractions with radioactive samples, and enable quantification of cap methyltransferase activity. I note that an alternative, nonradioactive assay has been reported for the analysis of cap methyltransferase reactions (Peyrane et al., 2007), but this method requires HPLC instrumentation that may not be available to all labs and may differ from the one presently reported in terms of sensitivity and sample compatibility. Additionally, a fluorescent assay for measuring cap methyltransferase activity was recently described (Aouadi et al., 2017), but this assay indirectly measures activity by monitoring the accumulation of S-adenosylhomocysteine (SAH) and may be incompatible with biological samples containing SAH. I hope that the level of detail in the protocol presented here enables future investigators to easily repeat and build upon my work.

Materials and Reagents

1. 10 cm or 15 cm culture dishes (*e.g.*, Alkali Scientific, catalog numbers: TD0100, TD0150)
2. Cell lifters (*e.g.*, GeneMate, catalog number: T-2443-4)
3. Sterile, RNase-free tips for P10, P20, P100, and P1000 pipets
4. 1.7 ml plastic, sterile, RNase-free microcentrifuge tubes (*e.g.*, GeneMate, catalog number: C-3262-1)
5. 0.2 ml PCR tubes (*e.g.*, GeneMate, catalog number: T-3225-1)

6. Plastic, disposable cuvettes for Bradford assay
7. NucAway spin columns (Thermo Fisher, catalog number: AM10070)
8. Plastic wrap (*e.g.*, Saran or Stretch-Tite brand)
9. Paper lab tape
10. Polyethylenimine (PEI) cellulose TLC plates (Macherey-Nagel, catalog number: 801053; see Note 2)
11. U2OS cells (ATCC, catalog number: HTB-96) or HEK293 cells (ATCC, catalog number: CRL-1573)
12. RNase-free water (*e.g.*, from a Millipore Synergy water purification system, 18.2 MΩ.cm)
13. McCoy's 5A medium (for U2OS cells; ThermoFisher, catalog number: 16600082)
14. Dulbecco's modified Eagle medium (DMEM; for HEK293 cells; ThermoFisher, catalog number: 21013024)
15. Fetal bovine serum (FBS; Atlanta Biologicals, catalog number: S10350)
16. Single-stranded DNA sense oligo

    5′

    CATGCAAATTAACCCTCACTAAA**GGGAGA**CCGGAATTCGAGCTCGCCC GGGGATC 3′ for T3 transcription template, resuspended in RNase-free water to 100 μM (*e.g.*, synthesized by Integrated DNA Technologies (IDT); underlined is T3 promoter sequence, bold sequence matches the transcribed 32-nucleotide (nt) pppRNA)
17. Single-stranded DNA antisense oligo

5′

GATCCCCGGGCGAGCTCGAATTCCGGTCTCCCTTTAGTGAGGGTTAATTTG

CATG 3′ for T3 transcription template, resuspended in RNase-free water to 100 μM (*e.g.*, synthesized by IDT)

18. MEGAscript T3 Transcription Kit (Ambion, catalog number: 1138)
19. SYBR Gold Nucleic Acid Gel Stain (Thermo Fisher, catalog number: S11494)
20. 40 U/μl RNaseOUT Recombinant Ribonuclease Inhibitor (Thermo Fisher, catalog number: 10777019)
21. Recombinant triphosphatase-guanylyltransferase capping enzyme (see Note 1)
22. [α-^{32}P]GTP (3,000 Ci/mmol, PerkinElmer, catalog number: BLU506H250UC)
23. RNA Clean & Concentrator-5 kit (Zymo Research, catalog number: R1016)
24. ScintiSafe Econo 1 scintillation fluid (Fisher Scientific, catalog number: SX20-5)
25. 1 M dithiothreitol (DTT)
26. 20 mM DTT
27. 100 mM phenylmethylsulfonyl fluoride (PMSF) in isopropanol
28. Protease inhibitor cocktail (Sigma, catalog number: P8340)
29. Phosphatase inhibitor cocktail 2 (Sigma, catalog number: P5726)
30. Phosphatase inhibitor cocktail 3 (Sigma, catalog number: P0044)
31. Phosphate-buffered saline (PBS; *e.g.*, Thermo Fisher, catalog number: 10010049)
32. Bio-Rad Protein Assay Dye Reagent Concentrate (Bio-Rad, catalog number: 5000006)

33. Bovine serum albumin (BSA; *e.g.*, Fisher, catalog number: BP1600-100) dissolved in water to 1 µg/µl
34. 32 mM S-adenosylmethionine (SAM; NEB, catalog number: B9003)
35. 1 µM SAM
36. 500 mM sodium acetate, pH 5.2
37. P1 nuclease (US Biological, catalog number: N7000), resuspended in RNase-free water to 0.625 U/µl
38. Cap analog GpppG (NEB, catalog number: S1407), resuspended in RNase-free water to 10 mM
39. Cap analog m^7GpppG (NEB, catalog number: S1404), resuspended in RNase-free water to 10 mM
40. 0.4 M ammonium sulfate
41. 1 M Tris-HCl, pH 7.5 (*e.g.*, Amresco, catalog number: E691)
42. 5 M sodium chloride (NaCl)
43. 1 M magnesium chloride ($MgCl_2$)
44. 500 mM ethylenediaminetetraacetic acid, pH 8.0 (EDTA; *e.g.*, Thermo Fisher, catalog number: 15575020)
45. Glycerol
46. 80% (v/v) glycerol in water
47. 1 M HEPES pH 7.3 (*e.g.*, Amresco, catalog number: J848)
48. 1 M potassium chloride (KCl)
49. IGEPAL CA-630 (Sigma, catalog number: I8896)

50. 10% IGEPAL CA-630 (v/v) in water
51. 10x annealing buffer (see Recipes)
52. 4x capping buffer (see Recipes)
53. YO Lysis Buffer (see Recipes)
54. YO Buffer A (see Recipes)
55. 10x cap methylation buffer (see Recipes)

Equipment

1. Ruler
2. Scissors
3. Forceps
4. P10, P20, P100, and P1000 pipets
5. Thermal cycler (*e.g.*, MJ Research, model: PTC-200)
6. Nanodrop spectrophotometer (Thermo Fisher Scientific, model: NanoDrop™ 1000, catalog number: ND-1000)
7. Heating block (*e.g.*, Bioer, model: MB-101)
8. -80 °C freezer
9. Handheld 254 nm UV light (*e.g.*, UVP, model: 95-0016-14)
10. Liquid scintillation counter (*e.g.*, Beckman Coulter, model: LS 6000IC)
11. Water-jacketed incubator (*e.g.*, Thermo Fisher Forma Series II) set to 37 °C with 5% CO_2
12. Refrigerated centrifuge (Eppendorf, model: 5415R)

13. Programmable rotator-mixer (Grant-Bio, model: PTR-30) at 4 °C and set to 10 rpm orbital rotation
14. UV-vis spectrophotometer (*e.g.*, Beckman, model: DU 640) set to 595 nm
15. Rectangular glass TLC chamber (*e.g.*, Miles Scientific, model: A70-22, formerly Analtech)
16. Storage phosphor screen (*e.g.*, GE/Amersham Biosciences)
17. Light eraser for storage phosphor screen (*e.g.*, Molecular Dynamics Image Eraser)
18. Typhoon imaging system (*e.g.*, GE/Amersham Biosciences, model: 9200)

Procedure

A schematic overview of this protocol is presented in Figure 12. In short, an *in-vitro*-transcribed short RNA is capped using [α-^{32}P]GTP to generate a Gp*ppRNA substrate, with the radiolabeled phosphate indicated by an asterisk. This GpppRNA substrate is briefly incubated with nuclear or cytoplasmic extracts (or other biological samples) and SAM. Different levels of cap methyltransferase activity in each extract will result in differential methylation of the GpppRNA substrate to produce m^{7}GpppRNA. The mixtures of GpppRNA and m^{7}GpppRNA are then digested to individual nucleotides with P1 nuclease, leaving intact the radiolabeled cap dinucleotide structures that are finally analyzed by TLC and phosphorimaging.

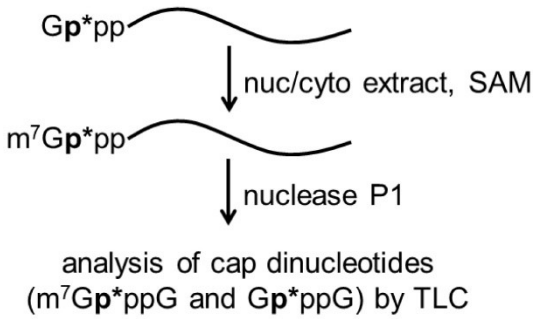

Figure 12. Schematic overview of cap methyltransferase activity assay.

A. Preparation of GpppRNA substrate for cap methyltransferase activity assay (see Note 3)

1. Prepare a 30 µl mixture in a 0.2 ml PCR tube by combining the following: 15 µl RNase-free water, 3 µl 10x annealing buffer (see Recipes), 6 µl 100 µM ssDNA sense oligo, 6 µl 100 µM ssDNA antisense oligo.
2. To denature and then slowly anneal the two oligos to create the dsDNA template for T3 transcription, place the mixture on a thermal cycler at 98 °C for 2 min, followed by 60 1 min steps, each 1.3 °C cooler than the previous step (the final step will be at 20 °C). Transfer this tube of dsDNA onto ice, and in a separate tube, prepare a 1 µM (1 pmol/µl) working stock by diluting it 20-fold with RNase-free water.
3. Using the MEGAscript T3 Transcription Kit, prepare a 20 µl reaction in a 0.2 ml PCR tube by combining in the following order: 6 µl RNase-free water, 2 µl 75 mM ATP, 2 µl 75 mM CTP, 2 µl 75 mM GTP, 2 µl 75 mM UTP, 2 µl 10x T3

reaction buffer, 2 µl 1 µM dsDNA template, 2 µl T3 RNA polymerase enzyme mix. Gently mix, and incubate at 37 °C for 16-24 h. This prolonged reaction time enables transcription of high yields of 32 nt 5′ triphosphate RNA (pppRNA).

4. Bring the T3 transcription reaction product mixture to 50 µl by adding 30 µl RNase-free water and purify using a NucAway Spin Column according to manufacturer′s instructions.
5. Measure the concentration of the purified pppRNA using a Nanodrop. In my experience, at least 7-8 µg of pppRNA should be recovered after a 24 h transcription reaction. Calculate the molar concentration of the pppRNA assuming a molecular mass of 10830.3 g/mol.
6. Further assess the purity of the pppRNA by 15% polyacrylamide urea-PAGE. As little as 150 fmol pppRNA per lane should be sufficient to visualize under UV light using SYBR Gold to post-stain the gel.
7. The pppRNA should be stored in small aliquots at -20 °C or -80 °C to avoid multiple freeze-thaw cycles.
8. To prepare a 40 µl capping reaction, combine in order the following components in a 1.7 ml tube on ice: RNase-free water (for 40 µl total volume), 10 µl 4x capping buffer (see Recipes), 1 µl RNaseOUT, 24 pmol 32 nt pppRNA, 2 pmol recombinant capping enzyme (see Note 1), 24 pmol (total GTP) [α-^{32}P]GTP (see Note 4). Gently mix and incubate at 30 °C for 3 h, then heat-inactivate by incubating at 65 °C for 10 min.

9. Transfer 1.33 µl (1/30) of the capping reaction product to a new tube on ice to save as 'input' for scintillation counting. Bring the capping reaction to 50 µl by adding 11.33 µl RNase-free water. Purify the RNA using the Zymo RNA Clean & Concentrator-5 kit according to manufacturer's instructions, using 30 µl RNase-free water for the final elution step. Return the purified RNA to ice, and transfer 1 µl (1/30) to a new tube on ice for scintillation counting.
10. Mix the set-aside 1/30 capping reaction 'input' and purified RNA samples each with 1.5 ml ScintiSafe Econo 1 scintillation fluid and transfer to scintillation vials. Measure the radioactivity in each mixture by scintillation counting. Determine the concentration of purified [^{32}P]G-capped RNA according to the following equation: [GpppRNA] (in µM) = (24 pmol) x (purified counts/input counts)/(30 µl).
11. The purified [^{32}P]G-capped RNA may be stored at -20 °C but should be used within a few days to limit radioactive decay. Be sure to account for radioactive decay when determining the appropriate amount to use in the cap methyltransferase activity assay.

B. Preparation of nuclear and cytoplasmic extracts of mammalian cells

1. Two to three days in advance, seed 10-cm or 15-cm dishes with U2OS, HEK293, or other type of adherent mammalian cells such that the dishes will be ~80-90% confluent at the time of harvesting. U2OS cells should be grown in McCoy's 5A medium containing 10% (v/v) FBS; HEK293 cells should be grown in DMEM

containing 10% (v/v) FBS. Cells should be grown in an incubator set to 37 °C with 5% CO_2.

2. On the day of harvesting the cells, prepare YO Lysis Buffer and YO Buffer A (see Recipes) on ice, leaving out the DTT, PMSF, protease inhibitor cocktail, and phosphatase inhibitor cocktails until immediately before using the buffers.
3. Remove culture medium from adherent cells, rinse with PBS and remove, and then harvest by scraping into 1 ml PBS and transferring to 1.7 ml centrifuge tubes. Gently pellet the cells (70 *x g* for 10 min at 4 °C), and then carefully remove the supernatant PBS by aspiration. Make note of the approximate volume of the cell pellets, and place the tubes on ice.
4. For the preparation of cytoplasmic extracts, immediately add YO Lysis Buffer equivalent to 4-5 times the volume of each cell pellet. Gently resuspend the cells with 10 up-down strokes of a P1000 pipet. Incubate the cells on ice for 10 min, and then mix with 5 additional up-down strokes of the P1000 pipet. Pellet nuclei (16,100 *x g* for 10 min at 4 °C), and then transfer the cytoplasmic extract supernatants to new, pre-chilled 1.7 ml tubes on ice.
5. Carefully remove any residual cytoplasmic extract from the nuclear pellets using a P10 pipet. To prepare nuclear extracts, add 4-5 original-cell-pellet volumes of YO Buffer A, and resuspend each nuclear pellet with 15 up-down strokes of a P200 pipet. Incubate the tubes end-over-end at 4 °C for 20 min, and then pellet nuclear debris (16,100 *x g* for 5 min at 4 °C). Transfer the nuclear extract supernatants to new, pre-chilled 1.7 ml tubes on ice.

6. Measure the concentration of protein in each extract by Bradford assay, using the Bio-Rad Protein Assay Dye Reagent Concentrate according to manufacturer's instructions and using a standard curve of bovine serum albumin (BSA) at 0, 1, 2, 4, 6, and 8 μg/ml. Diluting the extracts 250- to 500-fold in the 1x dye reagent typically gives measurements within the linear range of the assay. Using a program such as Microsoft Excel, calculate the protein concentrations using the best-fit line of the BSA standard curve.
7. For the cap methyltransferase activity assay, prepare 15-20 μl samples of each extract in new, pre-chilled tubes on ice. If comparing nuclear and cytoplasmic extracts, it is critical to ensure that these are in the same buffer composition. This can be accomplished by first bringing the extracts all to the same protein concentration (typically 0.5-1.0 μg/μl; such calculations can be greatly aided by Microsoft Excel) with the same buffer used prior (*i.e.*, YO Lysis Buffer for cytoplasmic extracts and YO Buffer A for nuclear extracts) and then mixing each sample with an equal volume of the other buffer (*i.e.*, YO Buffer A for cytoplasmic extracts and YO Lysis Buffer for nuclear extracts). Store these extract samples in small aliquots at -80 °C.
8. Assess the quality of subcellular fractionation by running the nuclear and cytoplasmic extracts on SDS-PAGE followed by Western blot analysis. The use of nuclear and cytoplasmic control antibodies (*e.g.*, against nucleolin and tubulin) can determine whether cross-contamination occurred during the fractionation procedure.

C. Preparation of TLC plate for cap methyltransferase activity assay

1. Wearing clean gloves, use a clean ruler and scissors to cut a 20 x 20 cm PEI cellulose TLC plate into four 10 x 10 cm squares. I recommend using clean forceps to handle the plate to limit contact with any contaminants that may be present on gloves. Store any unused plates at 4 °C. See Note 2 regarding TLC performance.
2. Use the ruler and a pencil to lightly draw a faint, straight line (origin) 1.5 cm from the bottom edge of a 10 x 10 cm plate. Draw faint tick marks on the origin 1 cm apart to indicate where samples will be spotted. An example TLC plate is shown in Figure 13.

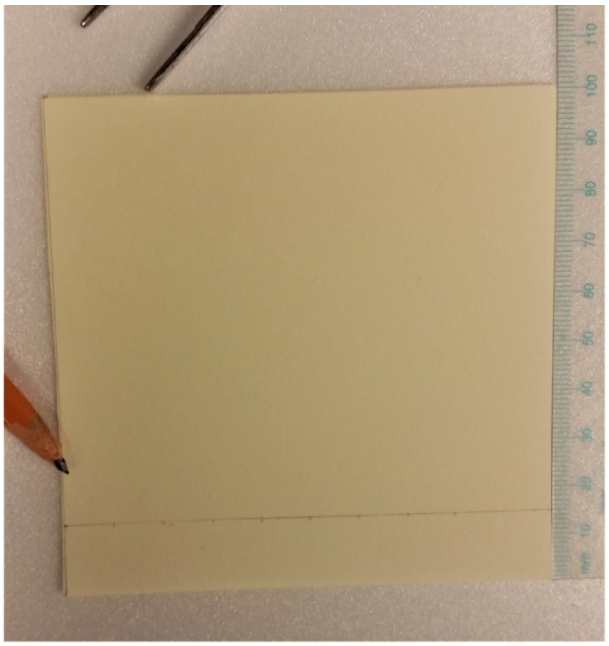

Figure 13. Example of TLC plate preparation.

3. Pre-run the TLC plate with RNase-free water. To do so, fill a rectangular glass TLC chamber with just enough water to cover the bottom (approximately 60 ml in the model listed above) such that the water depth does not exceed 0.75 cm. Using long forceps, gently place the TLC plate upright in the water. Take care to ensure that the left and right edges enter the water simultaneously, as this will promote even migration of water up the TLC plate. This pre-running step forces contaminants to the top of the TLC plate and greatly improves performance for the subsequent chromatographic analysis of the cap methyltransferase activity assay samples.
4. Once water has reached the top of the TLC plate, remove the TLC plate from the chamber and allow it to air-dry. Shaking the plate by hand or using a commercial hair dryer (without heating) can help speed up this process.
5. Pre-run TLC plates can be stored at 4 °C for at least 2 weeks.

D. Cap methyltransferase activity assay

1. After thawing components on ice, prepare 10 µl cap methyltransferase reactions in 1.7 ml tubes on ice by combining the following in order: RNase-free water (for 10 µl total volume), 1 µl 10x cap methylation buffer (see Recipes), 1 µl 1 µM SAM, 1 µl 20 mM DTT, 1 µl RNaseOUT, nuclear or cytoplasmic extract for 1 µg total protein, 5 fmol [^{32}P]G-capped RNA. Using a master mix of the reaction components (omitting the extracts) is recommended if working with a large

number of extract samples. Gently mix, incubate at 37 °C for 30 min, and then immediately return to ice.

2. Add 40 µl RNase-free water to each tube and purify the RNA samples using the Zymo Clean & Concentrator-5 kit according to manufacturer's instructions, using 7 µl RNase-free water for the final elution step. Place the purified RNA on ice.
3. Prepare 7 µl P1 nuclease digestion reactions in 1.7 ml tubes on ice by combining the following in order: 0.6 µl RNase-free water, 0.7 µl 500 mM sodium acetate pH 5.2, 5.0 µl purified RNA from cap methyltransferase reactions, 0.7 µl 0.625 U/µl P1 nuclease. Gently mix and incubate at 37 °C for 30 min. The samples may now be stored at -20 °C or analyzed immediately.
4. On the 1 cm tick marks on the origin of a pre-run PEI cellulose TLC plate, carefully spot 1 µl of the P1 nuclease digestion products using a P10 pipet. Allow the spots to completely air-dry, and then spot an additional 1 µl of the P1 digestion products on the same positions as before. As controls, also spot 2 µl (1 µl at a time) of 10 mM GpppG and 10 mM m^7GpppG standards on a separate tick mark (or marks).
5. After allowing the spots to completely air-dry, use long forceps to evenly place the TLC plate upright in a rectangular TLC chamber containing approximately 60 ml 0.4 M ammonium sulfate mobile phase. Allow the mobile phase to develop upward, approximately 6-7 cm beyond the origin, and then remove the TLC plate from the chamber. Allow the TLC plate to completely air-dry, which can be sped up by hand-shaking or using a hair dryer without heat.

6. Wearing proper eye and skin protection, observe the TLC plate under a handheld 254 nm UV light to determine the positions of the GpppG and m^7GpppG standards. These can be noted by marking their positions with a pencil or by taking a photo with a handheld camera.
7. Wrap the TLC plate in plastic wrap so that the front side is covered by one layer. Place the TLC plate in a storage phosphor screen cassette, taping the top edge to the cassette to keep it in place. Place a recently light-erased storage phosphor screen over the TLC plate, close the cassette, and expose at room temp for at least 16 h for maximum signal.
8. Remove the TLC plate from the cassette and image the storage phosphor screen with a Typhoon imager set to phosphor mode. Typical results are shown in Figure 14.

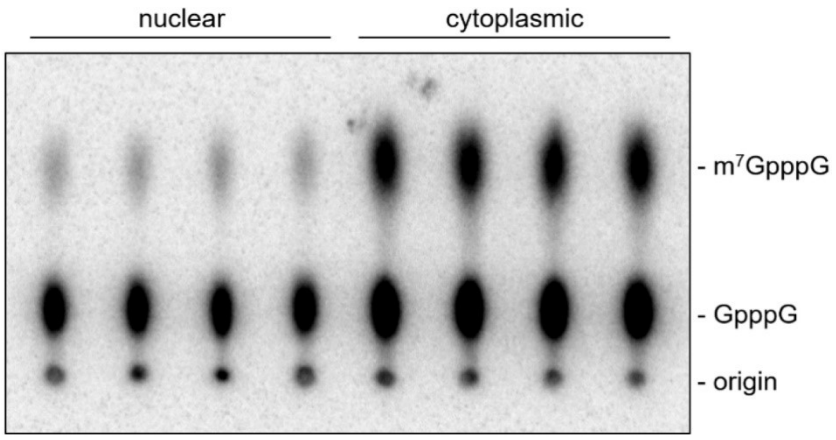

Figure 14. Typical phosphor image results.

To demonstrate reproducibility, four technical replicates of the described activity assay were performed with U2OS cell nuclear and cytoplasmic extracts.

Data Analysis

The extent of conversion of GpppRNA to m^7GpppRNA during a cap methyltransferase reaction (and by extension, the cap methyltransferase activity present in the corresponding biological sample) is represented by the ratio of the m^7GpppG spot intensity to the sum of the GpppG and m^7GpppG spot intensities on the TLC plate phosphor image. The spot intensities can be determined using any image software that includes densitometry analysis, such as ImageQuant TL. To ensure consistent calculation of spot intensities for multiple samples, use lanes or boxes of the same size that are large enough to just fit the entire spot for densitometry analysis. Also ensure that any background signal is subtracted; in ImageQuant TL, I use the 'rubberband' setting for establishing the baseline for peak signal integration. To account for biological variability among samples when comparing multiple conditions, it is good practice to perform this assay with at least three biological replicates to enable appropriate statistical testing.

Notes

1. The recombinant human capping enzyme I used to generate the radiolabeled GpppRNA was produced in-house as described in Trotman et al., 2017. Despite this enzyme stock having robust capping activity with non-radiolabeled GTP, the

production of radiolabeled GpppRNA was rather inefficient. If a recombinant capping enzyme is not available, I recommend using a commercially available enzyme, such as the Vaccinia Capping Enzyme (NEB M2080S), to produce the GpppRNA as was used in previous reports (Cowling, 2010b; Pillutla et al., 1998). If Vaccinia Capping Enzyme is used to generate GpppRNA, be sure to omit SAM from this reaction, as this enzyme also contains cap methyltransferase activity.

2. Unlike most types of chromatographic systems, the flow rate of TLC is variable and cannot be easily adjusted to optimize performance according to the van Deemter Equation (van Deemter et al., 1956; Guiochon et al., 1979). In TLC, the capillary flow rate is dependent on properties such as the particle size of the TLC plate, which can vary substantially from manufacturer to manufacturer. I have thus found that some manufacturers' PEI cellulose plates give streakier, more poorly resolved results than others, with the Macherey-Nagel plates listed here giving the best performance of those I have tested under the given conditions.
3. Any short, *in-vitro*-transcribed RNA (with a 5′ triphosphate) should be suitable for generating the radiolabeled GpppRNA substrate, and this protocol can be modified to produce other GpppRNA substrates if desired. The protocol presented here simply describes an easy way to generate the same 32 nt substrate RNA used in the initial characterization of human RNMT (Pillutla et al., 1998) and in my recent study (Trotman et al., 2017).
4. Use fresh [α-^{32}P]GTP to maximize the ratio of radioactive-to-nonradioactive GTP in the stock, which will allow for greater signal intensity during phosphorimaging. To

account for radioactive decay of the [α-^{32}P]GTP stock, I recommend using the PerkinElmer radioactivity calculator (https://www.perkinelmer.com/tools/calculatorrad) to determine the concentration of total GTP on the day of its use.

Recipes

1. 10x annealing buffer

   100 mM Tris-HCl pH 7.5

   500 mM NaCl

2. 4x capping buffer

   40 mM Tris pH 7.5

   12 mM $MgCl_2$

   4 mM DTT

   0.4 mM EDTA

   80% (v/v) glycerol

3. YO Lysis Buffer

   10 mM HEPES pH 7.3

   10 mM KCl

   10 mM $MgCl_2$

   0.2% (v/v) IGEPAL CA-630

   2 mM dithiothreitol (DTT)

   0.5 mM PMSF

7.5 µl/ml protease inhibitor cocktail (Sigma)

7.5 µl/ml phosphatase inhibitor cocktail 2 (Sigma)

7.5 µl/ml phosphatase inhibitor cocktail 3 (Sigma)

4. YO Buffer A

   10 mM HEPES pH 7.3

   25% (v/v) glycerol

   420 mM NaCl

   1.5 mM $MgCl_2$

   0.2 mM EDTA

   1 mM DTT

   0.5 mM PMSF

   7.5 µl/ml protease inhibitor cocktail (Sigma)

   7.5 µl/ml phosphatase inhibitor cocktail 2 (Sigma)

   7.5 µl/ml phosphatase inhibitor cocktail 3 (Sigma)

5. 10x cap methylation buffer

   500 mM Tris pH 8

   60 mM KCl

   12.5 mM $MgCl_2$

Acknowledgments

This work was supported by R01 grant GM084177 from the National Institutes of Health (to D.R.S). J.B.T. was funded by NIH T32 training grant GM08512 (to The Ohio

State University) and by a pre-doctoral fellowship from The Ohio State University Center for RNA Biology. The protocol presented here was adapted from those in Pillutla et al., 1998; Otsuka et al., 2009; and Cowling, 2010 and was used for experiments in Trotman et al., 2017. The authors declare no conflicts of interest or competing interests.

Chapter 4. Protein Interactome Analysis Reveals Stabilization of Mammalian Capping Enzyme by Heat Shock Protein 90[8]

Abstract

A defining feature of eukaryotic messenger RNAs (mRNAs) is the presence of a 5′ N7-methylguanosine cap, which is essential for proper RNA processing, localization, and translation. Beyond the canonical nuclear cap synthesis pathway, mammalian cells also possess cytoplasmic machinery capable of restoring a cap structure onto uncapped and/or partially degraded RNA 5′ ends. Central to both pathways is capping enzyme (CE), a bifunctional triphosphatase-guanylyltransferase that localizes to both the nucleus and the cytoplasm. To gain broader insight into the cellular context of cytoplasmic recapping, I sought to characterize the protein interactome of cytoplasmic CE (cCE). Stable U2OS cell lines were generated to inducibly express a tagged form of cCE or negative control EGFP, and these bait proteins were affinity purified and analyzed by bottom-up proteomics to identify interacting partners. Several cCE-interacting proteins were identified and validated, including the 90-kDa heat shock protein (HSP90). Inhibiting the ATP-binding activity of HSP90 with geldanamycin rapidly and

[8] This chapter has benefited from the experimental and conceptual contributions of the following: Bernice Agana[a,b,c], Andrew J. Giltmier[a,d], Vicki H. Wysocki[a,c], and Daniel R. Schoenberg[a,d] ([a]Center for RNA Biology, [b]Ohio State Biochemistry Program, [c]Department of Chemistry and Biochemistry, [d]Department of Biological Chemistry and Pharmacology, The Ohio State University, Columbus, Ohio, USA).

significantly reduced the levels of both nuclear and cytoplasmic CE, thus establishing CE as an HSP90 client protein.

Introduction

Cap homeostasis, enabled by cytoplasmic decapping and recapping of RNAs, has emerged as a novel mechanism of post-transcriptional gene regulation. A subpopulation of the transcriptome is regulated by cap homeostasis, with cytoplasmic recapping modulating the stability of some transcripts and the translatability of others in a manner independent of changes to poly(A) length (Kiss et al., 2016; Mukherjee et al., 2012). Additionally, cytoplasmic recapping appears to be responsible for diversifying the transcriptome by acting on 5′-end-shortened products of post-transcriptional processing (Djebali et al., 2012; Fejes-Toth et al., 2009; Kiss et al., 2015a; Lim and Maquat, 1992; Mercer et al., 2010, 2011; Otsuka et al., 2009).

Enzymes capable of regenerating caps on cytoplasmic RNAs have been described in diverse eukaryotic systems (Chen et al., 2017; Ignatochkina et al., 2015), but the most thoroughly characterized recapping system is that of mammalian cells. In mammals, CE and the guanine-N7 cap methyltransferase RNMT localize to both the nucleus and cytoplasm to participate in canonical cap synthesis and recapping, respectively (Otsuka et al., 2009; Thul et al., 2017; Trotman et al., 2017). Cytoplasmic CE and RNMT interact directly and associate with the adaptor protein Nck1, which recruits an uncharacterized 5′ monophosphate RNA kinase capable of generating diphosphate substrates for CE (Mukherjee et al., 2014; Trotman et al., 2017).

Despite targeted studies of cCE-interacting proteins, the full complement of proteins that associate with cCE is unknown. Identifying interacting partners of cCE would be informative for better understanding how cytoplasmic recapping may be regulated and how its specificity for target RNAs is achieved. The small protein cofactor RAM functions to regulate the catalytic activity of RNMT (Gonatopoulos-Pournatzis et al., 2011; Grasso et al., 2016; Trotman et al., 2017; Varshney et al., 2016), and regulation of CE is also possible through an unidentified inhibitor of its guanylyltransferase activity (Mullen and Price, 2017).

Proteomics analysis was used to identify the proteins that copurify with a cytoplasmically restricted form of CE. A preponderance of RNA-binding proteins that may define the specificity of recapping were found, and I unexpectedly identified HSP90 as a cCE interactor. Targeted inhibition of HSP90 with the drug geldanamycin destabilized CE protein levels, establishing CE as an HSP90 client protein and suggesting a link between recapping and the cellular stress response.

Materials and Methods

Plasmid Constructs

The sequence of plasmid pcDNA4/TO-bio-myc-NES-mCEΔNLS (bio-cCE) was described previously in Mukherjee et al., 2014. To generate pcDNA4/TO-bio-myc-NES-EGFP (bio-EGFP), a dsDNA gBlocks Gene Fragment (IDT) encoding the bio-myc-NES-EGFP sequence was inserted into KpnI-digested pcDNA4/TO (Thermo Fisher V102020)

using In-Fusion cloning (Clontech). The ORF sequences in both plasmids were confirmed by Sanger sequencing.

Cell Culture and Stable Cell Generation

All cells were grown at 37 °C under 5% CO_2 and were discarded after no more than 15 passages. U2OS-derived cell lines were grown in McCoy's 5A medium (Thermo Fisher 116600) supplemented with tetracycline-free fetal bovine serum (FBS, Atlanta Biologicals S10350) to 10% (v/v). Tetracycline-inducible U2OS (U2OS-TR) cells were described previously in Otsuka et al., 2009. To generate stable U2OS-TR cell lines expressing bio-EGFP or bio-cCE, U2OS-TR cells were transfected with either pcDNA4/TO-bio-myc-NES-EGFP or pcDNA4/TO-bio-myc-NES-mCEΔNLS using FuGene 6 (Promega E2691) according to manufacturer's instructions. Cells were passaged two days following transfection and then maintained for two weeks in medium containing 400 μg/mL Zeocin (Thermo Fisher R25001). Maintaining selective pressure with 400 μg/mL Zeocin, cells were passaged to low densities to allow formation of individual colonies that were isolated using cloning cylinders. Cell lines were expanded over several weeks in medium containing 400 μg/mL Zeocin before confirming inducible expression of bio-EGFP and bio-cCE by western blotting and immunofluorescence.

Immunofluorescence

Glass coverslips in the wells of a 24-well plate were each seeded with 50,000 stable cells 17 h prior to induction. Expression of bio-EGFP or bio-cCE was induced by

addition of tetracycline-HCl to a working concentration of 0.2 μg/mL. After 24 h, medium was removed from the coverslips, and the cells were fixed for 20 min at room temperature in PBS containing 4% formaldehyde and 0.2% (v/v) Triton X-100. Coverslips were briefly washed three times with PBS before incubating in IF Block Solution (PBS containing 1% (w/v) BSA and 0.05% (v/v) Triton X-100) for 90 min at room temperature, followed by overnight incubation at 4 °C in IF Blocking Solution containing a 1:1000 dilution of mouse anti-myc antibody (Santa Cruz sc-40). Coverslips were washed three times with IF Wash Solution (PBS containing 0.5 mM $MgCl_2$ and 0.05% (v/v) Triton X-100) at room temp, 5 min per wash, and then incubated for 60 min in the dark at room temp in IF Block Solution containing 0.75 μg/mL DAPI and a 1:1000 dilution of anti-mouse Alexa Fluor 594 (Thermo Fisher A11005). After washing with IF Wash Solution as before, coverslips were mounted on mounted on glass microscope slides with ProLong Gold Antifade Mountant (Thermo Fisher P36930), and incubated overnight in the dark at room temp to allow the mountant to cure. Images were acquired at room temp with a Nikon Eclipse Ti-U inverted microscope fitted with a CFI Plan Apo VC 60X oil immersion objective and a Nikon DS-Qi1 monochrome digital camera. Images were analyzed using Nikon NIS-Elements AR 3.10 software. Specificity of the secondary antibody for the primary antibodies was confirmed by parallel preparation of control coverslips not treated with primary antibody.

Subcellular Fractionation

Cells were harvested and fractionated into cytoplasmic and nuclear extracts as described in Trotman and Schoenberg, 2018.

SDS-PAGE and Western Blotting

Samples in Laemmli Sample Buffer were heated at 95 °C for 5 min and centrifuged for 5 s in a microfuge before loading Mini-PROTEAN TGX gels (Bio-Rad) and electrophoresing at 150 V in Tris-glycine-SDS running buffer. Proteins were transferred to Immobilon-FL (EMD Millipore IPFL00010) PVDF membranes at 100 V for 60 min at 4 °C. Membranes were blocked in Blocking Buffer (TBS containing 3% (w/v) BSA) for at least 30 min at room temperature before incubating overnight at 4 °C in Blocking Buffer containing primary antibodies at the dilutions listed in the Antibodies section. Membranes were washed three times in TBST at room temperature, at least 10 min per wash. Secondary antibody incubations were performed for 30 min at room temperature in Blocking Buffer, with antibody dilutions listed in the Antibodies section. Membranes were washed again with TBST as before and then imaged with a Li-Cor Odyssey infrared scanner at 700 or 800 nm as appropriate.

Antibodies

Primary antibodies used in this study are as follows: mouse anti-myc (Santa Cruz sc-40; 1:1000 for WB, 1:1000 for IF), rabbit anti-CE/RNGTT (Novus NBP1-49972; 1:500 for WB), rabbit anti-FASN (Proteintech 10624-2-AP; 1:500 for WB), rabbit anti-

XPO2/CSE1L (Proteintech; 1:1000 for WB), rabbit anti-EEF2 (One World Labs; 1:500 for WB), rabbit anti-HSP90α/β (Santa Cruz sc-4947; 1:2000 for WB), rabbit anti-RUVBL1 (Proteintech 10210-2-AP; 1:1000 for WB), rabbit anti-RUVBL2 (Proteintech 10195-1-AP; 1:500 for WB), rabbit anti-WDR77/MEP50 (Cell Signaling #2823; 1:1000 for WB), mouse anti-α-tubulin (Sigma T6199; 1:5000 for WB), rabbit anti-U2AF35 (provided by Brenton Graveley, University of Connecticut; 1:3000 for WB). Secondary antibodies used in this study are as follows: anti-mouse Alexa Fluor 594 (Thermo Fisher ; 1:1000 for IF), anti-rabbit Alexa Fluor 680 (Thermo Fisher A21109; 1:10,000 for WB), anti-mouse Alexa Fluor 680 (Thermo Fisher A21057; 1:10,000 for WB). Qdot 800 streptavidin conjugate (Thermo Fisher Q10171MP; 1:10,000 for WB) was used to detect biotinylated proteins.

Streptavidin Pulldown

After 24 h induction with 0.2 μg/mL tetracycline-HCl, growth medium was completely removed from 3 or 4 80-90% confluent 15-cm dishes each of bio-EGFP and bio-cCE stable cells. To each dish, 10 mL of PBS containing 0.15% formaldehyde (VWR 0493) was added and incubated at room temp for 10 min. To quench the crosslinking reaction, 1 mL of ice-cold PBS containing 1.25 M ice-cold glycine was added to each dish. Dishes were gently mixed by tilting and incubated for 5-10 min at room temp. The preceding steps were all performed in a staggered manner to ensure consistent treatment. Cells were then washed with PBS and harvested by scraping into PBS, pooling the bio-EGFP and bio-cCE cells into one 1.6-mL tube each. Cytoplasmic extracts were prepared

as described in Trotman and Schoenberg 2018. For the experiment in Figure 12, $CaCl_2$ was added to cytoplasmic extracts to 5 mM, micrococcal nuclease (Thermo Fisher 88216) was added to 0.46 U/mL, and samples were incubated at room temp for 15 min. To 1.6-mL tubes containing 15 µL (stock slurry volume) of pre-equilibrated MyOne Streptavidin T1 Dynabeads (Thermo Fisher 65601), equal mass amounts of protein (~1000 µg per sample) were added, brought to 1 mL with YO Lysis Buffer (Trotman et al., 2017), and brought to 150 mM upon addition of 30 µL of 5 M NaCl. Tubes were incubated end-over-end for 1 h at 4 °C to bind biotinylated proteins to the beads. The beads were washed 2 or 3 times with 500 µL of ice-cold YO Lysis Buffer containing 150 mM NaCl and then 2 or 3 times with 500 µL of ice-cold 50 mM ammonium bicarbonate, incubating end-over-end at 4 °C for 10 min per wash. After removal of the final wash, beads were resuspended in either 50 mM ammonium bicarbonate (for proteomics analysis) or 2× Laemmli Sample Buffer (Bio-Rad 1610737) containing 5% (v/v) β-mercaptoethanol. Samples were stored at -20 °C.

Proteomics Analysis

Beads from streptavidin pulldowns were reconstituted in 80 µL of 50 mM ammonium bicarbonate containing 0.02% ProteaseMAX surfactant (Promega V2071) and incubated at 95 °C for 5 min. After adding 13 µL of 50 mM ammonium bicarbonate, 1 µL of 0.5 M DTT was added, and samples were incubated at 56 °C for 20 min for the reduction of disulfides. Cysteine alkylation of was then performed by adding 3 µL of 0.55 M iodoacetamide and incubating at room temp in the dark for 15 min. Tryptic digests

were performed by adding 1 µL of 1% ProteaseMAX surfactant and 2 µL of 1 µg/µL trypsin and incubating at 37 °C for 3 h. Trypsin was inactivated upon addition of trifluoroacetic acid (TFA) to a final concentration of 0.5%. The digestion products were centrifuged 16,000 × *g* for 10 min, and the supernatants were cleaned up with C18 cartridge columns. Approximately 0.5 µg of peptides per sample were separated by reversed-phase ultra-performance liquid chromatography (RP-UPLC) on a Waters nanoACQUITY UPLC system and mass analyzed by a ThermoFisher Orbitrap Elite using top 15 data dependent acquisition in positive ion mode.

BioID

Treatment of cells for BioID was performed as in Trotman et al., 2017, with the exception that cells were supplemented with biotin to a working concentration of 1 µM. Following cytoplasmic extract preparation, streptavidin pulldowns were carried out as described above.

Results and Discussion

Generation of Stable Cells for Proteomics Analysis

To probe the interactome of cytoplasmic CE (cCE) in its native context, I generated a tetracycline-inducible U2OS cell line stably transfected with a tagged form of cCE. In this tagged construct ("bio-cCE"), I introduced an N-terminal biotinylation peptide sequence that is biotinylated *in vivo* to enable efficient recovery on streptavidin resin (Mukherjee et al., 2014; Tagwerker et al., 2006). I also included a myc epitope tag

as well as the HIV REV nuclear export signal (NES); this NES coupled with the deletion of the KRKY nuclear localization signal at the C-terminus of CE ensures exclusively cytoplasmic localization of the construct (Otsuka et al., 2009). To control for interacting proteins that may bind to the tags or interact non-specifically, I also generated a cell line expressing enhanced green fluorescence protein (EGFP) with the same tags as bio-cCE ("bio-EGFP"). A schematic view of each construct is presented in Figure 11A. Immunofluorescence analysis of both stable cell lines demonstrated that bio-EGFP and bio-cCE are only expressed upon induction with tetracycline (Figure 11B and C). Both constructs were shown to localize throughout the cytoplasm while being absent from the nucleus. Likewise, subcellular fractionation of the bio-cCE cell line confirmed that bio-cCE is present only in the cytoplasm (Figure 11D). Endogenous CE is more abundant in the nucleus than the cytoplasm, and consistent with results in Otsuka et al., 2009, similar levels of CE were seen by Western blot when three times more cytoplasmic extract was loaded than nuclear extract (on a microgram basis). I examined the levels of bio-cCE that were expressed when stable cells were grown for 24 h in the presence of 0, 0.2, 0.5, and 1.0 μg/mL tetracycline and found that levels of bio-cCE did not increase in a dose-dependent manner. Western blotting with an anti-CE antibody unfortunately revealed a cross-reacting band that co-migrates with bio-cCE, making it difficult to discern conditions at which bio-cCE levels mirrored those of endogenous cytoplasmic CE. Nonetheless, the level of bio-cCE expressed at 0.2 μg/mL was not considerably overexpressed relative to endogenous cCE, so any proteins that interact with bio-CE should be relevant to the physiology of endogenous cCE.

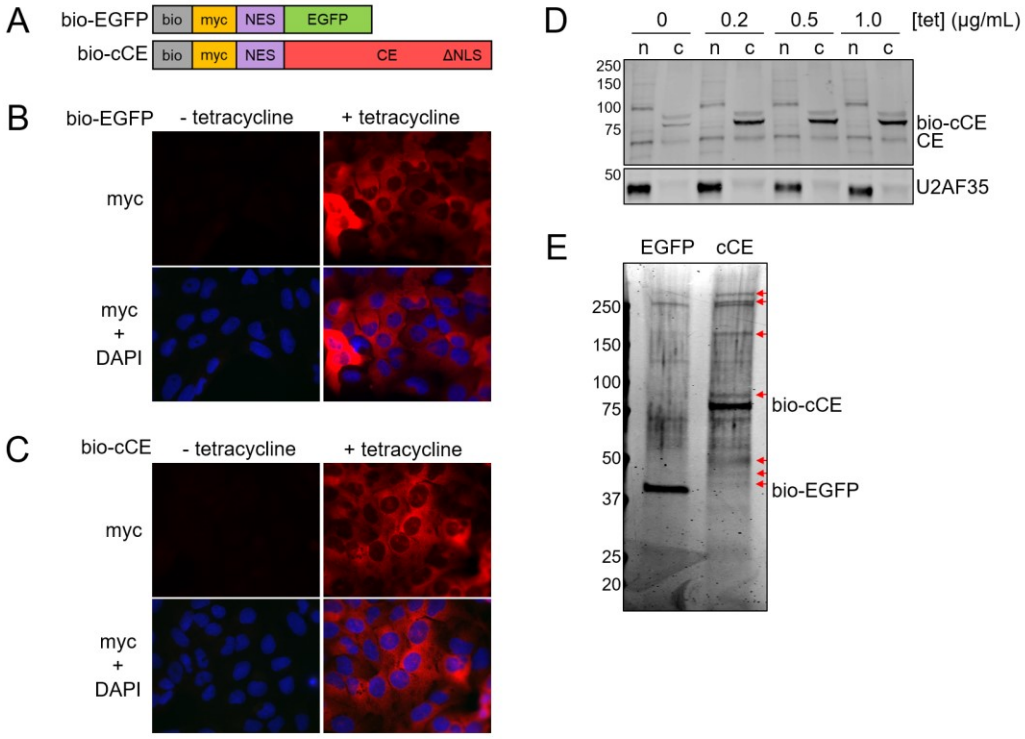

Figure 15. Generation and characterization of tetracycline-inducible U2OS cell lines stably transfected with bio-EGFP or bio-cCE.

A. Schematic showing the bio-EGFP and bio-cCE constructs stably transfected into U2OS cells. Each contains at its N-terminus a biotinylation tag, a myc tag, and the HIV REV NES. B and C. Immunofluorescence images of stable bio-EGFP (B) and bio-cCE (C) cell lines grown in the presence or absence of 0.2 μg/mL tetracycline of 24 h. Cells were stained with anti-myc antibody and DAPI. D. Western blot analysis of 10 μg of nuclear (n) and 30 μg of cytoplasmic (c) extracts of bio-cCE stable cells grown for 24 h in the indicated concentration of tetracycline. The top panel was generated using anti-CE

antibody, and the bottom panel was generated using anti-U2AF35 antibody as a nuclear fractionation control. Note that a cross-reacting band co-migrates with bio-cCE, which is apparent in the cytoplasmic extract of the uninduced cells (lane 2). The positions of protein markers of the indicated sizes (in kDa) are labeled on the left. E. Global view of proteins that interact with bio-EGFP and bio-cCE. Stable cells were grown for 24 h in the presence of 0.2 μg/mL tetracycline, crosslinked with formaldehyde, harvested, and lysed to produce cytoplasmic extracts. Streptavidin beads were incubated with these extracts and washed. Bound proteins were analyzed by SDS-PAGE and staining with Coomassie blue. Red arrows indicate bands highly enriched or exclusively visible in the bio-cCE interacting profile.

Analysis of the cCE Interactome

To preserve *in vivo* interactions between bio-EGFP and bio-cCE and other proteins, I employed a strategy where stable cells were briefly crosslinked with formaldehyde prior to harvesting, allowing any transient interactions to be stabilized (Srinivasa et al., 2015). Interacting proteins were then copurified with bio-EGFP and bio-cCE on streptavidin beads. Coomassie staining of the purified material revealed some proteins that appear to be common to both bio-EGFP and bio-cCE, underscoring the importance of bio-EGFP as a specificity control (Figure 11E). Importantly, multiple proteins were visibly enriched in the bio-cCE interactome relative to bio-EGFP.

Identification of proteins that copurify with bio-EGFP and bio-cCE was achieved by liquid chromatography coupled to tandem mass spectrometry (LC-MS/MS) analysis of

peptides produced by tryptic digestion. MS/MS spectra were searched against a database containing tryptic peptide sequences of the human proteome, and the numbers of peptide spectral matches (PSMs) were tallied for each protein identified. Results from three independent experiments are presented in Table 1, with proteins sorted by enrichment in the bio-cCE samples relative to the bio-EGFP samples. As expected, PSMs for CE (RNGTT) were exclusive to the bio-cCE samples. Surprisingly, no peptides were matched to the known cCE-interacting proteins Nck1 or RNMT (Mukherjee et al., 2014; Trotman et al., 2017). The reason for this is unknown but could be due to complications arising from less-abundant peptide signals being overwhelmed by those from more abundant proteins during MS/MS analysis. Likewise, no obvious candidate protein was identified that may harbor 5′ monophosphate kinase activity, though the possibility of uncharacterized kinase activity in the identified proteins cannot be ruled out. Regardless, it is apparent that cytoplasmic CE forms protein complexes beyond the previously described cytoplasmic capping complex, as 45 novel candidate cCE-interacting proteins were identified with a cCE enrichment index of at least 1.5 over the EGFP negative control (Table 1). Thirty-two of these have been previously suggested to be mRNA-binding proteins as determined by proteomics analysis (Baltz et al., 2012; Castello et al., 2012), which may prove to be important for understanding the selectivity of cCE for particular recapping target mRNAs (Mukherjee et al., 2012). Notably, none of the cCE-interacting proteins I identified are in common with the list of high-confidence proteins reported to interact with CE in a recent study of the interactomes of mRNA-processing factors (Youn et al., 2018). Most of the CE-interacting proteins identified in that study

reside in the nucleus, consistent with the majority of CE being nuclear (Figure 11D; Otsuka et al., 2009). In contrast, my focus on the cytoplasmic population of CE enabled identification of a novel set interacting proteins, most of which are cytoplasmic. Taken together, it appears that disparate sets of proteins interact with CE in the nucleus and cytoplasm, suggesting opportunities for distinct function and regulation in each compartment.

Gene Symbol	Gene Name	Experiment 1		Experiment 2		Experiment 3		cCE Enrichment Index	mRNA-binding?	
		cCE PSMs	EGFP PSMs	cCE PSMs	EGFP PSMs	cCE PSMs	EGFP PSMs		Ref. 1	Ref. 2
RNGTT	mRNA-capping enzyme	8		36		9		17.67		
FASN	Fatty acid synthase	12	3	24	5	40	1	6.33	Y	Y
KPNB1	Importin subunit beta-1	4		6		7		5.67	Y	
EEF2	Elongation factor 2	13		14	4	20	2	5.22	Y	Y
CLTC	Clathrin heavy chain 1	4	1	12	2	24	2	5.00	Y	*
CCT5	T-complex protein 1 subunit epsilon	2		7		9	1	4.50		*
CCT7	T-complex protein 1 subunit eta	3	1	4	1	13		4.00		
CSE1L	Exportin-2	3		4		5		4.00		
CCT3	T-complex protein 1 subunit gamma	3	1	4	1	17	1	4.00	Y	*
RUVBL2	RuvB-like 2	1		5		5		3.67		
CCT2	T-complex protein 1 subunit beta	2		8	1	12	2	3.67		
TUBA3C	Tubulin alpha-3C/D chain					35	7	3.50		
TCP1	T-complex protein 1 subunit alpha	2	1	6	2	12		3.33	Y	
TUBB6	Tubulin beta-6 chain	7		21	6	18	5	3.29		
CCT8	T-complex protein 1 subunit theta	5	2	14	3	13	2	3.20		*
TUBA1B	Tubulin alpha-1B chain	5	2	12	3	53	14	3.18		
TUBB	Tubulin beta chain	26	5	40	14	57	18	3.08		*
TUBB4B	Tubulin beta-4B chain	25	5	38	14	46	14	3.03		
PSMD2	26S proteasome non-ATPase regulatory subunit 2	1		5		3		3.00		*
CCT6A	T-complex protein 1 subunit zeta	4		4	1	6	1	2.80		Y
PHGDH	D-3-phosphoglycerate dehydrogenase	1		4		3		2.67		
FSCN1	Fascin	1		3		4		2.67		Y
TIMM50	Mitochondrial import inner membrane translocase subunit TIM50			4		4		2.67		
AHNAK	Neuroblast differentiation-associated protein AHNAK	2		12	3	2		2.67		Y
HSP90AB1	Heat shock protein HSP 90-beta	17	6	22	12	46	11	2.66	Y	Y
HSP90AA1	Heat shock protein HSP 90-alpha	13	5	16	7	19	4	2.53	Y	Y
FKBP4	Peptidyl-prolyl cis-trans isomerase FKBP4	1	1	7		2		2.50		Y
TLN1	Talin-1	4		4	1	2		2.50		*
CCT4	T-complex protein 1 subunit delta	1	1	9	2	12	3	2.44		Y
EIF2S1	Eukaryotic translation initiation factor 2 subunit 1	3	1	7	1	2		2.40	Y	Y
RNH1	Ribonuclease inhibitor	1		1		5		2.33		*
MTHFD1	C-1-tetrahydrofolate synthase, cytoplasmic	3		4	1	2		2.25		
PCBP2	Poly(rC)-binding protein 2			3	1	6		2.25	Y	Y
HSPA1A	Heat shock 70 kDa protein 1A/1B	3	1	8	1			2.20	Y	
STIP1	Stress-induced-phosphoprotein 1	3	1	4	1	4		2.20		Y
FLNC	Filamin-C	2	1	13	3	9	4	2.18		
TUBA1C	Tubulin alpha-1C chain	4	2	12	3			2.00		*
GAPDH	Glyceraldehyde-3-phosphate dehydrogenase	10	2	2	1	7	4	1.90		*
PCBP1	Poly(rC)-binding protein 1			3	1	6	1	1.80	Y	Y
ENO1	Alpha-enolase	7	1					1.75		Y
KIF5B	Kinesin-1 heavy chain	3		2				1.67		
RUVBL1	RuvB-like 1	1		1		3		1.67		*
FLNA	Filamin-A	9	5	20	16	17	4	1.64	Y	Y
RAN	GTP-binding nuclear protein Ran	2		3	1	1		1.50	Y	Y
PFN1	Profilin-1			2		4	1	1.50	Y	*
EIF5A	Eukaryotic translation initiation factor 5A-1	4	3			5		1.50	Y	*
PRDX1	Peroxiredoxin-1	7		5	5	2	2	1.40	Y	Y
ANXA2	Annexin A2	4	1	8	6	8	5	1.33		Y
RPL28	60S ribosomal protein L28	1		2		1		1.33		Y
PGD	6-phosphogluconate dehydrogenase, decarboxylating	1		1		2		1.33		
EPRS	Bifunctional glutamate/proline--tRNA ligase			3		1		1.33		
CACYBP	Calcyclin-binding protein	1		3				1.33		*
IPO4	Importin-4	2		2				1.33		
IPO5	Importin-5	1		1		2		1.33	Y	*
PLAA	Phospholipase A-2-activating protein			3		1		1.33		
GCN1L1	Translational activator GCN1	1		3				1.33	Y	
HSPB1	Heat shock protein beta-1			1	1	7	2	1.33		Y
ACTA2	Actin, aortic smooth muscle	7	2	5	4			1.33		

Table 1. Candidate cCE-interacting proteins identified by proteomics analysis.[9]

Proteins identified by three independent LC/MS-MS experiments are listed in order of decreasing cCE Enrichment Index, which is calculated as the average of bio-cCE PSMs

[9] Table 1 was generated using data contributed by Bernice Agana in the lab of Vicki H. Wysocki.

divided by the average of bio-EGFP PSMs (plus 1 to prevent division by zero). Prior identification of a protein as "mRNA-binding" (Y) or "candidate mRNA-binding" (*) is detailed in the last columns, with Baltz et al., 2012 as Ref 1. and Castello et al., 2012 as Ref. 2. Rows are color-coded according to broad protein class or function: blue for metabolic enzymes, green for nucleocytoplasmic transport proteins, purple for translation factors, orange for chaperones, pink for RuvB-like nucleic acid helicases, and yellow for cytoskeletal proteins.

To validate interactions between cCE and candidate cCE-interacting proteins, streptavidin pulldowns were performed with bio-EGFP and bio-cCE stable cells as was done for LC/MS-MS analysis. Material recovered with streptavidin beads was analyzed by Western blotting with antibodies against several candidates, as shown in Figure 12. I confirmed that bio-cCE interacts with fatty acid synthase (FASN), exportin-2 (XPO2/CSE1L), heat-shock protein 90 (HSP90), translation elongation factor 2 (EEF2), and RuvB-like proteins 1 and 2 (RUVBL1 and RUVBL2). As a negative control, I also probed the streptavidin-bound material with an antibody against methylosome protein 50 (MEP50/WDR77), a protein not identified by the proteomics analysis. The lack of recovery of this protein demonstrates the specificity of the interactions with bio-cCE. Despite the LC-MS/MS identification of all 8 T-complex proteins recovered with bio-cCE, I was unable to detect CCT4 or CCT5 even in cytoplasmic extracts, pointing to either poor antibody performance or an artifact of the mass spectrometry analysis.

It was possible that the detected interactions are mediated by mutual binding to RNA instead of through protein-protein interactions. To address this possibility, cytoplasmic extracts were treated with micrococcal nuclease to digest RNA prior to incubation with streptavidin beads. I noted no difference in recovery as a function of micrococcal nuclease treatment (Figure 12), suggesting that these interactions are not mediated by mutual binding to RNA but are likely instead through direct or indirect protein binding.

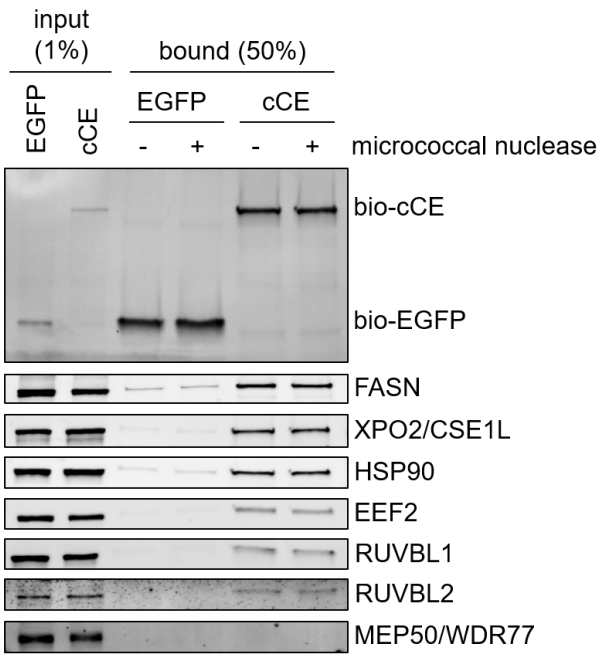

Figure 16. Validation of candidate cCE-interacting proteins.

Streptavidin pulldowns were performed as was done for proteomics analysis, except bio-EGFP and bio-cCE cytoplasmic extracts were pre-incubated in the presence or absence of

micrococcal nuclease prior to incubation with streptavidin beads. Following SDS-PAGE, the input extracts and bound material were analyzed by Western blotting with streptavidin-800 conjugate (top panel) and antibodies to the following proteins: FASN, XPO2/CSE1L, HSP90, EEF2, RUVBL1, RUVBL2, and MEP50/WDR77.

Investigation of CE Stabilization by HSP90

Both the α and β isoforms of HSP90 were identified by the proteomics analysis as cCE-interacting proteins (Table 1), and the large number of PSMs for each led me to investigate whether HSP90 plays an important role in the biology of CE. HSP90 is a well-characterized, ATP-dependent protein chaperone that helps fold and stabilize a select but diverse group of client proteins, including protein kinases, transcription factors, and disease-related factors such as p53 and Tau (Karagöz and Rüdiger, 2015; Röhl et al., 2013). HSP90 was also recently found to play a chaperoning role during the maturation of hemoglobin (Ghosh et al., 2018). HSP90 functions as a chaperone constitutively, but its expression increases in response to protein-denaturing stressors to help stabilize client proteins (Ullrich et al., 1989; Whitesell and Lindquist, 2005).

The cCE-HSP90 interaction was confirmed to occur *in vivo* using proximity-dependent biotinylation, or BioID (Figure 13A; Roux et al., 2012). This method takes advantage of the promiscuous biotin ligase BirA* fused to a protein of interest. Cells expressing this fusion construct are supplemented with excess biotin, and the BirA* generates reactive biotinoyl-AMP molecules that react with primary amines of proteins

within 100 Å (Kim et al., 2014). As a result, proteins proximal to the protein of interest are biotinylated, marking them as having interacted in their native cellular environment. HEK293 cells were transfected to express either BirA*-tagged cCE or BirA* fused only to the NES, incubated them in the presence of biotin, and recovered cytoplasmic proteins on streptavidin beads. The preferential recovery of HSP90 from cells expressing BirA*-tagged cCE demonstrated that HSP90 indeed interacts with CE *in vivo*.

Next, I examined whether HSP90 functions to stabilize cCE. To do so, I employed geldanamycin, a natural product that specifically inhibits HSP90 by binding to its unique ATP-binding site. Bio-cCE stable cells were induced with tetracycline for 24 h while simultaneously treating with geldanamycin or DMSO vehicle control (Figure 13B). In geldanamycin-treated cells, the levels of bio-cCE were reduced to 32% relative to DMSO-treated cells. Repeating this experiment with non-transfected U2OS cells, I tested the effect of geldanamycin on endogenous CE (Figure 13C). I found that endogenous cytoplasmic CE levels were significantly reduced to similar levels in geldanamycin-treated cells, a result that was mirrored by a similar decrease in the levels of nuclear CE. These results establish that HSP90 activity stabilizes CE in both compartments and that CE is a bona fide HSP90 client protein. Examining the kinetics of CE destabilization upon geldanamycin treatment (Figure 13D) revealed that nuclear and cytoplasmic CE are lost at similar rates. While the majority of HSP90 localizes to the cytoplasm, a small population has been reported to function in the nucleus as well (Fang et al., 2014; Tago et al., 2004). Thus, the simultaneous loss of nuclear and cytoplasmic CE upon HSP90

inhibition could be due to redistribution of CE via nucleocytoplasmic shuttling or due to direct action of HSP90 on mature nuclear CE.

A previous report showed that HSP90 inhibition prevents the cap-binding protein eIF4E and its binding partner 4E-T from localizing to stress granules, cytoplasmic aggregates of translationally silenced mRNAs that form upon cellular stress (Suzuki et al., 2009). The mechanism behind this observation remains largely unknown, as neither eIF4E nor 4E-T were found to be HSP90 client proteins, and geldanamycin treatment had no effect on the ability of eIF4E to bind to a cap analog. While a number of HSP90 client proteins may underlie the effect of geldanamycin on eIF4E and 4E-T recruitment to stress granules, one possible explanation is that upon HSP90 inhibition, reduced cCE levels cause fewer mRNAs sequestered in stress granules to be capped. Consistent with this hypothesis, CE localizes to stress granules upon oxidative stress (C. Mukherjee, unpublished results), and cytoplasmic recapping is known to enhance cell viability following recovery from stress (Otsuka et al., 2009). Future studies will focus on uncovering how HSP90 stabilization of CE affects the cap status of cytoplasmic RNAs and whether this impacts the composition of stress granules and the cellular response to stress.

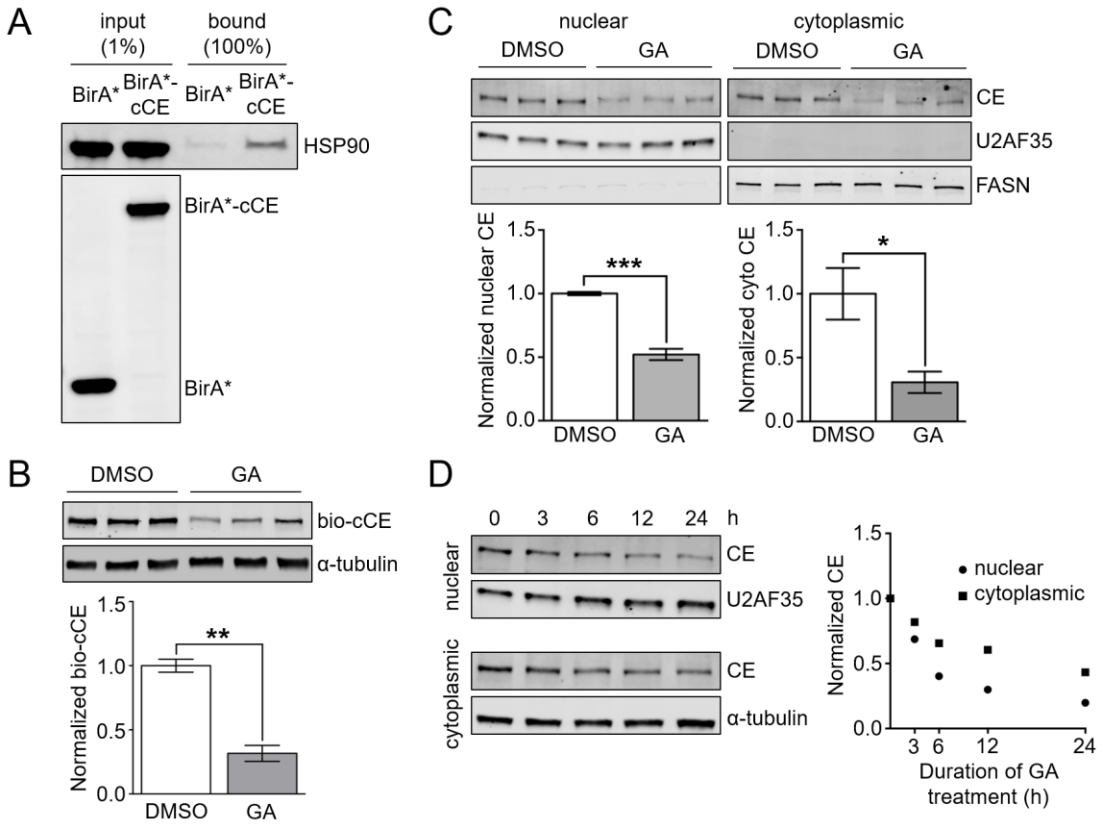

Figure 17. CE is stabilized by its interaction with HSP90.[10]

A. BioID analysis of the CE-HSP90 interaction. HEK293 cells were transfected with plasmids expressing myc-BirA*-NES (BirA*) or myc-BirA*-cCE (BirA*-cCE) and grown in the presence of 1 μM biotin. Cytoplasmic extracts of these cells were incubated with streptavidin beads and washed, and input and bound proteins were analyzed by SDS-PAGE and Western blotting with antibodies to HSP90 (top panel) and myc (bottom panel). B. Triplicate cultures of stable bio-cCE cells were grown for 24 h in the presence of 0.2 μg/mL tetracycline and either 0.2 μM geldanamycin (GA) or DMSO vehicle

[10] Figure 17A was generated by Andrew J. Giltmier in the lab of Daniel R. Schoenberg.

control. Cytoplasmic extracts were analyzed by SDS-PAGE and Western blotting with anti-myc antibody (top panel) or anti-α-tubulin antibody (bottom panel) as a loading control. Levels of bio-cCE were normalized to α-tubulin, arbitrarily set to 1, and plotted as the average of the three replicates for each condition, with error bars representing s.e.m. C. U2OS-TR cells were grown for 24 h in the presence of either 0.2 μM GA or DMSO vehicle control. Cytoplasmic and nuclear extracts were prepared and analyzed by SDS-PAGE and Western blotting with antibodies against CE (top panel), U2AF35 (middle panel), and FASN (bottom panel). Levels of endogenous CE were quantified as in (B), using U2AF35 and FASN for normalization of nuclear and cytoplasmic CE, respectively. D. U2OS-TR cells were treated with 0.2 μM GA for the indicated time prior to harvesting. Nuclear and cytoplasmic extracts were prepared and analyzed for CE levels as in (B) and (C). Asterisks indicate level of significance by two-tailed, unpaired *t*-test: * indicates $p < 0.05$, ** indicates $p < 0.01$, and *** $p < 0.001$.

Chapter 5. Future Prospects and Concluding Remarks

The findings of my work have important implications for the function and regulation of cytoplasmic RNA recapping. First, the association of RNMT with the cytoplasmic capping complex and with RAM presents the cell with opportunities to regulate cap methylation and in turn, mRNA stability and translation. RNMT is subject to many post-translational modifications that could modulate its ability to bind CE and/or RAM (Aregger and Cowling, 2017; Aregger et al., 2016). Despite the requirement of RAM for optimal RNMT activity, the stoichiometry of these two proteins is variable among different cell types, and RAM availability diminishes during neurodifferentiation of embryonic stem cells (Grasso et al., 2016). It is thus conceivable that regulation of cytoplasmic RAM levels may be a strategy that cells use to regulate cytoplasmic recapping.

My work also sheds light on the likely connection between recapping and the cellular stress response. When cells are stressed, cap-dependent translation is inhibited, and mRNAs are sequestered in ribonucleoprotein particles called stress granules (SGs). Additionally, HSP90 is upregulated upon stress to help fold client proteins that may become denatured in the stressed environment (Prodromou, 2016). SGs normally contain the cap-binding translation initiation factor eIF4E, but this association is abrogated upon HSP90 inhibition (Suzuki et al., 2009). HSP90 inhibition also causes a downregulation in

both the nuclear and cytoplasmic levels of CE. The cap status of translationally silenced mRNAs in SGs has yet to be explored, but the present data suggest that HSP90 stabilizes CE such that it may readily catalyze recapping of SG mRNAs upon recovery from stress. Recapped SG mRNAs could then be recognized by eIF4E, enabling their translation to resume. Such a model would be consistent with cytoplasmic recapping promoting cell viability following stress (Otsuka et al., 2009).

Research over the past decade has established RNA recapping as a novel mechanism of gene expression control; however, many other questions remain unanswered. One of the biggest challenges is to define the rules, if any, for the selectivity of recapped sites. Biochemically, such selectivity could be achieved through preferential activity of any of the recapping enzymes or by preferential decapping, exonuclease, and/or endonuclease activities. Sequence motifs provide a possible avenue for this selectivity in a manner that may be species-specific. Motif analyses found only a slight preference for a guanosine at presumptive novel 5′ ends in mouse (Mercer et al., 2010), but in *Drosophila*, 59% of the most abundant signals in downstream capped read clusters mapped to genomic TC dinucleotides (Ni et al., 2010). This finding implies that recapping frequently occurs after processing events that target UC dinucleotides in fruit flies. Emerging data reported in this dissertation suggest coordination of cCE with an array of RNA-binding proteins, which could explain why only particular transcripts are detectably recapped (Mukherjee et al., 2012). It also remains unknown whether RNA secondary structure is important for recapping. XRN1 exonuclease activity is inhibited by strong secondary structures (Charley et al., 2018; Moon et al., 2015; Muhlrad et al.,

1994), so 5′ monophosphate ends at such structures may be preferentially stabilized and targeted for recapping. Insight into any such rules could guide the development of reporter mRNAs as new tools to aid studies of recapping. Further, does cap homeostasis depend on or influence epitranscriptomic marks such as pseudouridine or N6-methyladenosine (m^6A)? N6-methylation of adenosine at the cap-proximal nucleotide is one of the most prevalent internal modifications in the transcriptome, and its reversibility and ability to modulate sensitivity to decapping by DCP2 (Mauer et al., 2017) warrant investigating how m^6A affects the selection of recapped sites.

Another major hurdle regarding mammalian recapping is elucidating the identity of the 5′ monophosphate RNA kinase. Is it a previously uncharacterized protein? Or does a known protein possess this as-of-yet uncharacterized activity? Additionally, considering the discovery that the trypanosome TbCe1 kinase domain is highly similar to the adenylate kinase family of proteins (Ignatochkina et al., 2015), nucleoside monophosphate kinases (NMPKs) are obvious candidates for investigation. The chemistry of any previously unrecognized 5′ monophosphate RNA kinase activity would presumably be analogous to NMPKs, and given the abundance of NMPK genes in mammals (nine different adenylate kinases, two different uridylate/cytidylate kinases, one guanylate kinase, and one thymidylate kinase (Panayiotou et al., 2014)), it is conceivable that some NMPKs may act upon 5′ monophosphate RNA ends to generate diphosphate substrates for the guanylyltransferase activity of CE. Methods capable of detecting 5′ diphosphate ends have recently been developed (Ettwiller et al., 2016; Luciano et al., 2017) and have shown that 5′ diphosphate mRNAs are surprisingly

common in bacteria. Do the transcriptomes of eukaryotic species contain prevalent 5′ diphosphate RNAs as well?

Are there non-mRNA targets of cytoplasmic (re)capping? m^7G caps have been observed on tRNA precursors (Ohira and Suzuki, 2016), and because these RNAs are synthesized by Pol III instead of Pol II, it appears unlikely that pre-tRNA capping occurs through the canonical co-transcriptional pathway. Capped pre-tRNAs in yeast were most prevalent on those that had undergone splicing, and because tRNA splicing occurs on the cytoplasmic surface of mitochondria in yeast, it will be interesting to learn where in the yeast cell pre-tRNA capping occurs. Likewise, human pre-tRNAs were recovered with anti-cap antibody, consistent with CAGE tags mapping to the 5′ regions of mammalian tRNA genes (Ohira and Suzuki, 2016). Analyses of RNAs shorter than 200 nucleotides have uncovered the existence of short, capped RNAs that appear to be derived from post-transcriptional processing of tRNAs, mature mRNAs and snoRNAs (Abdelhamid et al., 2014; Fejes-Toth et al., 2009; Mercer et al., 2010). What role cytoplasmic capping plays in the processing of tRNAs and short, processed RNAs remains to be determined.

Are the caps added in the cytoplasm distinguishable from those added in the nucleus? Cap 1 and cap 2 ribose methylations would be preserved following recapping at canonical 5′ ends but would potentially be absent upon recapping at downstream sites generated by post-transcriptional processing. The cap 1 methyltransferase CMTR1 is mostly nuclear and binds to the C-terminal repeat domain of Pol II, suggesting that cap 1 methylation is co-transcriptional and restricted to the nucleus (Bélanger et al., 2010; Haline-Vaz et al., 2008). Thus, caps added at downstream sites may be translationally

regulated by IFIT proteins that bind cap 0 more tightly than cap 1 (Johnson et al., 2018; Kumar et al., 2014). Such regulation could be further mediated by IFIT2, which binds AU-rich elements that are prevalent in recapping target RNAs (Fensterl and Sen, 2015; Mukherjee et al., 2012; Yang et al., 2012). In contrast to CMTR1, the cap 2 methyltransferase CMTR2 localizes to both the nucleus and cytoplasm and is able to methylate both cap 0 and cap 1 structures (Werner et al., 2011). Analysis of cap 2 methyltransferase activity revealed considerably higher activity in cytoplasmic extracts than in nuclear extracts of HeLa cells (Langberg and Moss, 1981), so it is possible that cap 2 methylation is a primarily cytoplasmic event and may be involved in cytoplasmic recapping.

In addition to encoding their own capping enzymes and "snatching" caps from host RNAs, (Ferron et al., 2012), do any RNA viruses hijack the cytoplasmic capping machinery (Snijder et al., 2016)? Is recapping a strategy used by neurons to control localized translation, particularly at around synapses (Rangaraju et al., 2017)? With so much left to discover, it is my hope that the decades to come continue to reveal new insights into how cytoplasmic recapping impacts RNA biology.

References

Abdelhamid, R.F., Plessy, C., Yamauchi, Y., Taoka, M., De Hoon, M., Gingeras, T.R., Isobe, T., and Carninci, P. (2014). Multiplicity of 5′ cap structures present on short RNAs. PLoS One *9*, e102895.

Afik, S., Bartok, O., Artyomov, M.N., Shishkin, A.A., Kadri, S., Hanan, M., Zhu, X., Garber, M., and Kadener, S. (2017). Defining the 5′ and 3′ landscape of the Drosophila transcriptome with Exo-seq and RNaseH-seq. Nucleic Acids Res. *45*, e95.

Aouadi, W., Eydoux, C., Coutard, B., Martin, B., Debart, F., Vasseur, J.J., Contreras, J.M., Morice, C., Quérat, G., Jung, M.L., et al. (2017). Toward the identification of viral cap-methyltransferase inhibitors by fluorescence screening assay. Antiviral Res. *144*, 330–339.

Aregger, M., and Cowling, V.H. (2013). Human cap methyltransferase (RNMT) N-terminal non-catalytic domain mediates recruitment to transcription initiation sites. Biochem. J. *455*, 67–73.

Aregger, M., and Cowling, V.H. (2017). Regulation of mRNA capping in the cell cycle. RNA Biol. *14*, 11–14.

Aregger, M., Kaskar, A., Varshney, D., Fernandez-Sanchez, M.E., Inesta-Vaquera, F.A., Weidlich, S., and Cowling, V.H. (2016). CDK1-Cyclin B1 activates RNMT, coordinating mRNA cap methylation with G1 phase transcription. Mol. Cell *61*, 734–746.

Arribas-Layton, M., Wu, D., Lykke-Andersen, J., and Song, H. (2013). Structural and functional control of the eukaryotic mRNA decapping machinery. Biochim. Biophys. Acta - Gene Regul. Mech. *1829*, 580–589.

Baltz, A.G., Munschauer, M., Schwanhäusser, B., Vasile, A., Murakawa, Y., Schueler, M., Youngs, N., Penfold-Brown, D., Drew, K., Milek, M., et al. (2012). The mRNA-bound proteome and its global occupancy profile on protein-coding transcripts. Mol. Cell *46*, 674–690.

Batut, P.J., Dobin, A., Plessy, C., Carninci, P., and Gingeras, T.R. (2012). High-fidelity promoter profiling reveals widespread alternative promoter usage and transposon-driven developmental gene expression. Genes Dev. *23*, 169–180.

Bélanger, F., Stepinski, J., Darzynkiewicz, E., and Pelletier, J. (2010). Characterization of hMTr1, a human cap1 2′-O-ribose methyltransferase. J. Biol. Chem. *285*, 33037–33044.

Benarroch, D., Smith, P., and Shuman, S. (2008). Characterization of a trifunctional mimivirus mRNA capping enzyme and crystal structure of the RNA triphosphatase domain. Structure *16*, 501–512.

Bradrick, S.S., and Gromeier, M. (2009). Identification of gemin5 as a novel 7-methylguanosine cap-binding protein. PLoS One *4*, 1–10.

Calero, G., Wilson, K.F., Ly, T., Rios-Steiner, J.L., Clardy, J.C., and Cerione, R. a

(2002). Structural basis of m7GpppG binding to the nuclear cap-binding protein complex. Nat. Struct. Biol. *9*, 912–917.

Cartolano, M., Huettel, B., Hartwig, B., Reinhardt, R., and Schneeberger, K. (2016). cDNA library enrichment of full length transcripts for SMRT long read sequencing. PLoS One *11*, e0157779.

Castello, A., Fischer, B., Eichelbaum, K., Horos, R., Beckmann, B.M., Strein, C., Davey, N.E., Humphreys, D.T., Preiss, T., Steinmetz, L.M., et al. (2012). Insights into RNA biology from an atlas of mammalian mRNA-binding proteins. Cell *149*, 1393–1406.

Chang, J.H., Jiao, X., Chiba, K., Oh, C., Martin, C.E., Kiledjian, M., and Tong, L. (2012). Dxo1 is a new type of eukaryotic enzyme with both decapping and 5′-3′ exoribonuclease activity. Nat. Struct. Mol. Biol. *19*, 1011–1017.

Charley, P.A., Wilusz, C.J., and Wilusz, J. (2018). Identification of phlebovirus and arenavirus RNA sequences that stall and repress the exoribonuclease XRN1. J. Biol. Chem. *293*, 285–295.

Chen, P., Zhou, Z., Yao, X., Pang, S., Liu, M., Jiang, W., Jiang, J., and Zhang, Q. (2017). Capping enzyme mRNA-cap/RNGTT regulates hedgehog pathway activity by antagonizing protein kinase A. Sci. Rep. *7*, 2891.

Chiu, Y.-L., Ho, C.K., Saha, N., Schwer, B., Shuman, S., and Rana, T.M. (2002). Tat stimulates cotranscriptional capping of HIV mRNA. Mol. Cell *10*, 585–597.

Cowling, V.H. (2010a). Regulation of mRNA cap methylation. Biochem. J. *425*, 295–302.

Cowling, V.H. (2010b). Enhanced mRNA cap methylation increases cyclin D1 expression and promotes cell transformation. Oncogene *29*, 930–936.

van Deemter, J.J., Zuiderweg, F.J., and Klinkenberg, A. (1956). Longitudinal diffusion and resistance to mass transfer as causes of nonideality in chromatography. Chem. Eng. Sci. *5*, 271–289.

Djebali, S., Davis, C.A., Merkel, A., Dobin, A., Lassmann, T., Mortazavi, A., Tanzer, A., Lagarde, J., Lin, W., Schlesinger, F., et al. (2012). Landscape of transcription in human cells. Nature *489*, 101–108.

Ettwiller, L., Buswell, J., Yigit, E., and Schildkraut, I. (2016). A novel enrichment strategy reveals unprecedented number of novel transcription start sites at single base resolution in a model prokaryote and the gut microbiome. BMC Genomics *17*, 1–14.

Fang, Q., Inanc, B., Schamus, S., Wang, X.H., Wei, L., Brown, A.R., Svilar, D., Sugrue, K.F., Goellner, E.M., Zeng, X., et al. (2014). HSP90 regulates DNA repair via the interaction between XRCC1 and DNA polymerase β. Nat. Commun. *5*, 1–16.

Fattahi, S., Langroudi, M.P., and Akhavan-Niaki, H. (2018). Hedgehog signaling pathway: epigenetic regulation and role in disease and cancer development. J. Cell. Physiol. *TBD*, TBD.

Fejes-Toth, K., Sotirova, V., Sachidanandam, R., Assaf, G. Hannon, G.J., Kapranov, P.,

Foissac, S., Willingham, A.T., Dattagupta, R., Dumais, E., and Gingeras, T.R. (2009). Post-transcriptional processing generates a diversity of 5′-modified long and short RNAs. Nature *457*, 1028–1032.

Fensterl, V., and Sen, G.C. (2015). Interferon-induced Ifit proteins: Their role in viral pathogenesis. J. Virol. *89*, 2462–2468.

Ferron, F., Decroly, E., Selisko, B., and Canard, B. (2012). The viral RNA capping machinery as a target for antiviral drugs. Antiviral Res. *96*, 21–31.

Flaherty, S.M., Fortes, P., Izaurralde, E., Mattaj, I.W., and Gilmartin, G.M. (1997). Participation of the nuclear cap binding complex in pre-mRNA 3′ processing. Proc. Natl. Acad. Sci. *94*, 11893–11898.

Frese, S., Schubert, W.D., Findeis, A.C., Marquardt, T., Roske, Y.S., Stradal, T.E.B., and Heinz, D.W. (2006). The phosphotyrosine peptide binding specificity of Nck1 and Nck2 Src homology 2 domains. J. Biol. Chem. *281*, 18236–18245.

Fujimura, T., and Esteban, R. (2010). Yeast double-stranded RNA virus L-A deliberately synthesizes RNA transcripts with 5′-diphosphate. J. Biol. Chem. *285*, 22911–22918.

Furuichi, Y. (2015). Discovery of m(7)G-cap in eukaryotic mRNAs. Proc. Jpn. Acad. Ser. B. Phys. Biol. Sci. *91*, 394–409.

Furuichi, Y., Morgan, M., Muthukrishnan, S., and Shatkin, A.J. (1975a). Reovirus messenger RNA contains a methylated, blocked 5′-terminal structure: m7G(5′)ppp(5′)GmpCp-. Proc. Natl. Acad. Sci. U. S. A. *72*, 362–366.

Furuichi, Y., Morgan, M., Shatkin, a J., Jelinek, W., Salditt-Georgieff, M., and Darnell, J.E. (1975b). Methylated, blocked 5′ termini in HeLa cell mRNA. Proc. Natl. Acad. Sci. U. S. A. *72*, 1904–1908.

Gebhardt, A., Habjan, M., Benda, C., Meiler, A., Haas, D.A., Hein, M.Y., Mann, A., Mann, M., Habermann, B., and Pichlmair, A. (2015). mRNA export through an additional cap-binding complex consisting of NCBP1 and NCBP3. Nat. Commun. *6*, 1–13.

Ghosh, A., and Lima, C.D. (2010). Enzymology of RNA cap synthesis. Wiley Interdiscip. Rev. RNA *1*, 152–172.

Ghosh, A., Garee, G., Sweeny, E.A., Nakamura, Y., and Stuehr, D.J. (2018). Hsp90 chaperones hemoglobin maturation in erythroid and nonerythroid cells. Proc. Natl. Acad. Sci. 201717993.

Gilmartin, G.M., McDevitt, M.A., and Nevins, J.R. (1988). Multiple factors are required for poly(A) addition to a mRNA 3′ end. Genes Dev. *2*, 588–597.

Gonatopoulos-Pournatzis, T., and Cowling, V.H. (2014). Cap-binding complex (CBC). Biochem. J. *457*, 231–242.

Gonatopoulos-Pournatzis, T., Dunn, S., Bounds, R., and Cowling, V.H. (2011). RAM/Fam103a1 is required for mRNA cap methylation. Mol. Cell *44*, 585–596.

Grasso, L., Suska, O., Davidson, L., Gonatopoulos-Pournatzis, T., Williamson, R.,

Wasmus, L., Wiedlich, S., Peggie, M., Stavridis, M.P., and Cowling, V.H. (2016). mRNA Cap Methylation in Pluripotency and Differentiation. Cell Rep. *16*, 1352–1365.

Grudzien-Nogalska, E., and Kiledjian, M. (2017). New insights into decapping enzymes and selective mRNA decay. Wiley Interdiscip. Rev. RNA *8*, e1379.

Gu, W., Lee, H.C., Chaves, D., Youngman, E.M., Pazour, G.J., Conte, D., and Mello, C.C. (2012). CapSeq and CIP-TAP identify Pol II start sites and reveal capped small RNAs as C. elegans piRNA precursors. Cell *151*, 1488–1500.

Guiochon, G., Bressolle, F., and Siouffi, A. (1979). Study of the Performances of Thin Layer Chromatography IV — Optimization of Experimental Conditions. J. Chromatogr. Sci. *17*, 368–386.

von der Haar, T., Gross, J.D., Wagner, G., and McCarthy, J.E.G. (2004). The mRNA cap-binding protein eIF4E in post-transcriptional gene expression. Nat. Struct. Mol. Biol. *11*, 503–511.

Haline-Vaz, T., Lima Silva, T.C., and Zanchin, N.I.T. (2008). The human interferon-regulated ISG95 protein interacts with RNA polymerase II and shows methyltransferase activity. Biochem. Biophys. Res. Commun. *372*, 719–724.

Hall, M.P., and Ho, C.K. (2006). Characterization of a Trypanosoma brucei RNA cap (guanine N-7) methyltransferase. RNA *12*, 488–497.

Le Hir, H., Izaurralde, E., Izaurralde, E., Maquat, Le Hir, H., and Maquat (2000). The spliceosome deposits multiple proteins 20-24 nucleotides upstream of mRNA exon-exon junctions. EMBO J. *19*, 6860–6869.

Le Hir, H., Gatfield, D., Izaurralde, E., and Moore, M.J. (2001). The exon-exon junction complex provides a binding platform for factors involved in mRNA export and nonsense-mediated mRNA decay. EMBO J. *20*, 4987–4997.

Ho, C.K., Sriskanda, V., McCracken, S., Bentley, D., Schwer, B., and Shuman, S. (1998a). The guanylyltransferase domain of mammalian mRNA capping enzyme binds to the phosphorylated carboxyl-terminal domain of RNA polymerase II. J. Biol. Chem. *273*, 9577–9585.

Ho, C.K., Schwer, B., and Shuman, S. (1998b). Genetic, physical, and functional interactions between the triphosphatase and guanylyltransferase components of the yeast mRNA capping apparatus. Mol. Cell. Biol. *18*, 5189–5198.

Hornbeck, P. V., Chabra, I., Kornhauser, J.M., Skrzypek, E., and Zhang, B. (2004). PhosphoSite: A bioinformatics resource dedicated to physiological protein phosphorylation. Proteomics *4*, 1551–1561.

Hoskins, R.A., Landolin, J.M., Brown, J.B., Sandler, J.E., Takahashi, H., Lassmann, T., Yu, C., Booth, B.W., Zhang, D., Wan, K.H., et al. (2011). Genome-wide analysis of promoter architecture in Drosophila melanogaster. Genome Res. *21*, 182–192.

Hyde, J.L., and Diamond, M.S. (2015). Innate immune restriction and antagonism of viral RNA lacking 2′-O methylation. Virology *480*, 66–74.

Ignatochkina, A. V, Takagi, Y., Liu, Y., Nagata, K., and Ho, C.K. (2015). The messenger RNA decapping and recapping pathway in Trypanosoma. Proc. Natl. Acad. Sci. 201424909.

Izaurralde, E., Lewis, J., McGuigan, C., Jankowska, M., Darzynkiewicz, E., and Mattaj, I.W. (1994). A nuclear cap binding protein complex involved in pre-mRNA splicing. Cell *78*, 657–668.

Jarmolowski, A., Boelens, W.C., Izaurralde, E., and Mattaj, I.W. (1994). Nuclear export of different classes of RNA is mediated by specific factors. J. Cell Biol. *124*, 627–635.

Jiao, X., Chang, J.H., Kilic, T., Tong, L., and Kiledjian, M. (2013). A mammalian pre-mRNA 5′ end capping quality control mechanism and an unexpected link of capping to pre-mRNA processing. Mol. Cell *50*, 104–115.

Johnson, B., VanBlargan, L.A., Xu, W., White, J.P., Shan, C., Shi, P.Y., Zhang, R., Adhikari, J., Gross, M.L., Leung, D.W., et al. (2018). Human IFIT3 modulates IFIT1 RNA binding specificity and protein stability. Immunity *48*, 487–499.

Karagöz, G.E., and Rüdiger, S.G.D. (2015). Hsp90 interaction with clients. Trends Biochem. Sci. *40*, 117–125.

Kim, D.I., KC, B., Zhu, W., Motamedchaboki, K., Doye, V., and Roux, K.J. (2014). Probing nuclear pore complex architecture with proximity-dependent biotinylation. Proc. Natl. Acad. Sci. U. S. A. *111*, E2453-61.

Kiss, D.L., Oman, K., Bundschuh, R., and Schoenberg, D.R. (2015a). Uncapped 5′ ends of mRNAs targeted by cytoplasmic capping map to the vicinity of downstream CAGE tags. FEBS Lett. *589*, 279–284.

Kiss, D.L., Oman, K., Bundschuh, R., and Schoenberg, D.R. (2015b). Uncapped 5′ ends of mRNAs targeted by cytoplasmic capping map to the vicinity of downstream CAGE tags. FEBS Lett. *589*, 279–284.

Kiss, D.L., Oman, K.M., Dougherty, J. a., Mukherjee, C., Bundschuh, R., and Schoenberg, D.R. (2016). Cap homeostasis is independent of poly(A) tail length. Nucleic Acids Res. *44*, 304–314.

Kramer, S. (2017). The ApaH-like phosphatase TbALPH1 is the major mRNA decapping enzyme of trypanosomes. PLoS Pathog. *13*, 1–20.

Kuge, H., Brownlee, G.G., Gershon, P.D., and Richter, J.D. (1998). Cap ribose methylation of c-mos mRNA stimulates translation and oocyte maturation in Xenopus laevis. Nucleic Acids Res. *26*, 3208–3214.

Kumar, P., Sweeney, T.R., Skabkin, M.A., Skabkina, O. V., Hellen, C.U.T., and Pestova, T. V. (2014). Inhibition of translation by IFIT family members is determined by their ability to interact selectively with the 5′-terminal regions of cap0-, cap1- and 5′ppp-mRNAs. Nucleic Acids Res. *42*, 3228–3245.

Kumar, P., Hellen, C.U.T., and Pestova, T. V. (2016). Toward the mechanism of eIF4F-mediated ribosomal attachment to mammalian capped mRNAs. Genes Dev. *30*, 1573–

1588.

Kyrieleis, O.J.P., Chang, J., De La Peña, M., Shuman, S., and Cusack, S. (2014). Crystal structure of vaccinia virus mRNA capping enzyme provides insights into the mechanism and evolution of the capping apparatus. Structure *22*, 452–465.

Langberg, S.R., and Moss, B. (1981). Post-transcriptional modifications of mRNA: Purification and characterization of cap I and cap II RNA (nucleoside-2′-)-methyltransferases from HeLa cells. J. Biol. Chem. *256*, 10054–10060.

Lee, A.S.Y., Kranzusch, P.J., Doudna, J.A., and Cate, J.H.D. (2016). eIF3d is an mRNA cap-binding protein that is required for specialized translation initiation. Nature *536*, 96–99.

Lim, S.K., and Maquat, L.E. (1992). Human beta-globin mRNAs that harbor a nonsense codon are degraded in murine erythroid tissues to intermediates lacking regions of exon I or exons I and II that have a cap-like structure at the 5′ termini. EMBO J. *11*, 3271–3278.

Lim, S., Mullins, J.J., Chen, C.M., Gross, K.W., and Maquat, L.E. (1989). Novel metabolism of several beta zero-thalassemic beta-globin mRNAs in the erythroid tissues of transgenic mice. EMBO J. *8*, 2613–2619.

Lim, S.K., Sigmund, C.D., Gross, K.W., and Maquat, L.E. (1992). Nonsense codons in human beta-globin mRNA result in the production of mRNA degradation products. Mol. Cell. Biol. *12*, 1149–1161.

Luciano, D.J., Vasilyev, N., Richards, J., Serganov, A., and Belasco, J.G. (2017). A novel RNA phosphorylation state enables 5′ end-dependent degradation in Escherichia coli. Mol. Cell *67*, 44–54.e6.

Machida, R.J., and Lin, Y.Y. (2014). Four methods of preparing mRNA 5′ end libraries using the illumina sequencing platform. PLoS One *9*.

Marcotrigiano, J., Gingras, A.C., Sonenberg, N., and Burley, S.K. (1997). Cocrystal structure of the messenger RNA 5′ cap-binding protein (eIF4E) bound to 7-methyl-GDP. Cell *89*, 951–961.

Mascarenhas, R., Dougherty, J.A., and Schoenberg, D.R. (2013). SMG6 cleavage generates metastable decay intermediates from nonsense-containing β-globin mRNA. PLoS One *8*, e74791.

Mauer, J., Luo, X., Blanjoie, A., Jiao, X., Grozhik, A. V., Patil, D.P., Linder, B., Pickering, B.F., Vasseur, J.J., Chen, Q., et al. (2017). Reversible methylation of m6Am in the 5′ cap controls mRNA stability. Nature *541*, 371–375.

Mayr, C. (2017). Regulation by 3′-untranslated regions. Annu. Rev. Genet. *51*, 171–194.

Mercer, T.R., Dinger, M.E., Bracken, C.P., Kolle, G., Szubert, J.M., Korbie, D.J., Askarian-Amiri, M.E., Gardiner, B.B., Goodall, G.J., Grimmond, S.M., et al. (2010). Regulated post-transcriptional RNA cleavage diversifies the eukaryotic transcriptome. Genome Res. *20*, 1639–1650.

Mercer, T.R., Wilhelm, D., Dinger, M.E., Soldà, G., Korbie, D.J., Glazov, E.A., Truong,

V., Schwenke, M., Simons, C., Matthaei, K.I., et al. (2011). Expression of distinct RNAs from 3′ untranslated regions. Nucleic Acids Res. *39*, 2393–2403.

Moon, S.L., Blackinton, J.G., Anderson, J.R., Dozier, M.K., Dodd, B.J.T., Keene, J.D., Wilusz, C.J., Bradrick, S.S., and Wilusz, J. (2015). XRN1 stalling in the 5′ UTR of hepatitis C virus and bovine viral diarrhea virus is associated with dysregulated host mRNA stability. PLoS Pathog. *11*, 1–21.

Moss, B. (2017). Investigating viruses during the transformation of molecular biology. J. Biol. Chem. *292*, 3958–3969.

Muhlrad, D., Decker, C.J., and Parker, R. (1994). Deadenylation of the unstable mRNA encoded by the yeast MFA2 gene leads to decappmg followed by 5′-->3′ digestion of the transcript. Genes Dev. Dev. *8*, 855–866.

Mukherjee, C., Patil, D.P., Kennedy, B.A., Bakthavachalu, B., Bundschuh, R., and Schoenberg, D.R. (2012). Identification of cytoplasmic capping targets reveals a role for cap homeostasis in translation and mRNA stability. Cell Rep. *2*, 674–684.

Mukherjee, C., Bakthavachalu, B., and Schoenberg, D.R. (2014). The cytoplasmic capping complex assembles on adapter protein Nck1 bound to the proline-rich C-terminus of mammalian capping enzyme. PLoS Biol. *12*, e1001933.

Mullen, N.J., and Price, D.H. (2017). Hydrogen peroxide yields mechanistic insights into human mRNA capping enzyme function. PLoS One *12*, 1–15.

Ni, T., Corcoran, D.L., Rach, E.A., Song, S., Spana, E.P., Gao, Y., Ohler, U., and Zhu, J. (2010). A paired-end sequencing strategy to map the complex landscape of transcription initiation. Nat. Methods *7*, 521–527.

Niedzwiecka, A., Marcotrigiano, J., Stepinski, J., Jankowska-Anyszka, M., Wyslouch-Cieszynska, A., Dadlez, M., Gingras, A.C., Mak, P., Darzynkiewicz, E., Sonenberg, N., et al. (2002). Biophysical studies of eIF4E cap-binding protein: Recognition of mRNA 5′ cap structure and synthetic fragments of eIF4G and 4E-BP1 proteins. J. Mol. Biol. *319*, 615–635.

Ohira, T., and Suzuki, T. (2016). Precursors of tRNAs are stabilized by methylguanosine cap structures. Nat. Chem. Biol. *12*, 648–655.

Otsuka, Y., Kedersha, N.L., and Schoenberg, D.R. (2009). Identification of a cytoplasmic complex that adds a cap onto 5′-monophosphate RNA. Mol. Cell. Biol. *29*, 2155–2167.

Panayiotou, C., Solaroli, N., and Karlsson, A. (2014). The many isoforms of human adenylate kinases. Int. J. Biochem. Cell Biol. *49*, 75–83.

Peyrane, F., Selisko, B., Decroly, E., Vasseur, J.J., Benarroch, D., Canard, B., and Alvarez, K. (2007). High-yield production of short GpppA- and 7MeGpppA-capped RNAs and HPLC-monitoring of methyltransfer reactions at the guanine-N7 and adenosine-2′O positions. Nucleic Acids Res. *35*, e26.

Pillutla, R.C., Yue, Z., Maldonado, E., and Shatkin, A.J. (1998). Recombinant human mRNA cap methyltransferase binds capping enzyme/RNA polymerase IIo complexes. J.

Biol. Chem. *273*, 21443–21446.

Prodromou, C. (2016). Mechanisms of Hsp90 regulation. Biochem. J. *473*, 2439–2452.

Ramanathan, A., Robb, G.B., and Chan, S.-H. (2016). mRNA capping: biological functions and applications. Nucleic Acids Res. *44*, 7511–7526.

Rangaraju, V., tom Dieck, S., and Schuman, E.M. (2017). Local translation in neuronal compartments: how local is local? EMBO Rep. *18*, 693–711.

Reyes, A., and Huber, W. (2018). Alternative start and termination sites of transcription drive most transcript isoform differences across human tissues. Nucleic Acids Res. *46*, 582–592.

Röhl, A., Rohrberg, J., and Buchner, J. (2013). The chaperone Hsp90: Changing partners for demanding clients. Trends Biochem. Sci. *38*, 253–262.

Roux, K.J., Kim, D.I., Raida, M., and Burke, B. (2012). A promiscuous biotin ligase fusion protein identifies proximal and interacting proteins in mammalian cells. J. Cell Biol. *196*, 801–810.

Saha, N., Schwer, B., and Shuman, S. (1999). Characterization of human, Schizosaccharomyces pombe, and Candida albicans mRNA cap methyltransferases and complete replacement of the yeast capping apparatus by mammalian enzymes. J. Biol. Chem. *274*, 16553–16562.

Schmidt, S.A., Foley, P.L., Jeong, D.H., Rymarquis, L.A., Doyle, F., Tenenbaum, S.A., Belasco, J.G., and Green, P.J. (2015). Identification of SMG6 cleavage sites and a preferred RNA cleavage motif by global analysis of endogenous NMD targets in human cells. Nucleic Acids Res. *43*, 309–323.

Schoenberg, D.R., and Maquat, L.E. (2009). Re-capping the message. Trends Biochem. Sci. *34*, 435–442.

Schuberth-Wagner, C., Ludwig, J., Bruder, A.K., Herzner, A.-M., Zillinger, T., Goldeck, M., Schmidt, T., Schmid-Burgk, J.L., Kerber, R., Wolter, S., et al. (2015). A conserved histidine in the RNA sensor RIG-I controls immune tolerance to N1-2′O-methylated self RNA. Immunity 41–51.

Schwer, B., and Shuman, S. (1996). Conditional inactivation of mRNA capping enzyme affects yeast pre-mRNA splicing in vivo. RNA *2*, 574–583.

Shafer, B., Chu, C., and Shatkin, A.J. (2005). Human mRNA cap methyltransferase: alternative nuclear localization signal motifs ensure nuclear localization required for viability. Mol. Cell. Biol. *25*, 2644–2649.

Sheinberger, J., and Shav-Tal, Y. (2017). mRNPs meet stress granules. FEBS Lett. *591*, 2534–2542.

Shiraki, T., Kondo, S., Katayama, S., Waki, K., Kasukawa, T., Kawaji, H., Kodzius, R., Watahiki, A., Nakamura, M., Arakawa, T., et al. (2003). Cap analysis gene expression for high-throughput analysis of transcriptional starting point and identification of promoter usage. Proc. Natl. Acad. Sci. U. S. A. *100*, 15776–15781.

Snijder, E.J., Decroly, E., and Ziebuhr, J. (2016). The nonstructural proteins directing coronavirus RNA synthesis and processing (Elsevier Inc.).

Song, M.G., Li, Y., and Kiledjian, M. (2010). Multiple mRNA decapping enzymes in mammalian cells. Mol. Cell *40*, 423–432.

Song, M.G., Bail, S., and Kiledjian, M. (2013). Multiple Nudix family proteins possess mRNA decapping activity. RNA *19*, 390–399.

Spencer, E., Loring, D., Hurwitz, J., and Monroy, G. (1978). Enzymatic conversion of 5′-phosphate-terminated RNA to 5′-di- and triphosphate-terminated RNA. Proc. Natl. Acad. Sci. U. S. A. *75*, 4793–4797.

Srere, P. (1987). Complexes of sequential metabolic enzymes. Annu. Rev. Biochem. *56*, 89–124.

Srere, P.A. (1985). The metabolon. Trends Biochem. Sci. *10*, 109–110.

Srinivasa, S., Ding, X., and Kast, J. (2015). Formaldehyde cross-linking and structural proteomics: bridging the gap (in press). Methods.

Stevens, A., Wang, Y., Bremer, K., Zhang, J., Hoepfner, R., Antoniou, M., Schoenberg, D.R., and Maquat, L.E. (2002). Beta-globin mRNA decay in erythroid cells: UG site-preferred endonucleolytic cleavage that is augmented by a premature termination codon. Proc. Natl. Acad. Sci. U. S. A. *99*, 12741–12746.

Suzuki, Y., Minami, M., Suzuki, M., Abe, K., Zenno, S., Tsujimoto, M., Matsumoto, K., and Minami, Y. (2009). The Hsp90 inhibitor geldanamycin abrogates colocalization of eIF4E and eIF4E-transporter into stress granules and association of eIF4E with eIF4G. J. Biol. Chem. *284*, 35597–35604.

Tago, K., Tsukahara, F., Naruse, M., Yoshioka, T., and Takano, K. (2004). Regulation of nuclear retention of glucocorticoid receptor by nuclear Hsp90. Mol. Cell. Endocrinol. *213*, 131–138.

Tagwerker, C., Flick, K., Cui, M., Guerrero, C., Dou, Y., Auer, B., Baldi, P., Huang, L., and Kaiser, P. (2006). A tandem affinity tag for two-step purification under fully denaturing conditions. Mol. Cell. Proteomics *5*, 737–748.

Takagi, Y., Sindkar, S., Ekonomidis, D., Hall, M.P., and Ho, C.K. (2007). Trypanosoma brucei encodes a bifunctional capping enzyme essential for cap 4 formation on the spliced leader RNA. J. Biol. Chem. *282*, 15995–16005.

Tamarkin-Ben-Harush, A., Vasseur, J.J., Debart, F., Ulitsky, I., and Dikstein, R. (2017). Cap-proximal nucleotides via differential eIF4E binding and alternative promoter usage mediate translational response to energy stress. Elife *6*, 1–21.

Thul, P.J., Åkesson, L., Wiking, M., Mahdessian, D., Geladaki, A., Ait Blal, H., Alm, T., Asplund, A., Björk, L., Breckels, L.M., et al. (2017). A subcellular map of the human proteome. Science (80-.). *356*, eaal3321.

Trotman, J.B., and Schoenberg, D.R. (2018). RNA cap methyltransferase activity assay. Bio-Protocol *8*, e2767.

Trotman, J.B., Giltmier, A.J., Mukherjee, C., and Schoenberg, D.R. (2017). RNA guanine-7 methyltransferase catalyzes the methylation of cytoplasmically recapped RNAs. Nucleic Acids Res. *45*, 10726–10739.

Ullrich, S.J., Moore, S.K., and Appella, E. (1989). Transcriptional and translational analysis of the murine 84- 86-kDa heat shock proteins. J. Biol. Chem. *264*, 6810–6816.

Varshney, D., Petit, A.P., Bueren-Calabuig, J.A., Jansen, C., Fletcher, D.A., Peggie, M., Weidlich, S., Scullion, P., Pisliakov, A. V., and Cowling, V.H. (2016). Molecular basis of RNA guanine-7 methyltransferase (RNMT) activation by RAM. Nucleic Acids Res. *44*, 10423–10436.

Visa, N., Izaurralde, E., Ferreira, J., Daneholt, B., and Mattaj, I.W. (1996). A nuclear cap-binding complex binds Balbiani ring pre-mRNA cotranscriptionally and accompanies the ribonucleoprotein particle during nuclear export. J. Cell Biol. *133*, 5–14.

Wei, C.M., and Moss, B. (1975). Methylated nucleotides block 5′-terminus of vaccinia virus messenger RNA. Proc. Natl. Acad. Sci. U. S. A. *72*, 318–322.

Weill, L., Belloc, E., Bava, F.A., and Méndez, R. (2012). Translational control by changes in poly(A) tail length: Recycling mRNAs. Nat. Struct. Mol. Biol. *19*, 577–585.

Wen, Y., Yue, Z., and Shatkin, A.J. (1998). Mammalian capping enzyme binds RNA and uses protein tyrosine phosphatase mechanism. Proc. Natl. Acad. Sci. U. S. A. *95*, 12226–12231.

Werner, M., Purta, E., Kaminska, K.H., Cymerman, I.A., Campbell, D.A., Mittra, B., Zamudio, J.R., Sturm, N.R., Jaworski, J., and Bujnicki, J.M. (2011). 2′-O-ribose methylation of cap2 in human: Function and evolution in a horizontally mobile family. Nucleic Acids Res. *39*, 4756–4768.

Whitesell, L., and Lindquist, S.L. (2005). HSP90 and the chaperoning of cancer. Nat. Rev. Cancer *5*, 761–772.

Wu, F., and Minteer, S. (2015). Krebs cycle metabolon: structural evidence of substrate channeling revealed by cross-linking and mass spectrometry. Angew. Chemie Int. Ed. *54*, 1851–1854.

Wu, B., Eliscovich, C., Yoon, Y.J., and Singer, R.H. (2016). Translation dynamics of single mRNAs in live cells and neurons. Science (80-.). *352*, 1430–1435.

Yan, X., Hoek, T.A., Vale, R.D., and Tanenbaum, M.E. (2016). Dynamics of translation of single mRNA molecules in vivo. Cell *165*, 976–989.

Yang, Z., Liang, H., Zhou, Q., Li, Y., Chen, H., Ye, W., Chen, D., Fleming, J., Shu, H., and Liu, Y. (2012). Crystal structure of ISG54 reveals a novel RNA binding structure and potential functional mechanisms. Cell Res. *22*, 1328–1338.

Youn, J.-Y., Dunham, W.H., Hong, S.J., Knight, J.D.R., Bashkurov, M., Chen, G.I., Bagci, H., Rathod, B., MacLeod, G., Eng, S.W.M., et al. (2018). High-density proximity mapping reveals the subcellular organization of mRNA-associated granules and bodies. Mol. Cell 1–16.

Yue, Z., Maldonado, E., Pillutla, R., Cho, H., Reinberg, D., and Shatkin, a J. (1997). Mammalian capping enzyme complements mutant Saccharomyces cerevisiae lacking mRNA guanylyltransferase and selectively binds the elongating form of RNA polymerase II. Proc. Natl. Acad. Sci. U. S. A. *94*, 12898–12903.

Appendix A. Supplementary Material for Chapter 2

Supplementary Materials and Methods

Plasmid Constructs

Primer sequences can be found in Table 2. To generate pGEX-2T-RNMT, the human RNMT coding sequence (amino acids 2-476) was PCR-amplified from pET16b-His-RNMT (provided by Stuart Shuman, Sloan Kettering; (Saha et al., 1999)) using primers JT6 and JT8 and inserted into EcoRI-digested pGEX-2T (GE Healthcare 28-9546-53) via In-Fusion cloning (Clontech). To generate pcDNA3-FLAG-RNMT, human RNMT with an N-terminal FLAG tag and linker sequence AGCAGCGGCCATATCGAAGGTCGTCAT was PCR-amplified using primers JT62 and JT63 and inserted into KpnI-digested pcDNA3. pcDNA3-FLAG-RNMT 1-120 was generated by PCR-amplifying FLAG-RNMT 1-120 from pcDNA3-FLAG-RNMT with primers JT62 and JT76 and inserting into KpnI-digested pcDNA3. pcDNA3-FLAG-RNMT 121-476 was generated via Change-IT site-directed mutagenesis (Affymetrix) using 5′-phosphorylated primer JT77 to delete RNMT amino acids 1-120 from pcDNA3-FLAG-RNMT. To generate pcDNA3-FLAG-NES-RNMT 121-476 D203A ("ΔN-RNMT"), pcDNA3-FLAG-RNMT 121-476 was used as a template for Change-IT SDM using 5′-phosphorylated primer JT121 to introduce the HIV-1 Rev NES and 5′-phosphorylated primer JT122 to mutate aspartic acid 203 to alanine. pET28b-His-CE was generated by PCR-amplifying the human CE coding region (amino acids 2-596) from pET21a-hCE (provided by David Price, University of Iowa; (Moteki and Price, 2002))

using primers JT10 and JT11 and inserting this into NheI-digested pET28b. The stop codon engineered at the very C-terminus of CE prevented tagging its C-terminus with the T7 tag encoded downstream in the pET28b sequence. To generate pcDNA3.1-myc-BirA*-cCE, pcDNA3.1-myc-BirA* (Addgene plasmid #35700, (Roux et al., 2012)) was first modified via Change-IT SDM using 5′-phosphorylated primer JT91 to change the NotI restriction site to a BsrGI restriction site, resulting in the plasmid pcDNA3.1-myc-BirA*-BsrGI. pcDNA3.1-myc-BirA*-cCE was generated by PCR-amplifying the cCE sequence from pcDNA3/TO-myc-cCE-bio (Mukherjee et al., 2014) using primers JT65 and JT92 and inserting into XhoI-digested pcDNA3.1-myc-BirA*-BsrGI. To generate pGEX-2T-eIF4E K119A, pGEX-2T-meIF4E (provided by Jerry Pelletier, McGill University) was modified by SDM. The following plasmids were described previously: pcDNA4/TO-myc-GFP-FLAG (Otsuka et al., 2009), pQCXIP-MS2-bio (provided by Marian Waterman, University of California Irvine; (Tsai et al., 2011)), pcDNA3-bio-myc-mCE (bio-CE) and pcDNA3-bio-myc-NES-mCE ΔNLS (bio-cCE) (Mukherjee et al., 2014), pECE-EGFP-bio (provided by Harold Fisk, The Ohio State University; (Sawant et al., 2015)).

Immunofluorescence Microscopy

U2OS cells grown on glass coverslips were fixed in ice-cold methanol for 20 min. Coverslips were washed three times with PBS before blocking in IF Block Solution (PBS containing 1% (w/v) BSA and 0.05% (v/v) Triton X-100) at room temperature for 90 min. Primary antibodies were added to appropriate dilutions (see Antibodies section) and

incubated at 4 °C overnight. Coverslips were washed three times for 5 min with IF Wash Buffer (PBS containing 0.5 mM $MgCl_2$ and 0.05% (v/v) Triton X-100) and then incubated in the dark at room temperature for 60 min in IF Block Buffer containing a 1:1000 dilution of anti-rabbit Alexa Fluor 488 conjugate secondary antibody (Thermo Fisher A11008) and 0.75 μg/mL DAPI. Coverslips were washed three times with IF Wash Buffer as before, mounted on glass microscope slides with ProLong Gold Antifade Mountant (Thermo Fisher P36930), and incubated in the dark at room temperature overnight to allow the mountant to cure. Images were acquired at room temperature with a Nikon Eclipse Ti-U inverted microscope fitted with a CFI Plan Apo VC 60X oil immersion objective and a Nikon DS-Qi1 monochrome digital camera. Images were analyzed using Nikon NIS-Elements AR 3.10 software. Specificity of the secondary antibody for the primary antibodies was confirmed by parallel preparation of control coverslips not treated with primary antibody.

Transfection and Subcellular Fractionation

Prior to transfection, cells were given fresh, pre-warmed medium. HEK293 cells were 60-70% confluent at time of transfection with 10 μg plasmid DNA per 10-cm dish using jetPRIME transfection reagent (Polyplus 114-15) according to manufacturer′s protocol. Cells were cultured 48 h before being harvested. U2OS cells were 70-75% confluent at time of transfection with 6 μg plasmid DNA per 10-cm dish using FuGENE 6 transfection reagent (Promega E2691) according to manufacturer′s protocol. These cells were then cultured 24 h before being harvested. One 10-cm dish of U2OS cells was used

per siRNA treatment. At the time of the first siRNA transfection, cells were 50% confluent. Transfection mixtures were prepared with jetPRIME transfection reagent (Polyplus) and added to culture medium to bring siRNA to a concentration of 10 nM. After 24 h, the culture medium was removed, and the same procedure was repeated for a second transfection. After another 24 h, the cells were harvested. Trilencer-27 siRNAs (OriGene) used in this study are as follows: universal scrambled control siRNA (SR30004), RNMT siRNA (SR305750B), RAM siRNA (SR313193A). To harvest, cells were washed with PBS and then scraped into 1 mL PBS. After centrifugation at 70 x g for 10 min at 4 °C, pellets were resuspended in 5 to 10 volumes of ice-cold YO Lysis Buffer (10 mM HEPES pH 7.3, 10 mM KCl, 10 mM $MgCl_2$, 0.2% (v/v) IGEPAL CA-630, 2 mM DTT, 0.5 mM PMSF, 7.5 µL/mL protease inhibitor cocktail (Sigma P8340), 7.5 µL/mL phosphatase inhibitor cocktail 2 (Sigma P5726), 7.5 µL/mL phosphatase inhibitor cocktail 3 (Sigma P0044)) by pipetting 10 times. Resuspended cells were incubated on ice for 10 min, pipetted 5 times, and centrifuged at 16,100 x g for 10 min at 4 °C. The supernatants (cytoplasmic extracts) were removed and kept on ice. Residual supernatants were completely removed from the nuclear pellets before resuspending in 4 to 10 cell-pellet volumes of ice-cold YO Buffer A (10 mM HEPES pH 7.3, 25% (v/v) glycerol, 420 mM NaCl, 1.5 mM $MgCl_2$, 0.2 mM EDTA, 1 mM DTT, 0.5 mM PMSF, 7.5 µL/mL protease inhibitor cocktail (Sigma), 7.5 µL/mL phosphatase inhibitor cocktail 2 (Sigma), 7.5 µL/mL phosphatase inhibitor cocktail 3 (Sigma)) by pipetting 15 times. This was incubated end-over-end for 20 min at 4 °C and then centrifuged (16,100 x g for 5 min at 4 °C) to pellet nuclear debris. Supernatants (nuclear extracts) were removed and

kept on ice. Total protein concentration in each extract was determined by Bradford assay using Bio-Rad Protein Assay Dye Reagent (Bio-Rad 5000006) normalized against a standard curve of BSA (Fisher Scientific BP1600-100). For cap methyltransferase activity assays, nuclear and cytoplasmic extracts were brought to the same buffer composition (Combo Buffer) by diluting to 50% with YO Lysis Buffer or YO Buffer A, respectively, and stored in small aliquots at -80 °C. For SDS-PAGE analysis, extracts were diluted to 75% with 4X Laemmli Sample Buffer.

Antibodies

Primary antibodies used in this study are as follows: rabbit polyclonal anti-RNMT antibody (Proteintech 13743-1-AP; 1:25 for IF, 1:500 for WB, 4 ng/µL for IP), normal rabbit IgG antibody (Santa Cruz sc-2027; 4 ng/µL for IP), rabbit polyclonal anti-RAM/FAM103A1 antibody (Proteintech 19422-1-AP; 1:25 for IF, 1:1000 for WB), rabbit polyclonal anti-nucleolin (Sigma N2662; 1:5000 for WB), rabbit polyclonal anti-U2AF35 (provided by Brenton Graveley, University of Connecticut, (Zuo and Maniatis, 1996); 1:3000 for WB), mouse monoclonal anti-α-tubulin (Sigma T6199; 1:10,000 for WB), mouse monoclonal anti-GAPDH (Sigma G8795; 1:10,000 for WB), rabbit polyclonal anti-phosphothreonine (Stressmarq SPC-154F; 1:125 for WB), rabbit polyclonal anti-CE (Novus NBP1-49973; 1:2000 for WB), mouse monoclonal anti-FLAG (Sigma F3165; 1:1000 for WB), mouse monoclonal c-myc IgG antibody (Santa Cruz sc-40, 1:2000 for WB). Secondary antibodies used in this study are as follows: anti-rabbit Alexa Fluor 680 (Thermo Fisher A21109; 1:10,000 for WB), anti-mouse Alexa Fluor 680

(Thermo Fisher A21057; 1:10,000 for WB), anti-mouse DyLight 800 (Rockland 610-145-121; 1:10,000 for WB), anti-rabbit Alexa Fluor 488 (Thermo Fisher A11008; 1:1000 for IF). For the detection of biotinylated proteins, Qdot 800 streptavidin (Thermo Fisher Q10171MP; 1:10,000 for WB) was used.

SDS-PAGE and Western Blot Analysis

Samples were heated at 95 °C for 5 min and briefly centrifuged prior to loading Bio-Rad Mini-PROTEAN TGX precast gels alongside pre-stained protein standards (Bio-Rad 1610373). Between 10 and 20 μg of nuclear or cytoplasmic extract was typically loaded per lane, and the same mass amount was always loaded when comparing nuclear and cytoplasmic extracts. SDS-PAGE was run at 150 V in Tris-glycine buffer containing 0.1% (w/v) SDS. For Coomassie staining, gels were washed three times in water and incubated in GelCode Blue Stain Reagent (Thermo Fisher 24590) for at least 1 h. Gels were destained with water and imaged with an Odyssey infrared imager (Li-Cor) at 700 nm. For Western blot analysis, electrophoresed proteins were transferred to Immobilon-FL (EMD Millipore IPFL00010) PVDF membranes at 100 V for 70 min at 4 °C. Membranes were blocked in Blocking Buffer (TBS containing 3% (w/v) BSA) for at least 30 min at room temperature. For primary antibody incubations, membranes were incubated overnight at 4 °C in Blocking Buffer containing antibody at the dilution indicated in the Antibodies section. Membranes were washed three times in TBST at room temperature, 10 min per wash. For secondary antibody incubations, membranes were incubated for 45 min at room temperature in Blocking Buffer containing appropriate

antibody at the dilution indicated in the Antibodies section. Membranes were washed in TBST as before and imaged with an Odyssey infrared imager (Li-Cor) at the appropriate wavelength.

Preparation of GST and GST-RNMT

Escherichia coli BL21(DE3)pLysS competent cells (Promega) were transformed with either pGEX-2T or pGEX-2T-RNMT. These cells were grown to OD_{600} of 0.5 in 400 mL lysogeny broth (LB) containing 100 μg/mL ampicillin sodium salt and 34 μg/mL chloramphenicol before inducing protein expression by adding isopropyl β-D-1-thiogalactopyranoside (IPTG) to 0.5 mM. Cells were cultured for 17 h at 25 °C (GST) or 17 °C (GST-RNMT) before harvesting by centrifugation. Pelleted cells were resuspended in GST Lysis Buffer (20 mM Tris pH 7.5, 20 mM NaCl, 1% (v/v) Triton X-100, 2 mM DTT, 1X SigmaFast EDTA-free Protease Inhibitor Cocktail (Sigma S8830), 50 μg/mL lysozyme) and lysed by sonication. Lysates were pre-cleared twice by centrifugation at 15,000 rpm at 4 °C for 20 min before adding 1 mL bead-volume glutathione Sepharose 4B beads (GE Healthcare 17075601). Mixtures were incubated end-over-end at 4 °C for 2 h before washing the protein-bound beads with 15 mL GST Wash Buffer (25 mM Tris pH 7.5, 150 mM NaCl, 0.1% (v/v) Triton X-100) by gravity flow. Protein-bound beads were resuspended in GST Wash Buffer containing 20% (v/v) glycerol and 1X SigmaFast EDTA-free Protease Inhibitor Cocktail (Sigma) and stored at -80 °C in small aliquots.

Preparation of GST-eIF4E K119A

E. coli BL21(DE3)pLysS competent cells (Promega) were transformed with pGEX-2T-eIF4E K119A and expressed and purified as described for GST (above), with the exception that after washing the protein-bound beads, the beads were incubated end-over-end three successive times with 500 µL GST Elution Buffer (50 mM Tris pH 8.0, 100 mM NaCl, 1 mM DTT, 10 mM glutathione, 1X SigmaFast EDTA-free Protease Inhibitor Cocktail (Sigma), 20% (v/v) glycerol) at 4 °C for 5 min. The eluates were pooled and buffer-exchanged into the same buffer lacking glutathione using an Amicon Ultra-15 10K centrifugal filter unit (EMD Millipore UFC901024). This final preparation was stored at -80 °C in small aliquots.

Preparation of His-CE

E. coli BL21(DE3)pLysS competent cells were transformed with pET28b-His-CE and grown to OD_{600} of 0.5 in 400 mL LB containing 35 µg/mL kanamycin sulfate and 34 µg/mL chloramphenicol. Protein expression was induced by adding IPTG to 0.4 mM and culturing for 19 h at 17 °C. Cells were pelleted by centrifugation and resuspended in His Lysis Buffer (50 mM Tris pH 7.5, 200 mM NaCl, 10% (w/v) sucrose, 0.1% (v/v) Triton X-100, 1X SigmaFast EDTA-free Protease Inhibitor Cocktail (Sigma), 50 µg/mL lysozyme) before lysing by sonication. Lysates were pre-cleared twice by centrifugation at 15,000 rpm at 4 °C for 20 min. To the pre-cleared lysate, imidazole (pH 7.5) was added to 10 mM, and 400 µL bead-volume of TALON-agarose beads (Clontech 635501) was added. The mixture was incubated end-over-end at 4 °C for 2 h, and the protein-bound beads were washed with 4 mL His Wash Buffer (50 mM Tris pH 7.5, 200 mM

NaCl, 10% (w/v) sucrose, 0.1% (v/v) Triton X-100, 25 mM imidazole) by gravity flow. Bead-bound proteins were eluted in successive 1-mL fractions with Elution Buffer (50 mM Tris pH 8.0, 100 mM NaCl, 10% (v/v) glycerol) containing increasing concentrations of imidazole (50, 75, 100, 200, and 750 mM). The purity and yield of each fraction was analyzed by SDS-PAGE and Coomassie staining, and the desired fractions were pooled. The pooled fractions were buffer-exchanged into His Storage Buffer (50 mM Tris pH 8.0, 100 mM NaCl, 10% (v/v) glycerol, 1X SigmaFast EDTA-free Protease Inhibitor Cocktail (Sigma)) and concentrated using an Amicon Ultra-15 10K centrifugal filter unit (EMD Millipore). This final preparation was stored at -80 °C in small aliquots.

Generation of G-Capped Luciferase RNA

To generate G-capped luciferase control RNA, 10 pmol 5′-triphosphate Luciferase Control RNA (Promega L4561) was incubated at 30 °C for 95 min in a 20-µL in-vitro capping reaction containing 10 mM Tris-HCl pH 7.5, 3 mM $MgCl_2$, 1 mM DTT, 0.1 mM EDTA, 20% (v/v) glycerol, 10 nmol GTP and 1 pmol recombinant His-CE. The reaction was heat-inactivated at 65 °C for 10 min before purifying the RNA with the RNA Clean & Concentrator-5 kit (Zymo Research). Concentration and purity of the prepared RNA were confirmed with a NanoDrop ND-1000 spectrophotometer and by urea-PAGE.

Name	Forward or Reverse	Sequence (5' to 3')
JT6	Forward	GATCCCCGGGAATTCATGCAAATTCTGCAAAAGCAGAAGAAT
JT8	Reverse	CAGTCACGATGAATTTCACTGCTGTTTCTCAAAGGCAAAC
JT10	Forward	CAGCCATATGGCTAGCGCTCACAACAAGATCCCGCC
JT11	Reverse	CACCAGTCATGCTAGTTATTAGGTTAAAGGGTGTGGTCTTTTGGGA
JT62	Forward	GGAGACCCAAGCTTGATGGGCGACTACAAAGACGATGACGACAAG
JT63	Reverse	GTGGATCCGAGCTCGTCATCACTGCTGTTTCTCAAAGGCAAACACCAA
JT65	Forward	CGCAGAGAAGCTCGAGCTTCAGCTACCACCGCTTGAGAGAC
JT76	Reverse	GTGGATCCGAGCTCGTCATCATCCAGTAGAAGATTTATCTTTTGGAACATC CTCAGTTTC
JT77	Forward	CAGCGGCCATATCGAAGGTCGTCATGATGGCACTCAAAATAAGAGAAAAA TAGCA
JT91	Forward	CCTGAGAAGCGCAGAGAAGCTCGAGTGTACACCACTGTGCTGGATATCT GCAGAAT
JT92	Reverse	GTGGTGTACACTCGAGTCATCAGGTTGGCCGATGCAGTCTTTTGGGC
JT121	Reverse	ATGACGACCTTCGATATGGCCATCAAGAGTAAGTCTCTCAAGCGGTGGTA GCTGAAGGCTGCTCTTGTCGTCATCGTC
JT122	Forward	CGACAGAAGAAAAAACGTGATATCACTGTTTTGGCCCTGGGATGTGGTAA AGGTGGAGAT

Table 2. Primers for plasmid construction.

Transcript Symbol	Transcript Name	Oligo Name	Forward or Reverse	Sequence (5' to 3')
EGFP	Enhanced green fluorescent protein	DLK327	Forward	ATGGTGAGCAAGGGCGAGGAGC
		DLK328	Reverse	TGCAGATGAACTTCAGGGTCAG
LUC	Firefly luciferase	DLK280	Forward	CTTATGCATGCGGCCGCATCTAGAGG
		DLK285	Reverse	CAGTTGCTCTCCAGCGGTTCCATCC
BOP1	Block of proliferation 1	DP348	Forward	TCTGAGCCCGAACTGGAGCCTGA
		DP349	Reverse	AGAATCGCTGCCGGTGCTGT
RPLP0	Ribosomal protein lateral stalk subunit P0	DLK297	Forward	GGAGAAACTGCTGCCTCATATC
		DLK298	Reverse	CAGCAGCTGGCACCTTATT
STRN4	Striatin 4	DLK270	Forward	AACCTGGCCGGCAATCAGAGAGGAT
		DLK273	Reverse	CCCAAACACCACTCTCCTGGACAATTA
POLR2B	RNA polymerase II subunit B	DP276	Forward	TACGACGCGGATGAGGATATGCAA
		DP277	Reverse	CAATCCAGCATGCTTCTTGCCACA
ZNF207	Zinc-finger protein 207	DLK219	Forward	CGTGGTGGTAGCCGTTGGGTTGGGAAAG
		DLK73	Reverse	TACAATACCAGCACCACGGCTTCA
VDAC3	Voltage dependent anion channel 3	DLK223	Forward	CGTTGGTTTGAAGACCTTCAGCGT
		DLK224	Reverse	GGCTCTTATGAAACCAAAGACCTCCACC
EXOSC2	Exosome component 2	DP272	Forward	AAGATGGCGATGGAGATGAGGCTT
		DP273	Reverse	CCCGGCACCACTAGATGTTTCTTAG
MAPK1	Mitogen-activated protein kinase 1	DLK58	Forward	TCTGGCAGGCAGGCAGGCAAT
		DLK59	Reverse	TGACCGGGAGGAGGAAGGAAGA
STAT3	Signal transducer and activator of transcription 3	DP314	Forward	TAGCAGGATGGCCCAATGGAATCA
		DP315	Reverse	AGCTGTCACTGTAGAGCTGATGGA

Table 3. Primers for RT-qPCR.